

UNIVERSITY OF OKLAHOMA

GRADUATE COLLEGE

PHENOMENOLOGY OF THE STRING THEORY LANDSCAPE

A DISSERTATION

SUBMITTED TO THE GRADUATE FACULTY

in partial fulfillment of the requirements for the

Degree of

DOCTOR OF PHILOSOPHY

By

MOHAMMED SHADMAN SALAM

Norman, Oklahoma

2022

PHENOMENOLOGY OF THE STRING THEORY LANDSCAPE

A DISSERTATION APPROVED FOR THE
HOMER L. DODGE DEPARTMENT OF PHYSICS AND ASTRONOMY

BY THE COMMITTEE CONSISTING OF

Dr. Howard Baer, Chair

Dr. Bruno Barboza

Dr. Braden Abbott

Dr. Eddie Baron

Dr. Michael Jablonski

To the memories of..

***Abbu** - from whom I learned about the importance of honesty, integrity and hard work,*

***Nanu** - for all the delicious food that is everlasting on my taste buds,*

***Nanabhai** - for those wonderfully deep conversations about history, politics and life,*

and

***Chokidar Chachu** - for we're bound not by blood, but more strongly by the heart.*

Acknowledgements

I want to begin by expressing my gratitude to my advisor Prof. Howie Baer. I have no qualms to state wholeheartedly that he is the reason why I survived graduate school. When I joined his group, my confidence was at an all-time low and I was in a bad place mentally and physically. Various issues, both personal and professional, had me seriously contemplating dropping out but being a stubborn stickler for seeing things through (to my own detriment sometimes), I went into his office one gloomy afternoon in Spring 2018 expressing my interest to work with him. At that point, I was lucky to have had several courses taught by him, and through his lucid lectures mixed with a healthy dose of humor, I started to fall in love with physics again. I will forever be indebted to Howie for accepting me into his group, believing in me, when even I didn't believe in myself, and handing me goal-oriented and exciting projects. Of course, I ran into brick walls countless times when I did not know what I was doing wrong or had no clue where to start with a project; his door was open for any questions and through deep, engaging conversations he clarified my confusions without ever getting angry or visibly frustrated by my many dumb questions. I always came out of his office with an uplifting feeling of having learned something new in addition to having my original queries answered. In short, Howie has been a father figure to me who has guided me through some of my toughest periods of life in academia and I will forever cherish my time working under his supervision.

I would also like to extend my gratitude and thanks to Dr. Bruno Barboza, Dr. Braden Abbott, Dr. Eddie Baron and Dr. Michael Jablonski for taking time out of their busy schedule to serve on my committee. Thank you all for listening to my concerns, answering my emails and filling out official forms well ahead of deadlines whenever I needed them. Additionally, I am grateful to Prof. Vernon Barger of Wisconsin-Madison for his wise inputs during our collaborations, and Prof. Xerxes Tata of Hawai'i for some very enlightening and heart-warming discussions over dinner and drinks at Pre-SUSY 2019.

To Shabnam Ahsan Esha, my partner in life, my best friend, my shoulder to lean on, words alone cannot express my gratitude for your constant love and support throughout the last eleven years of being together. From years of having a long-distance relationship, when we got into different schools - many states apart - in our pursuit of higher education, to being newly-weds but still separated indefinitely on opposite sides of the globe by a raging pandemic, many times it felt as if the Universe was plotting against us. Your love, dedication and trust kept my belief strong as we weaved our way through challenging circumstances. I can never repay the sacrifices you've made, especially in the last year, to be here with me while I finish my PhD. Richard Feynman once famously wrote, "physics is not the most important thing, love is"; I know it for a fact since whatever I accomplish would be as meaningless as the sky without the stars, if I didn't have you in my life. I love you.

I would like to thank my parents for without them, I would not even exist within any pocket universe in the vast multiverse. Through hard work and numerous sacrifices, they ensured that me and my brother get a good education and have all the necessary things for a comfortable existence. To my elder brother, Ezad, I am grateful for taking up a lot of responsibility upon my father's passing which allowed me to pursue my education with little worry. I want to also thank my maternal aunt and her husband, Farzana Ayub and

Mohammad Abul Bashar, for constantly being there as well-wishers. Additionally, I want to mention my maternal uncle, Nasser Ayub, whom I always looked up to as a kid and aspired to work at NASA one day, following in his footsteps. His stories about space exploration birthed my curiosity for science and the cosmos. I am also very grateful to the family I chose, my in-laws, Afroza Amin and Ahsan Habib. Since before I became a member of their family, they were very accepting of me and thereafter always treated me like their own son. I truly cherish their kindness, love and warmth.

I am also very thankful to my friends Tahsin, Zia, Rohan and Shahriar for all the shenanigans we got up to in days past. Countless cups of tea, all the terrace *addas* through lazy afternoons to late evenings, and infinite hours of gaming that grew from being a coping mechanism to deal with many issues I was having, into something that was an indispensable part of most of my days. I also extend my thanks to Rafid Mahbub, my neighbor and friend, for our many aimless walks through the alleyways of Paltan. Now, it would be a disservice to not mention a friend whom I always considered to be like a brother, Siam. Sometimes, even after decades of knowing someone feels like you don't really know them - he is the epitome of such a person. We are not connected anymore but I would still like to thank him for the many hours of phone calls of, often pointless, conversations about all things life.

At OU, I have had the pleasure of befriending John Truden, Geo Jose, Daniel Wilbern, Burak Mustafa, Joseph Choi, Xin Guo, Rajeeb Sharma, Eric Ashby, Matthew Goodman, Andrea Cristini, Hasan Serce and Dibyashree Sengupta, among some others whose names have slipped my mind as I write this. Thank you John for being a good friend and roommate and for always making me feel valued and appreciated. I thank Daniel for being my coding *guru* since without his willingness to train me in various aspects of shell scripting and python, I would be lost at sea in my research. To Burak, Choi, Xin, Eric, Rajeeb and Geo, I am eternally grateful for sharing your knowledge and wisdom with me while we were busy passing various classes and qualifiers. Andrea, in a short period of time, we became pretty close friends so much so that we were comfortable opening up about our personal lives, over many meals we shared at *The Library*, which greatly helped me get over difficult phases of life for which I am truly grateful to you. To Hasan and Dibyashree, thanks for always keeping your door open to my constant research questions, some of which, in hindsight, were annoyingly trivial. To Matt, I really appreciate how you kept in touch with your sporadic texts even after many years of leaving OU. To all, thanks for making my years in Norman a bit more livable.

Lastly, I would like to mention members of the Bangladeshi student community here in Norman, especially to the following people. Thanks to Warid Islam, for being available to pick me up from the airport and making me feel at home upon landing in the US. Eternally grateful to Mohan Bhowmik for letting me share his home for the first few days when I didn't have any other accommodations, and helping me set up my new life here. Thanks to Shajid Islam Amit and Rowzat Faiz Shegufa for always being open and available to help me out of difficult situations by providing relevant information and lending good advice.

Finally, this dissertation is dedicated to four of the most beloved people in my life whom I've lost. Each of them have made unique contributions to the journey that got me where I am today.

To anyone I have missed, please know that my mind betrayed me and that it was purely unintentional and I am thankful to you regardless.

Table of Contents

Abstract	viii
List of Figures	xiii
List of Tables	xiv
1 Introduction	1
1.1 The Standard Model	1
1.2 Shortcomings of the Standard Model	3
1.3 Supersymmetry	4
1.3.1 Motivations for SUSY	5
1.3.2 Basics of SUSY Transformations	8
1.3.3 Minimal Supersymmetric Standard Model (MSSM)	11
1.3.4 Local SUSY/ Supergravity	14
1.3.5 SUSY Breaking	14
2 Discussion on String Theory	17
2.1 Superstring Theories	18
2.1.1 Global Worldsheet SUSY	21
2.1.2 Mode Expansions and Boundary Conditions	22
2.1.3 Canonical Quantization of the RNS Superstring Theory	25
2.1.4 GSO Projection	32
2.2 Types of Superstring Theories	35
3 String Compactifications	37
3.1 The General Construct	37
3.2 Moduli Stabilization	38
3.2.1 Promising Solutions to the Moduli Stabilization Problem	39
3.2.2 Vacuum Multiplicity	43
4 Naturalness and the Anthropic Landscape	45
4.1 Anthropic Resolution of the Cosmological Constant Problem	46
4.2 Anthropic Origin of the Weak-Scale	50
4.3 Naturalness Re-examined	52
4.3.1 CMSSM / mSUGRA and NUHM n models	53
4.3.2 Practical Naturalness Measures	55
4.3.3 Stringy Naturalness	61
4.4 Naturalness versus Stringy Naturalness	67
4.5 The Triumph of Natural SUSY in the Landscape	69
4.5.1 Fate of the SM and CMSSM in the Landscape	69
4.5.2 Radiative Natural SUSY emergent from the Landscape	72
5 String landscape guide to SUSY and DM searches	81
5.1 Soft terms in the low energy EFT	81
5.2 Results from gravity mediated SUSY breaking schemes	91
5.3 Results from Generalized Mirage-Mediation (GMM')	100

5.3.1	GMM' model and parameter space	100
5.3.2	Results in the m_0^{MM} vs. $m_{1/2}^{MM}$ plane	103
5.3.3	Higgs and sparticle mass distributions in the GMM' model for varying n_0	107
5.4	Results from Dynamical SUSY breaking in the landscape	112
5.4.1	Higgs and sparticle mass distributions in the landscape with DSB	115
5.5	Examination of soft terms drawn logarithmically on the landscape	121
5.5.1	Higgs and sparticle mass distributions in the landscape with logarithmic draw on soft terms	121
5.6	Landscape predictions for SUSY Dark Matter	131
5.6.1	Landscape implications for WIMP DM search results from Direct Detection (DD) and Indirect Detection (IDD) Experiments	132
5.6.2	LHC higgsino discovery plane	135
6	Summary and Outlook	147
	References	153

Abstract

In this dissertation, we perform a thorough phenomenological study of the string theory landscape [1]. To this end, we compare and contrast the data collected from particle accelerators and detectors against various models of observable particle phenomena. One stark indirect evidence of underlying string theory is the existence of *supersymmetric* (SUSY) particles, a variety of new particles resulting from a symmetry between the bosons and fermions observed in nature: *i.e.* every boson should be paired with a fermionic partner and vice versa. The discovery of the Higgs boson at the LHC in 2012, the particle responsible for giving mass to matter particles (e.g. electrons) and the massive gauge bosons, has provided us with strong bounds on the masses of these yet unobserved *superpartner* particles, which when combined with string theory landscape arguments, can yield strong statistical predictions for observing SUSY in future upgrades to particle accelerators. Various SUSY models are explored in the context of string landscape statistics by which we can rule some models out as realistic extensions to the Standard Model (SM). We also argue how realistic SUSY models requires the Higgs boson mass to be ~ 125 GeV with superpartners beyond current energy limits of the LHC - just what is observed experimentally. Additionally, we also analyze the prospect of detecting dark matter particles which only gravitate and exhibit at best only weak interactions. The emergence of SUSY also equips us with such Weakly Interacting Massive Particles (WIMPs), whose mass range can then be statistically predicted using string landscape arguments.

List of Figures

1.1	1-loop quantum corrections to $m_{H_{SM}}^2$ due to a fermion loop (left) and a scalar loop (right).	6
1.2	Gauge Coupling unification in the MSSM.	7
3.1	Flux Compactification Topology.	40
3.2	D-branes in String Theory.	42
4.1	Distribution of Λ_{cc} on a log scale.	47
4.2	String landscape finds a natural home in the multiverse.	48
4.3	Open versus Closed Universe.	49
4.4	A simplified picture of the ABDS window.	51
4.5	Naturalness contours for the CMSSM and NUHM2 SUSY models.	59
4.6	Annuli of soft SUSY breaking F-terms in the complex plane.	63
4.7	RG Evolution of $m_{H_u}^2$ vs. Q for several choices of $m_{H_u}^2(\Lambda)$ for a given benchmark point for the NUHM2 model [2].	64
4.8	Contributions of $\text{sign}(\Sigma_u^u(\tilde{t}_{1,2})) \cdot \sqrt{ \Sigma_u^u(\tilde{t}_{1,2}) }$ to the weak-scale vs. $A_t(\text{weak})$ for the given NUHM2 model benchmark point [2].	66
4.9	m_h vs. A_t for the given NUHM2 model benchmark point [2].	67
4.10	m_0 vs. $m_{1/2}$ plane for the given NUHM2 model with $A_0 = -1.6m_0$, $\mu = 200$ GeV, $m_A = 2$ TeV.	68
4.11	m_H vs. μ_{SM} for various theory cut-off values Λ_{SM}	70
4.12	m_Z^{PU} vs. μ for various values of naturalness measure Δ_{EW}	71

4.13	The expected $\sqrt{-m_{H_u}^2(weak)}$ vs. μ^{PU} parameter space in a toy model ignoring radiative corrections to the Higgs potential.	74
4.14	The $\sqrt{-m_{H_u}^2(weak)}$ vs. μ^{PU} parameter space wherein the green points denote vacua with appropriate EWSB within ABDS constraints.	76
4.15	m_Z^{PU} vs. μ^{PU} parameter space wherein the green points denote vacua with appropriate EWSB within ABDS constraints.	78
4.16	The $\sqrt{-m_{H_u}^2(weak)}$ vs. μ^{PU} parameter space from Isajet wherein the green points denote vacua with appropriate EWSB within ABDS constraints. . . .	79
5.1	Regions of $\Delta_{EW} > 30$ (blank) and CCB minima (lower left) in the scalar potential.	93
5.2	LHC Run 2 limit for $m_{\tilde{g}} \geq 2.25$ TeV is shown by the red contour. [3]	93
5.3	Locus of $n = 1$ landscape scan points for the NUHM3 model with $\mu = 100 - 360$ GeV in the $m_{\tilde{\chi}_1^0}$ vs. $m_{\tilde{g}}$ plane versus recent LHC Run2 constraints. [3]	94
5.4	Locus of $n = 1$ landscape scan points for the NUHM3 model with $\mu = 100 - 360$ GeV in the $m_{\tilde{\chi}_1^0}$ vs. $m_{\tilde{t}_1}$ plane versus recent LHC Run2 constraints. [3]	94
5.5	Locus of $n = 1$ landscape scan points for the NUHM3 model with $\mu = 100 - 360$ GeV in the $m_{\tilde{t}_1}$ vs. $m_{\tilde{g}}$ plane versus recent LHC Run2 constraints (black) and projected HE-LHC 95% CL reach contours (purple-dashed). [3]	95
5.6	Locus of $n = 1$ landscape scan points for the NUHM3 model in the $m_0(1,2)$ vs. $m_0(3)$ plane for $\mu = 100 - 360$ GeV. [3]	95
5.7	Locus of $n = 1$ landscape scan points for the NUHM3 model with $\mu = 100 - 360$ GeV in the μ vs. $m_{\tilde{w}_2}$ plane versus projected HL-LHC 95% CL search limits. [3]	96

5.8	Locus of $n = 1$ landscape scan points for the NUHM3 model with $\mu = 100 - 360$ GeV in the $m_{\tilde{z}_2} - m_{\tilde{z}_1}$ vs. $m_{\tilde{z}_2}$ plane versus projected HL-LHC 95% CL search limits. [3]	96
5.9	Feynman diagram for the SSdB decay signature.	97
5.10	Feynman diagram for the OSDLJMET decay signature.	98
5.11	Locus of $n = 1$ landscape scan points for the NUHM3 model with $\mu = 100 - 360$ GeV in the $\tan \beta$ vs. m_A plane versus recent LHC Run2 constraints.	99
5.12	m_0^{MM} vs. $m_{1/2}^{MM}$ plane of the GMM' model for a value of $n_{1/2} = 1$ but with a) $n_0 = 1$, b) $n_0 = 2$, c) $n_0 = 3$, d) $n_0 = 4$	105
5.13	Probability distribution dP/dm_h vs. m_h for $n_{1/2} = 1$ and $n_0 = 1, 2, 3, 4$ for scans of the GMM' model for $m_{3/2} = 20$ TeV, $\mu = 200$ GeV, $m_A = 2$ TeV, $\tan \beta = 10$ and $a_3 = 1.6\sqrt{c_m}$ while enforcing $m_Z^{PU} < 4m_Z^{OU}$. [4]	106
5.14	Probability distribution dP/dm_h vs. m_h for $n_{1/2} = 1$ and $n_0 = 1$ blue, 2 red for general statistical scans over the GMM' model for $m_{3/2} = 20$ TeV, $\mu = 200$ GeV. [4]	108
5.15	Various Probability distributions of the GMM' spectra.	109
5.16	Probability distribution $dP/dm_{\tilde{u}_L}$ vs. $m_{\tilde{u}_L}$ for $n_{1/2} = 1$ and $n_0 = 1$ blue, 2 red for general statistical scans over the GMM' model for $m_{3/2} = 20$ TeV, $\mu = 200$ GeV. [4]	111
5.17	Expected SUSY breaking scale m_{hidden} vs. hidden sector coupling g^2 from DSB. [5]	114
5.18	Probability distributions for various DSB input parameters.	117
5.19	Probability distributions of light and heavy Higgs in DSB scenario.	118

5.20	Various probability distributions for the DSB spectra.	119
5.21	Probability distributions for various input scan parameters for $f_{SUSY} \sim$ $\log(m_{soft})$	123
5.22	Various probability distributions in the Higgs/higgsino sector for $f_{SUSY} \sim$ $\log(m_{soft})$	124
5.23	Scatter plot of models with appropriate EWSB and $m_Z^{PU} < 4m_Z^{OU}$ in the m_h vs. A_0 plane with $\mu = 150$ GeV. [6]	126
5.24	Scatter plot of models with appropriate EWSB and $m_Z^{PU} < 4m_Z^{OU}$ in the m_A vs. $\tan \beta$ plane with $\mu = 150$ GeV.	127
5.25	Scatter plot of models with appropriate EWSB and $m_Z^{PU} < 4m_Z^{OU}$ in the m_h vs. Δm^0 plane with $\mu = 150$ GeV.	128
5.26	Various probability distributions for the spectra generated with $f_{SUSY} \sim$ $\log(m_{soft})$	129
5.27	Locus of $n = 1$ landscape scan points for the NUHM3 model in the $\xi \sigma^{SI}(\tilde{\chi}_1^0, p)$ vs. $m_{\tilde{\chi}_1^0}$ plane versus recent WIMP search constraints $\mu = 100 - 360$ GeV.	132
5.28	Locus of $n = 1$ landscape scan points for the NUHM3 model in the a) $\xi \sigma^{SD}(\tilde{\chi}_1^0, p)$ vs. $m_{\tilde{\chi}_1^0}$ and b) $\xi^2 \langle \sigma^{SI} v \rangle$ vs. $m_{\tilde{\chi}_1^0}$ planes versus recent WIMP search constraints [3].	134
5.29	ATLAS Collaboration results presented in Fig. 11a of Ref. [7] depicting number of events against the dilepton invariant mass.	137
5.30	Deviations in loop-corrected chargino mass as compared to simplified model value $\Delta m(\tilde{\chi}_1^\pm)$ a) in the NUHM2 model and b) in the GMM' model.	139

5.31	Regions of naturalness Δ_{EW} in the light higgsino discovery plane $m_{\tilde{\chi}_2^0}$ vs, $\Delta m^0 \equiv m_{\tilde{\chi}_2^0} - m_{\tilde{\chi}_1^0}$ from <i>a)</i> the NUHM2 model and <i>b)</i> the GMM' model. . . .	141
5.32	Regions of stringy naturalness in the higgsino discovery plane $m_{\tilde{\chi}_2^0}$ vs, $\Delta m^0 \equiv$ $m_{\tilde{\chi}_2^0} - m_{\tilde{\chi}_1^0}$ from <i>a)</i> the NUHM2 model and <i>b)</i> the GMM' model.	145

List of Tables

1.1	The Standard Model Gauge Group.	1
1.2	MSSM Gauge Group.	12
2.1	Superstring Spectrum.	34
5.1	Expected range of Higgs and sparticle masses in the GMM' model from the string landscape with $n_{1/2} = 1$ but with $n_0 = 1$ or $n_0 = 2$	111
5.2	Three models of moduli stabilization along with expected form of soft terms, expected soft term distribution in string II-B landscape and reference for associated statistical distributions of Higgs and sparticle masses. [6]	130

Chapter 1

Introduction

1.1 The Standard Model

The Standard Model (SM) is a collection of gauge theories based on gauge groups $SU(3)_C$ and $SU(2)_L \times U(1)_Y$. This framework arranges fundamental particles into two main categories, namely *fermions* and *bosons*. Fermions are spin-1/2 particles that include the quarks and leptons while the force mediators (spin-1) and the Higgs (spin-0) fall under the umbrella of bosons. The group representations of the first generation fermions and bosons along with their corresponding gauge quantum numbers are given in the table below.

	Field	$SU(3)_C$	$SU(2)_L$	$U(1)_Y$
Leptons	$L = \begin{pmatrix} \nu_L \\ e_L \end{pmatrix}$	1	2	-1
	e_R	1	1	-2
Quarks	$Q = \begin{pmatrix} u_L \\ d_L \end{pmatrix}$	3	2	1/3
	u_R	3	1	4/3
	d_R	3	1	-2/3
Gauge Bosons	B	1	1	0
	W	1	3	0
	G	8	1	0
Higgs Boson	$\phi = \begin{pmatrix} \phi^+ \\ \phi^0 \end{pmatrix}$	1	2	1

Table 1.1: Group Representation of first generation fermions, gauge bosons and the Higgs boson.

The $SU(3)_C$ group is called *Quantum Chromodynamics* (QCD) and describes the interaction of particles with color charge, like the quarks, via exchange of *gluons*, the particles that mediate the strong nuclear force. The gluons themselves carry color charge and hence have strong self interactions, as a result of which gluons are always observed as confined states

such as hadrons (a state made up of multiple quarks and antiquarks). The requirement of local gauge invariance means that the gluons form a color octet under $SU(3)_C$ i.e. there are 8 gluons in the SM and all of these are necessarily massless. Furthermore, the quarks come in three different color charges namely, red (r), blue(b) and green(g) and so they form a color triplet under $SU(3)_C$. A consequence of $SU(3)_C$ symmetry is that strong interactions must conserve color charge.

The $SU(2)_L \times U(1)_Y$ group describes the *electroweak* interactions, the unified framework of electromagnetism and the weak nuclear force pioneered by Glashow, Weinberg and Salam [8, 9, 10]. The $SU(2)_L \times U(1)_Y$ symmetry breaks down to $U(1)_{em}$, which describes the interaction of electrically charged particles via the exchange of *photons*, a field theory framework termed *Quantum Electrodynamics* (QED). The symmetry is unbroken at high energies but at low energies it breaks spontaneously when the Higgs boson, a spin-0 (scalar) field, acquires a non-zero vacuum expectation value (VEV), in a process known as the Higgs mechanism [11, 12]. Consequently this symmetry breaking gives rise to the massive W^\pm and Z^0 bosons which are the mediators for the weak force, along with the photon which remains massless. The L subscript in $SU(2)_L$ refers to the fact that only left-chiral fields interact via the weak force which is a consequence of the observation that weak interactions do not respect *parity* symmetry. Therefore, left-chiral fermions are $SU(2)_L$ doublets while right-chiral fermions are $SU(2)_L$ singlets, as shown in Table 1.1. Additionally, the Y subscript in the $U(1)_Y$ label is identified as the weak hypercharge, the group generator for the $U(1)$ part of the electroweak gauge group. Since all SM fermions and the Higgs are charged under $U(1)_Y$ they exhibit weak interactions; in fact, quarks interacting via the weak force is what causes nuclear β - decay. The complete SM framework consists of 3 generations each of 6

leptons and 6 *flavors* of quarks termed as *up* (u), *down* (d), *charm* (c), *strange* (s), *top* (t), *bottom* (b) coming in 3 colors each (so 18 quarks). There are also 12 force mediators and the Higgs boson which is required to give mass to the massive gauge bosons, quarks and the charged leptons. Additionally, paired with leptons and quarks there are 6 antileptons and 6 antiquarks (6 flavors) which have the same masses as their particle counterparts but with all charges with their signs flipped. Thus, altogether the SM consists of an assortment of 62 fundamental particles which helps to explain three of the four fundamental forces in nature.

1.2 Shortcomings of the Standard Model

Despite its successes however, the SM is incomplete. Most obviously, the SM is devoid of gravity. The quantum field theory behind it fails to quantize gravity in that the theory becomes non-renormalizable when following traditional particle or field approaches of introducing a *graviton* as the force mediator.

Furthermore, even after the discovery of the Higgs boson with its mass precisely measured at $m_h \sim 125$ GeV, the SM suffers from instability in the Higgs mass calculation in that it is quadratically divergent. Technically, the mass is theoretically obtained as, $m_H^2 = m_{H_0}^2 + \delta m_H^2$ wherein the radiative corrections $\delta m_H^2 \sim \Lambda^2$ where Λ is the cutoff energy of the theory with $\Lambda \gg m_H$. The only remedy to these quadratic divergences is to require an incredible amount of *fine-tuning* in the $m_{H_0}^2$ term to obtain the measured Higgs mass. Inevitably, the question then arises as to why the measured Higgs mass is so much smaller than the Planck scale ($\Lambda_{m_P} \sim 10^{18}$ GeV) or the GUT scale ($\Lambda_{m_{GUT}} \sim 10^{16}$ GeV). This kind of tuning is considered *unnatural* and the SM cannot account for such a scenario. Conversely, this is one of the

leading unsolved mysteries of the SM and has been termed “The Big Hierarchy Problem” (BHP) or the “*fine-tuning problem*”.

Then there is the question of Dark Matter (DM) and Dark Energy (DE) content of the Universe, whose existence is evident from astronomical observations [13, 14]. In fact, data suggests that only $\sim 5\%$ of the constituents of the known Universe is comprised of matter particles of the SM while the rest is accredited to the DM ($\sim 27\%$) and DE ($\sim 68\%$) content, of whose presence the SM is oblivious to.

Moreover, the cosmological constant in Einstein’s field equations, Λ_{cc} , which is equivalent to the *vacuum energy* has been experimentally measured from observation of supernovae redshift to be $\Lambda_{cc} \simeq 10^{-122} m_P^2$ [15]. This is in outrageous disagreement to the value expected from naive dimensional analysis i.e. $\Lambda_{cc} \simeq m_P^2$ where m_P is the reduced Planck mass. This is the infamous cosmological constant (CC) problem which is devoid of explanation in the SM framework.

The above list is not exhaustive however and the SM suffers from a number of other ailments, such as the strong CP problem, that have been left out. These are just a few issues listed that are enough to motivate thinking about a theory that lies beyond the SM (BSM). One of the most promising BSM theories is discussed in the following section, followed by a study of the most compelling UV-complete theory till date - *string theory*, in Chapter 2.

1.3 Supersymmetry

Supersymmetry (SUSY) is one of the most popular class of BSM models. It posits the existence of a symmetry between bosons and fermions, i.e. for every boson (fermion) there

exists a partner fermion (boson), a relation which is yet to be observed in experiments. Nevertheless, there are encouraging signs that nature respects this symmetry, some of which will be discussed shortly. Additionally, the existence of SUSY serves to ameliorate a lot of the problems that plague the SM.

1.3.1 Motivations for SUSY

The principle motivation for SUSY is its ability to neatly solve the fine-tuning problem or BHP, referred to in the previous section. Loop integrals that one encounters in field theories are often divergent; the structure of these divergences determine if they are tameable by conventional regularization methods or if new degrees of freedom need to be introduced to avoid them. For instance, fermion mass integrals are protected by their chiral symmetry which results in mild logarithmic divergences up to a cut-off scale Λ ,

$$\delta m \propto m \ln \frac{\Lambda}{m}.$$

However, the divergence structure of field theories with elementary scalars often leads to dangerous quadratic divergences. For instance, calculation of the physical Higgs mass at one-loop level yields,

$$m_{H_{SM}}^2(\text{phys}) \simeq m_{H_{SM}}^2 + \frac{c}{16\pi^2} \Lambda^2 \tag{1.1}$$

where $m_{H_{SM}}^2$ is the Higgs mass squared parameter in the Lagrangian, c contains various coupling constants while $1 \text{ TeV} \ll \Lambda < m_P \simeq 10^{18} \text{ GeV}$ is some high scale cut-off for which the SM ceases to be a valid theory. The second term includes various contributions such as the Higgs coupling to a fermion loop or to itself as shown by the Feynman diagrams in Figure 1.1.

Astonishingly this implies a fine-tuning of 1 part in 10^{26} to mathematically obtain the observed Higgs mass, $m_H(\text{phys}) \simeq 125 \text{ GeV} \sim 100 \text{ GeV}$ for a scale choice, $\Lambda = m_{GUT} \sim 10^{16} \text{ GeV}$. To render the Higgs mass ‘natural’, or conversely, not fine-tuned, large cancellations between fermionic and bosonic loops would seemingly need to occur. Therein arises the notion of a symmetry between fermions and bosons i.e. SUSY which accounts for the loop cancellations, thereby stabilizing the Higgs mass and solving the BHP.

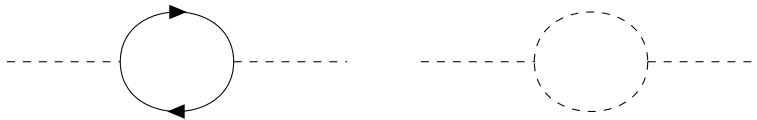


Figure 1.1: 1-loop quantum corrections to $m_{H_{SM}}^2$ due to a fermion loop (left) and a scalar loop (right).

SUSY is also a well-motivated extension to the SM due to its ability to explain the values of empirically obtained parameters in the SM like the gauge couplings. Any candidate complete theory beyond the SM should necessarily explain these precisely measured values; most favorable of these theories should manifest a *unification* of these couplings at energy scale $m_{GUT} \sim 10^{16} \text{ GeV}$ and so named **Grand Unified Theories (GUTs)**. Although the SM is a renormalizable quantum theory with its own set of Renormalization Group Equations (RGE), when extrapolated up to m_{GUT} from $m_{weak} \sim 100 \text{ GeV}$ this set of RGE shows only rough unification of the $SU(2)$, $SU(3)$ and $U(1)$ gauge couplings. However, SUSY RGE’s successfully unifies the couplings at m_{GUT} , another strong evidence for SUSY as a BSM framework. This is shown in Figure 1.2, where we follow convention and plot the inverse of $\alpha_i = g_i^2/4\pi$, where g_i are the gauge coupling constants with $i = 1, 2, 3$ against the $t = \ln Q$ with Q being the energy scale. The plot results from the running of the gauge couplings

from the weak-scale ($Q \sim 100$ GeV) where the couplings have been measured to very high precision, up to the GUT scale dictated by their Renormalization Group Equations (RGEs) in the SM and the Minimal Supersymmetric SM (MSSM).

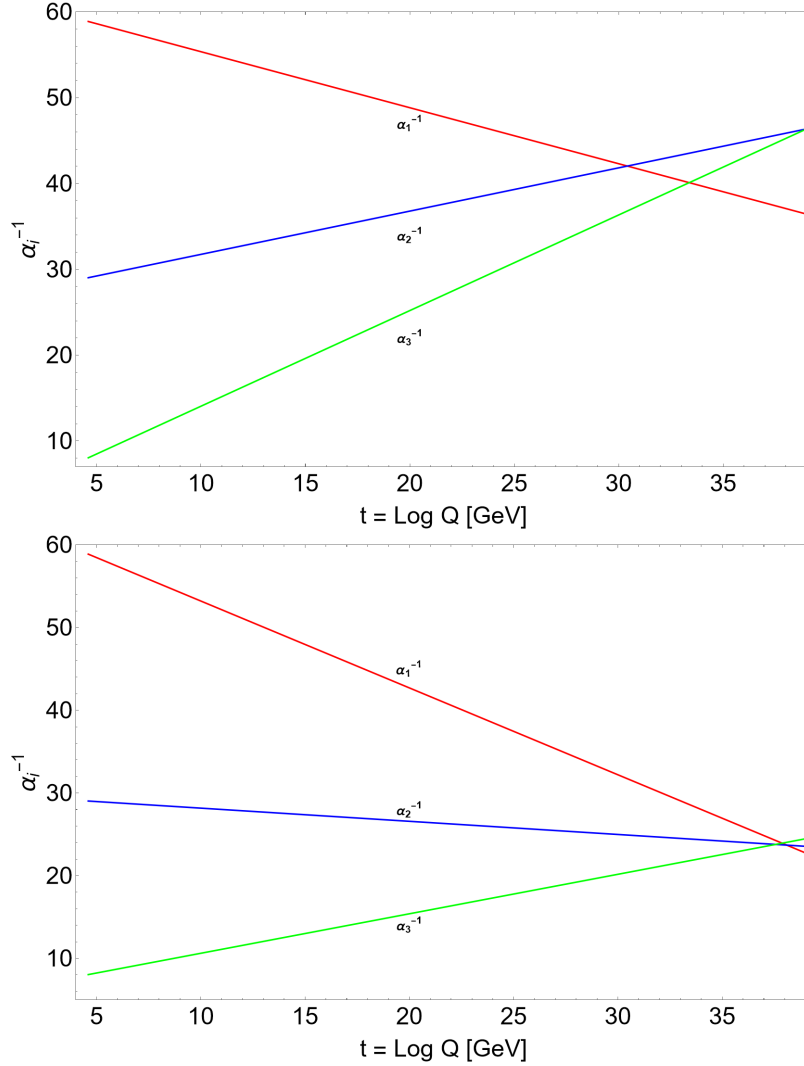


Figure 1.2: Evolution of the $SU(3)_C \times SU(2)_L \times U(1)_Y$ gauge coupling constants from the weak-scale to the GUT scale in the SM (top frame) and in the MSSM with 2-Higgs doublets (bottom frame).

Additionally, all R – parity conserving SUSY models accommodate DM particles in their spectrum. Such a particle should be massive, electrically and color neutral. Moreover, *local* SUSY exhibits an inherent connection to gravity in that it necessitates the existence of

a massless spin-2 gauge boson which mediates the gravitational interactions, the *graviton* along with its spin-3/2 *superpartner*, the *gravitino*, in the SUSY model spectrum. This is an example of *supergravity* model which includes Einstein's theory of General Relativity (GR). Like any 4 – D theory of gravity, supergravity is non-renormalizable but nevertheless the SUSY-gravity connection proves useful when pursuing robust quantum gravity theories, as will be discussed later in this dissertation.

A further important ability of the SUSY framework is to explain the fundamentals of Electroweak Symmetry Breaking (EWSB) that is observed when the W and Z bosons become massive via the Higgs mechanism, as was discussed earlier. Even though appropriate gauge and parameter choices can accommodate proper EWSB in the SM, no explanation is provided for the required choices. In contrast, EWSB is fueled by the SUSY RGE effects driving the Higgs boson squared mass parameters to small negative values and hence negates any need for arbitrary parameter selection. However, this phenomena termed *Radiative Electroweak Symmetry Breaking* (REWSB), only works if the top quark mass is large enough e.g $m_t \sim 100 - 200$ GeV; as a result REWSB holds since the measured top quark mass happens to be $m_t \sim 173$ GeV [16]. REWSB has profound implications for particle physics as will be studied in more detail later in the work.

1.3.2 Basics of SUSY Transformations

As established in the discussion above, SUSY is a symmetry that relates fermions and bosons. More technically, SUSY is a spacetime transformation that converts a bosonic state to a fermionic state and vice versa. Using operator notation, a SUSY transformation is

written as,

$$Q|Boson\rangle = |Fermion\rangle, \quad Q|Fermion\rangle = |Boson\rangle$$

where Q is the generator of SUSY transformations which is an anti-commuting *spinor*. Since spinors are intrinsically complex valued objects, its complex conjugate operator \bar{Q} is also a symmetry generator. Since SUSY is a spacetime symmetry, we must expand the Poincaré group into the complete set of SUSY transformations. Thus, augmented by the usual spacetime transformations of rotations and boosts generated by the six component rank-2 tensor $M_{\mu\nu}$ and translations generated by the energy-momentum operator P_μ , the SUSY transformations generated by the spinor Q_a form the *super-Poincaré algebra*, as

$$[P_\mu, P_\nu] = 0, \tag{1.2}$$

$$[M_{\mu\nu}, P_\lambda] = i(g_{\nu\lambda}P_\mu - g_{\mu\lambda}P_\nu), \tag{1.3}$$

$$[M_{\mu\nu}, M_{\rho\sigma}] = i(g_{\mu\rho}M_{\nu\sigma} - g_{\mu\sigma}M_{\nu\rho} - g_{\nu\rho}M_{\mu\sigma} - g_{\nu\sigma}M_{\mu\rho}), \tag{1.4}$$

$$[P_\mu, Q_a] = [P_\mu, Q_a^\dagger] = 0, \tag{1.5}$$

$$[M_{\mu\nu}, Q_a] = -\left(\frac{1}{2}\sigma_{\mu\nu}\right)_{ab}Q_b, \tag{1.6}$$

$$\{Q_a, \bar{Q}_a\} = 2(\gamma^\mu)_{ab}P_\mu, \tag{1.7}$$

$$\{Q_a, Q_b\} = -2(\gamma^\mu C)_{ab}P_\mu, \tag{1.8}$$

$$\{\bar{Q}_a, \bar{Q}_b\} = 2(C^{-1}\gamma^\mu)_{ab}P_\mu. \tag{1.9}$$

The above algebra is the most general extension of the Poincaré algebra provided that there is only a single ($N = 1$) spinor generator Q ; these are known as $N = 1$ SUSY. For a supersymmetric theory then, single-particle states form an irreducible representation of the SUSY algebra, termed as *supermultiplets*. These supermultiplets contain both bosonic and fermionic states which are *superpartners* of each other. In the irreducible representation, the P^2 operator with eigenvalue m^2 (square of the mass), commutes with all the group generators implying that the superpartners in a supermultiplet must have the same mass. However, therein lies the conundrum: such a bosonic counterpart with the same mass as say, the electron, could not have evaded detection at past or current detectors. The solution then is to consider SUSY to be a broken symmetry and so that superpartners necessarily have different masses and differ by a spin-1/2 from their SM counterparts. As a result the SM gauge bosons with spin-1 are partnered up with their spin-1/2 superpartners, the *gauginos*, the SM fermions with spin-1/2 form chiral supermultiplets with their scalar (spin-0) superpartners, the *sfermions*. The Higgs boson (spin-0) on the other hand, resides in two chiral supermultiplets with its superpartners, the spin- $\pm 1/2$ *higgsinos*, each of which is required to give rise to masses of the up-type and down-type quarks. Thus, to build SUSY models, one needs to combine bosonic (scalar and vector) and fermionic (spinor) fields into a single entity, the *superfield* $\Phi \equiv \hat{\Phi}(x, \theta)$ where the θ are anti-commuting Grassman coordinates which correspond physically to Majorana spinor field which is a Dirac spinor that obey the Majorana condition,

$$\theta = \bar{\theta} = \theta^T C,$$

where C is the charge conjugation matrix. The above relation tells us that a Majorana

spinor is its own antiparticle. Then, a general superfield $\Phi \equiv \hat{\Phi}(x, \theta)$ is defined as an object consisting of fields that transform into each other via the following Lorentz transformation,

$$\delta\hat{\Phi} = i[\bar{\alpha}Q, \hat{\Phi}] = \left(-\bar{\alpha}\frac{\partial}{\partial\bar{\theta}} - i\bar{\alpha}\not{\partial}\theta \right)\hat{\Phi}, \quad (1.10)$$

where α are Majorana spinor parameters that characterize SUSY transformations and the bar on top refers to it being the conjugate spinor.

1.3.3 Minimal Supersymmetric Standard Model (MSSM)

With the machinery in hand, we can now extend the SM to include $N = 1$ SUSY in a way that solves the bulk of the issues plaguing the SM without introducing an intractable number of parameters. This can be achieved by building the Minimal Supersymmetric Standard Model (MSSM) where one takes the SM gauge group, $SU(3)_C \times SU(2)_L \times U(1)_Y$, elevates the SM gauge fields to gauge superfields and the fermion fields to chiral superfields, and chooses a *superpotential* to describe the interactions between the various chiral superfields in the theory before writing down the Lagrangian. Furthermore, in addition to promoting the SM higgs doublet to a doublet of left-chiral superfields that transforms as a $\mathbf{2}$ under $SU(2)_L$ and has weak hypercharge $Y = 1$,

$$\phi = \begin{pmatrix} \phi^+ \\ \phi^0 \end{pmatrix} \rightarrow \hat{H}_u = \begin{pmatrix} \hat{h}_u^+ \\ \hat{h}_u^0 \end{pmatrix}, \quad (1.11)$$

we need to introduce another Higgs doublet superfield,

$$\hat{H}_d = \begin{pmatrix} \hat{h}_d^- \\ \hat{h}_d^0 \end{pmatrix} \quad (1.12)$$

which transforms as a $\mathbf{2}^*$ under $SU(2)_L$ and has a weak hypercharge $Y = -1$. The need for the second Higgs doublet of the MSSM stems from the inability of the scalar component of \hat{h}_u^0 to give mass to the down-type quarks and charged leptons. This is because the superpotential, the source of Yukawa interactions between Higgs scalar component and matter fermions, allows only terms containing left-chiral superfields; to give mass to the down-type quarks and the charged leptons however, the scalar component of right-chiral superfield $\hat{h}_u^{0\dagger}$ is required. This requirement can only be fulfilled by introducing the second doublet which has the correct hypercharge and chirality. Also, the introduction of spin-1/2 higgsinos upsets the celebrated anomaly cancellation of the SM unless one introduces a second Higgs doublet with opposite quantum numbers. The matter and Higgs superfield content of the MSSM in a single generation is summarized in Table 1.2.

Field	$SU(3)_C$	$SU(2)_L$	$U(1)_Y$
$\hat{L} = \begin{pmatrix} \hat{\nu}_{eL} \\ \hat{e}_L \end{pmatrix}$	$\mathbf{1}$	$\mathbf{2}$	-1
\hat{E}^c	$\mathbf{1}$	$\mathbf{1}$	2
$\hat{Q} = \begin{pmatrix} \hat{u}_L \\ \hat{d}_L \end{pmatrix}$	$\mathbf{3}$	$\mathbf{2}$	1/3
\hat{U}^c	$\mathbf{3}^*$	$\mathbf{1}$	-4/3
\hat{D}^c	$\mathbf{3}^*$	$\mathbf{1}$	2/3
$\hat{H}_u = \begin{pmatrix} \hat{h}_u^+ \\ \hat{h}_u^0 \end{pmatrix}$	$\mathbf{1}$	$\mathbf{2}$	1
$\hat{H}_d = \begin{pmatrix} \hat{h}_d^- \\ \hat{h}_d^0 \end{pmatrix}$	$\mathbf{1}$	$\mathbf{2}^*$	-1

Table 1.2: Matter and Higgs superfield content of the MSSM in a single generation along with their gauge group properties.

With the matter and Higgs superfield framework, we are free to choose the superpotential term in the MSSM Lagrangian. In contrast to the SM Lagrangian, baryon and lepton number violating terms are allowed in the MSSM Lagrangian if such terms respect gauge invariance. However, presence of such terms in a theory that potentially describes the $4 - D$ world leads to a plethora of problems such as faster than observed proton decay. To avoid this, one requires all terms to respect R -parity defined as, $R = (-1)^{3(B-L)+2s}$, where s is the spin of the field while B and L are baryon and lepton numbers respectively. Thus, the MSSM superpotential is chosen to be [17],

$$\hat{W} = \mu \hat{H}_u^a \hat{H}_{da} + \sum_{i,j=1,3} [(\mathbf{f}_u)_{ij} \epsilon_{ab} \hat{Q}_i^a \hat{H}_u^b \hat{U}_j^c + (\mathbf{f}_d)_{ij} \hat{Q}_i^a \hat{H}_{da} \hat{D}_j^c + (\mathbf{f}_e)_{ij} \hat{L}_i^a \hat{H}_{da} \hat{E}_j^c], \quad (1.13)$$

where the a and b are $SU(2)$ doublet indices, ϵ_{ab} is the completely antisymmetric tensor and \mathbf{f} terms are the elements of 3×3 Yukawa coupling matrices with $i, j = 1 - 3$ indices corresponding to the various generations which, along with superpotential μ parameter, is generally complex. At this point we can write down a *globally* supersymmetric MSSM Lagrangian with unbroken $N = 1$ SUSY using a master formula used to calculate SUSY Lagrangians with gauge invariant terms, that can be read off Eq.(6.44) in [17]. To ensure proper EWSB as in the SM to give rise to massive W and Z bosons, it is sufficient to minimize the scalar potential of the MSSM Lagrangian in a way that leads to non-zero VEV's for the neutral fields i.e. $\langle h_u^0 \rangle \equiv v_u \neq 0$, $\langle h_d^0 \rangle \equiv v_d \neq 0$. Lastly, it must also be ensured that SUSY is properly broken, which will be discussed shortly.

1.3.4 Local SUSY/ Supergravity

Thus far in our discussion of supersymmetric theories we have implicitly assumed global SUSY i.e. theories wherein the SUSY transformation parameter α from Eq.(1.10) had no spacetime coordinate dependence. We can elevate a global symmetry to a local one if we consider spacetime dependent transformation parameters which in our case would mean $\alpha \equiv \alpha(x^\mu)$, giving rise to locally supersymmetric theories which are necessary since gravity is defined locally in GR. As with any local gauge theory, the method of invoking local SUSY transformation parameters necessarily introduces a corresponding gauge field to maintain the invariance of the SUSY Lagrangian. This gauge field is identified as the massless, spin-3/2 gravitino field which then is required to be paired with its massless bosonic superpartner, the spin-2 graviton field. Upon SUSY breaking at some energy scale, the gravitino acquires mass in a manner similar to the W and Z gauge bosons in the theory of weak interactions. As a result, since it necessarily brings a graviton into the spectrum, local SUSY is also known as *supergravity (SUGRA)*. However, it turns out that the gravitational coupling constant has dimensions of inverse mass and as such gives rise to non-renormalizable terms in the SUGRA Lagrangian. This means SUGRA cannot be the complete theory valid at all energies but rather can be understood as the low energy limit of a more fundamental theory with local SUSY, namely *superstring theory* which will be discussed in the next chapter.

1.3.5 SUSY Breaking

As has been discussed earlier, SUSY must be a broken symmetry in nature which necessitates there be a mechanism via which this occurs. Since in models with global SUSY, spontaneous SUSY breaking (SSB) is ruled out by experiments [18], it must be broken

explicitly by terms in the Lagrangian. Such SUSY breaking contributions are called F and/or D - breaking terms and an elaborate discussion can be found in [17]. It is necessary that any such terms that appear in the Lagrangian cause *soft* breaking of SUSY i.e. only logarithmic divergences are introduced into the calculations which ensures the stability of the observed Higgs mass. Since the exact mechanism is not known, one assumes the SUSY breaking occurs in a “hidden” sector and communicated to the “visible” sector via some mediating process. To that end, multiple SUSY breaking mediation mechanisms are promoted, each having unique features. Categorically, these are Gravity Mediated SUSY Breaking, Anomaly Mediated SUSY Breaking (AMSB), Gauge Mediated SUSY Breaking and Gaugino Mediated SUSY breaking. The latter two mechanisms can be all but ruled out while the others remain highly motivated.

For models with local SUSY, SSB is the most widely promoted mechanism in the literature. SUSY can be broken spontaneously, while retaining Poincaré symmetry, when either $\langle 0|F_i|0\rangle \neq 0$ or $\langle 0|D_A|0\rangle \neq 0$, i.e. when either the F or D -field attains a non-zero VEV. These two types of SSB is therefore called F -type SUSY breaking and D -type SUSY breaking respectively. It is well established that spontaneous breaking of a global symmetry leads to a massless Nambu-Goldstone boson corresponding to every symmetry generator that does not annihilate the ground state [19, 20]. In contrast, for local symmetries the Nambu-Goldstone boson is “eaten by the gauge fields” thereby becoming longitudinal components of a gauge field which then gain mass; this is the Higgs mechanism we alluded to in our discussion of EWSB in the SM. In case of global SUSY however, upon SSB the resultant Nambu-Goldstone mode is in fact a massless spin-1/2 fermion since the generator of SUSY transformations is a spin-1/2 spinor; the massless Nambu-Goldstone boson is then

called the *goldstino*. Upon invoking locality of SUSY transformations, the massless goldstino is absorbed by the gravitino which then becomes massive in a process aptly termed the *super-Higgs* mechanism.

Chapter 2

Discussion on String Theory

As has been discussed in the earlier chapter, quantizing gravity is a persistent issue plaguing the SM. Quantizing gravitational force requires a marriage between Einstein's general theory of relativity and conventional quantum field theory but any attempt at such a union results in non-renormalizable solutions, as briefly studied in Ref. [21]. String theory makes its grand entrance here by providing the proper tools to not only successfully quantize gravity but also as a UV-complete *theory of everything*. In its most basic form, string theory posits the existence of extremely tiny strings of order the Planck length to be the most fundamental objects in nature which can oscillate in various modes and these oscillations manifest themselves as the observed particles of a low energy *effective field theory* (EFT) such as the MSSM. Originally, string theory was formulated solely for bosons (bosonic string theory) [22] but was later extended to include fermions in the string spectrum by supersymmetrizing it. Such string theories with spacetime fermions alongside bosons are called *superstring theories* [23]. A crucial feature that makes superstring theory so attractive, besides the mathematical aesthetics, is that all superstring theories successfully manifest quantization of gravity via the emergence of a spin-2 *graviton* in the particle spectrum. It would seem like we have filled all the blanks in our incomplete understanding of how nature works at the fundamental level by replacing the existing SM framework by this appealing new string framework but alas superstring theories present their own set of challenges to be tackled. In this chapter we aim to address these issues semi-qualitatively, discuss potential solutions and present their compatibility with observable phenomena. Much of the following

discussion is summarized from [24] while other sources used for specific points are cited accordingly when needed.

2.1 Superstring Theories

From classical field theories we know that a point particle traces out a *worldline* as it propagates through spacetime. When the point particles are replaced by $1 - D$ strings, its trajectory is defined on a $(1 + 1) - D$ *worldsheet*. Thus the starting point of any string theory is to write down the worldsheet action propagating in D -dimensional Minkowski space. The corresponding bosonic string action with D scalar fields, known as the *Polyakov action*, is [25]

$$S_P = -\frac{1}{2\pi} \int d^2\sigma \partial^\alpha X^\mu \partial_\alpha X_\mu \quad (2.1)$$

defined in the *conformal gauge* such that $h_{\alpha\beta} \mapsto \eta_{\alpha\beta}$ where $h_{\alpha\beta}$ is the worldsheet metric and $\eta_{\alpha\beta}$ is the Minkowski spacetime metric. Additionally, X^μ with $\mu = 0, \dots, D - 1$ are the target spacetime coordinates, σ^α with $\alpha = 0, 1$ such that $\sigma^0 \equiv \tau$ and $\sigma^1 \equiv \sigma$ are the worldsheet coordinates, while we set the length parameter $\alpha' = 1/2$ and the string tension is $T = 1/\pi$. In order to include fermions in the string formalism, there are two known approaches that one can employ, namely *Ramond-Neveu-Schwarz (RNS)* formalism and *Green-Schwarz (GS)* formalism. RNS theory introduces fermions on the string worldsheet by incorporating worldsheet SUSY while in contrast, the GS theory is supersymmetric in $10 - D$ Minkowski spacetime. While the GS formalism may seem more appealing with manifestly spacetime SUSY, it loses manifest Lorentz covariance upon quantization in the light-cone gauge [24]. Moreover, it will be briefly shown shortly that the RNS worldsheet SUSY can be

projected to spacetime SUSY via a process known as *Gliozzi-Scherck-Olive* (GSO) projection [26]. Hence, we'll restrict our discussion to RNS superstrings. The bosonic action therefore can be extended to include worldsheet fermions according to the RNS formalism as [24],

$$S = S_P + S_F = -\frac{1}{2\pi} \int d^2\sigma \left(\partial^\alpha X^\mu \partial_\alpha X_\mu + \bar{\psi}^\mu \rho^\alpha \partial_\alpha \psi_\mu \right) \quad (2.2)$$

where S_F is the fermionic action, ρ^α are the 2-D Dirac matrices

$$\rho^0 = \begin{pmatrix} 0 & -1 \\ 1 & 0 \end{pmatrix} \quad \text{and} \quad \rho^1 = \begin{pmatrix} 0 & 1 \\ 1 & 0 \end{pmatrix},$$

that obey the Clifford algebra, $\{\rho^\alpha, \rho^\beta\} = 2\eta^{\alpha\beta}$, and ψ^μ is a Dirac spinor on the worldsheet with two independent components,

$$\psi^\mu \equiv \begin{pmatrix} \psi_-^\mu \\ \psi_+^\mu \end{pmatrix}$$

and correspondingly the Dirac conjugate is defined as,

$$\bar{\psi}^\mu = \psi^\dagger i\rho^0$$

These components are real such that we impose the following reality condition,

$$(\psi^\mu)^T C = (\psi^\mu)^\dagger i\rho^0 \quad (2.3)$$

where C is a 2×2 charge conjugation matrix so that we have Dirac spinors with real components which are called Majorana spinors. Thus, in the Majorana representation, the components of the spinor are real i.e,

$$(\psi_{\pm}^{\mu})^* = \psi_{\pm}^{\mu}.$$

We can then define the light-cone coordinates in terms of the worldsheet coordinates as,

$$\sigma^{\pm} = \tau \pm \sigma$$

$$\text{and, } \partial_{\pm} \equiv \frac{1}{2}(\partial_{\tau} \pm \partial_{\sigma})$$

which make the left-moving (ψ_{+}^{ν}) and right-moving (ψ_{-}^{μ}) parts of the string explicit in the string action. Therefore, the fermionic action then assumes the form,

$$S_F = \frac{i}{\pi} \int d^2\sigma \left(\psi_{-}^{\mu} \partial_{+} \psi_{-}^{\nu} + \psi_{+}^{\mu} \partial_{-} \psi_{+}^{\nu} \right) \eta_{\mu\nu} \quad (2.4)$$

from which one obtains the free-field Dirac equation in light-cone coordinates i.e.

$$\delta S_F = 0 \implies \partial_{+} \psi_{-}^{\mu} = 0 \quad \text{and} \quad \partial_{-} \psi_{+}^{\mu} = 0 \quad (2.5)$$

that respectively describes the left-moving and right-moving parts of the string. This then allows us to clearly specify the boundary conditions of the fermions for closed and open strings which can further be utilized to yield the oscillating superstring mode expansions which ultimately lead to the superstring spectra.

2.1.1 Global Worldsheet SUSY

Invoking SUSY requires the introduction of the SUSY transformation parameter ϵ ,

$$\epsilon = \begin{pmatrix} \epsilon_- \\ \epsilon_+ \end{pmatrix},$$

which is a two-component Majorana spinor with components ϵ_- and ϵ_+ that are necessarily real, infinitesimal and anti-commuting Grassman numbers. Moreover, since there is no spacetime dependence associated to ϵ , the transformations defined by this parameter is a global symmetry of the worldsheet. It can be shown that the combined bosonic and fermionic action given in Eq.(2.2) is invariant under the transformations,

$$\delta X^\mu = \bar{\epsilon} \psi^\mu, \tag{2.6}$$

$$\delta \psi^\mu = \rho^\alpha \partial_\alpha X^\mu \epsilon, \tag{2.7}$$

where, $\bar{\epsilon} = \epsilon^\dagger i \rho^0$ is the complex conjugated parameter. Note that the transformations defined in Eq.(2.6) and Eq.(2.7) mix bosonic and fermionic fields and hence describes a supersymmetric transformation, thereby justifying that the RNS action (Eq.(2.2)) indeed describes a superstring theory with global worldsheet SUSY. It is also useful to express the above transformation equations in terms of the individual spinor components as,

$$\delta X^\mu = i(\epsilon_+ \psi_-^\mu - \epsilon_- \psi_+^\mu), \tag{2.8}$$

$$\delta \psi_+^\mu = 2\partial_+ X^\mu \epsilon_-, \tag{2.9}$$

$$\delta\psi_-^\mu = -2\partial_- X^\mu \epsilon_+. \quad (2.10)$$

As is known from Noether's theorem, a global symmetry leads to a conserved current; in our case, this set of global worldsheet SUSY transformations lead to a conserved *supercurrent* (j_A^α with spinor index A) while translational symmetry of the RNS action leads to the conservation of the energy-momentum tensor $T_{\alpha\beta}$. These conserved currents of the theory gives rise to the super-Virasoro constraints or the mass-shell conditions in the RNS formalism and assumes the form [27],

$$\begin{aligned} T_{\pm\pm} &\equiv (\partial_\pm x)^2 + \frac{i}{2}\psi_\pm \cdot \partial_\pm \psi_\pm = 0 \\ j_\pm &\equiv \psi_\pm \cdot \partial_\pm = 0. \end{aligned} \quad (2.11)$$

2.1.2 Mode Expansions and Boundary Conditions

The next step in realizing the superstring spectrum is to derive the Fourier mode expansions from the equations of motion. A brief examination of the fermionic action Fourier modes and boundary conditions is sufficient since the full superstring spectrum consisting of both fermions and bosons can be built out of considering different boundary conditions for the fermionic part, as will be shown. Explicitly writing out the variation of S_F given in Eq.(2.4) yields the surface terms,

$$\delta S_F \sim \int d\tau (\psi_- \delta\psi_- - \psi_+ \delta\psi_+) |_{\sigma=\pi} - \int d\tau (\psi_- \delta\psi_- - \psi_+ \delta\psi_+) |_{\sigma=0}$$

that are required to vanish according to the action principle.

Open Strings The above requirement admits two possible boundary conditions at each boundary, $\sigma = 0$ and $\sigma = \pi$. At the boundary $\sigma = 0$ one can choose either of $\psi_+(\tau, 0) =$

$\pm\psi_-(\tau, 0)$ but the choice of sign is a matter of convention such that one can set,

$$\psi_+^\mu(\tau, 0) = \psi_-^\mu(\tau, 0). \quad (2.12)$$

At the boundary $\sigma = \pi$, periodicity and anti-periodicity of fermions become relevant which allows two possible choices such that the superstring state space breaks down to two subspaces namely, the Ramond (R) sector and Neveu-Schwarz (NS) sector respectively,

$$\psi_+^\mu(\tau, \pi) = \psi_-^\mu(\tau, \pi) \quad (\text{R}), \quad (2.13)$$

$$\psi_+^\mu(\tau, \pi) = -\psi_-^\mu(\tau, \pi) \quad (\text{NS}). \quad (2.14)$$

The R-sector boundary condition applies to periodic fermions while the NS-sector applies to anti-periodic fermions. These boundary conditions are implemented to realize the Fourier mode expansions of the general solutions to the Dirac equations (Eq. (2.5)) in the following manner.

- *R-sector*: Since in this sector we have periodic fermions, $\psi_\pm(\tau, \sigma)$ can be expanded in terms of integrally moded oscillators i.e.

$$\psi_-^\mu(\tau, \sigma) = \frac{1}{\sqrt{2}} \sum_{n \in \mathbb{Z}} d_n^\mu e^{-in(\tau-\sigma)}, \quad (2.15)$$

$$\psi_+^\mu(\tau, \sigma) = \frac{1}{\sqrt{2}} \sum_{n \in \mathbb{Z}} d_n^\mu e^{-in(\tau+\sigma)}, \quad (2.16)$$

where the Majorana condition restricts the mode expansions to be real and as such

we must have $d_{-n}^\mu = d_n^{\mu\dagger}$. The normalization constant is chosen for convenience in quantization.

- *NS-sector*: In contrast, the NS-sector include anti-periodic fermions and their anti-periodicity is ensured by carrying out the mode expansions in terms of fractional modes i.e.

$$\psi_-^\mu(\tau, \sigma) = \frac{1}{\sqrt{2}} \sum_{r \in \mathbb{Z} + 1/2} b_r^\mu e^{-ir(\tau - \sigma)}, \quad (2.17)$$

$$\psi_+^\mu(\tau, \sigma) = \frac{1}{\sqrt{2}} \sum_{r \in \mathbb{Z} + 1/2} b_r^\mu e^{-ir(\tau + \sigma)}. \quad (2.18)$$

As will be shown later, the open string R-sector will result in spacetime fermions while NS-sector will yield spacetime bosons.

Closed Strings When considering strings with two ends fixed, we again need to consider two periodicity conditions of the fermions,

$$\psi_\pm(\sigma) = \pm \psi_\pm(\sigma + \pi) \quad (2.19)$$

and either choice leads to vanishing of the surface terms in the variation of the fermionic action; the positive sign choice describes periodic boundary conditions (R) while negative sign choice describes anti-periodic boundary conditions (NS). Furthermore, it is possible to impose R or NS boundary conditions on the left-moving waves and the right-moving waves separately. As such for the mode expansions one can choose,

$$\psi_-^\mu(\tau, \sigma) = \sum_{n \in \mathbb{Z}} d_n^\mu e^{-2in(\tau - \sigma)} \quad \text{or} \quad \psi_-^\mu(\tau, \sigma) = \sum_{r \in \mathbb{Z} + 1/2} b_r^\mu e^{-2ir(\tau - \sigma)} \quad (2.20)$$

for the right-movers while for the left-movers one can choose,

$$\psi_+^\mu(\tau, \sigma) = \sum_{n \in \mathbb{Z}} \tilde{d}_n^\mu e^{-2in(\tau+\sigma)} \quad \text{or} \quad \psi_+^\mu(\tau, \sigma) = \sum_{r \in \mathbb{Z}+1/2} \tilde{b}_r^\mu e^{-2ir(\tau+\sigma)}. \quad (2.21)$$

Thus we can consider the cases when both right and left-movers are periodic (R-R), when both the right and left-movers are anti-periodic (NS-NS) or when they are a superposition of periodic and anti-periodic waves (R-NS or NS-R). As a result, there are four distinct closed string sectors wherein states in NS-NS and R-R sectors are spacetime-bosons and states in the NS-R and R-NS sectors are spacetime fermions.

2.1.3 Canonical Quantization of the RNS Superstring Theory

In this subsection we summarize the procedure of obtaining the quantum superstring spectrum. The mode expansion coefficients are elevated to operators and since they describe a fermionic theory, they obey the following anti-commutation relations,

$$\{b_r^\mu, b_s^\nu\} = \{\tilde{b}_r^\mu, \tilde{b}_s^\nu\} = \delta_{r,-s} \eta^{\mu\nu} \quad (2.22)$$

$$\{d_m^\mu, d_n^\nu\} = \{\tilde{d}_m^\mu, \tilde{d}_n^\nu\} = \delta_{m,-n} \eta^{\mu\nu} \quad (2.23)$$

and the other combinations all anticommute to 0 (all relations are in natural units wherein $\hbar = c = 1$). Since the spacetime metric appears in the above anticommutator algebra, its negative time component gives rise to ghost states; the RNS formalism is cured of these ghost states by imposing what are known as the super-Virasoro constraints which directly influence the number of spacetime dimensions required for theoretical consistency. Then we define

a ground state for each of R-sector and NS-sector denoted as, $|0\rangle_R$ and $|0\rangle_{NS}$ respectively. Following from convention, we choose the negative mode oscillators to be creation operators while the positive mode oscillators are annihilation operators; for instance d_{-1}, d_{-2}, \dots are creation operators and d_1, d_2, \dots are annihilation operators in the R-sector while analogously in the NS-sector we have $b_{-1/2}, b_{-3/2}, \dots$ as creation operators and $b_{1/2}, b_{3/2}, \dots$ as annihilation operators. Thus it follows that all positive mode oscillators annihilate the ground state in their respective sectors such that,

$$d_n^\mu |0, k\rangle_R = 0 \quad \text{for } n > 0,$$

$$b_r^\mu |0, k\rangle_{NS} = 0 \quad \text{for } r > 0.$$

The super-Virasoro constraints in Eq.(2.11) gives rise to a Lie superalgebra. The corresponding generators of the super-Virasoro algebra are constructed by adding the bosonic generator to the fermionic generator built out of the vanishing components of $T_{\alpha\beta}$ and j_A . Moreover, since the fermionic part is split into two sectors, the contributions to the super-Virasoro generators will also be different depending on whether one works in the R or NS-sector.

Open Strings In general for an open string, one super-Virasoro generator is given by,

$$L_m = \frac{1}{\pi} \int_{-\pi}^{\pi} d\sigma e^{im\sigma} T_{++} = L_m^{(b)} + L_m^{(f)} \quad (2.24)$$

where the contribution from the bosonic modes is,

$$L_m^{(b)} = \frac{1}{2} \sum_{n \in \mathbb{Z}} : \alpha_{-n} \cdot \alpha_{m+n} : \quad m \in \mathbb{Z}.$$

- *R-sector*: In the R-sector, the fermionic mode contribution to the super-Virasoro generator is,

$$L_m^{(f)} = \frac{1}{2} \sum_{n \in \mathbb{Z}} \left(n + \frac{m}{2}\right) : d_{-n} \cdot d_{m+n} : \quad m \in \mathbb{Z}, \quad (2.25)$$

while the modes of the supercurrent are,

$$F_m = \frac{\sqrt{2}}{\pi} \int_{-\pi}^{\pi} e^{im\sigma} j_+ = \sum_{n \in \mathbb{Z}} \alpha_{-n} \cdot d_{m+n}. \quad (2.26)$$

This leads to the following super-Virasoro algebraic relations in the R-sector,

$$[L_m, L_n] = (m - n)L_{m+n} + \frac{D}{8} m^3 \delta_{m,-n} \quad (2.27)$$

$$[L_m, F_n] = \left(\frac{m}{2} - n\right) F_{m+n} \quad (2.28)$$

$$\{F_m, F_n\} = 2L_{m+n} + \frac{D}{2} m^2 \delta_{m,-n}. \quad (2.29)$$

- *NS-Sector*: Similarly, in the NS-sector we have the following fermionic and supercurrent mode contributions respectively,

$$L_m^{(f)} = \frac{1}{2} \sum_{r \in \mathbb{Z} + 1/2} \left(r + \frac{m}{2}\right) : b_{-r} \cdot b_{m+r} : \quad m \in \mathbb{Z}, \quad (2.30)$$

$$G_r = \frac{\sqrt{2}}{\pi} \int_{-\pi}^{\pi} e^{ir\sigma} j_+ = \sum_{n \in \mathbb{Z}} \alpha_{-n} \cdot b_{r+n}. \quad (2.31)$$

Consequently, these generators form the following super-Virasoro algebra,

$$[L_m, L_n] = (m - n)L_{m+n} + \frac{D}{8} m(m^2 - 1) \delta_{m,-n} \quad (2.32)$$

$$[L_m, G_r] = \left(\frac{m}{2} - r\right) G_{m+r} \quad (2.33)$$

$$\{G_r, G_s\} = 2L_{r+s} + \frac{D}{2} \left(r^2 - \frac{1}{4}\right) \delta_{r,-s}. \quad (2.34)$$

One can derive the number of spacetime dimensions (also known as the *critical dimension*), D , and the normal ordering constant, a , that arises as a result of quantum operator ordering, using the above algebra in conjunction with physical state constraints in each sector. The physical state conditions are an extension from bosonic theory in that for the superstring case we now have to consider multiple generators and two separate sectors. Denoting the physical state to be $|\text{phys}\rangle$ we have the following physical state conditions in the R-sector,

$$\begin{aligned} L_m |\text{phys}\rangle_R &= 0 \quad m > 0, \\ F_n |\text{phys}\rangle_R &= 0, \quad n \geq 0, \\ (L_0 - a_R) |\text{phys}\rangle_R &= 0. \end{aligned} \quad (2.35)$$

Analogously, the NS-sector super-Virasoro constraints yield the following physical state conditions,

$$\begin{aligned} L_m |\text{phys}\rangle_{NS} &= 0 \quad m > 0, \\ G_r |\text{phys}\rangle_{NS} &= 0, \quad r > 0, \\ (L_0 - a_{NS}) |\text{phys}\rangle_{NS} &= 0. \end{aligned} \quad (2.36)$$

It turns out that the superstring critical dimension is

$$D = 10, \quad (2.37)$$

and the normal ordering constant is deduced to be different depending on what sector of the open string is being considered such that,

$$a = \begin{cases} 0 & \text{(R)} \\ \frac{1}{2} & \text{(NS)}. \end{cases} \quad (2.38)$$

Mass Spectrum We can further define the number operator, N , defined as,

$$N = \sum_{n=1}^{\infty} \alpha_{-n}^i \cdot \alpha_n^i + \sum_{r>0} r b_{-r}^i \cdot b_r^i, \quad (2.39)$$

which can be used to simplify the open string mass formula obtained from the last condition in Eq.(2.35) in the R-sector and Eq.(2.36) in the NS-sector.

Open String Spectra The mass formula for the open string is,

$$\alpha' M^2 = N - a \quad (2.40)$$

and this becomes,

$$\alpha' M^2 = N \quad \text{in the R-sector}, \quad (2.41)$$

$$\alpha' M^2 = N - \frac{1}{2} \quad \text{in the NS-sector}, \quad (2.42)$$

where we used Eq.(2.38) to substitute in the proper value for the normal ordering constant a .

We can then analyze the open string spectrum for the two sectors separately.

- *NS-sector*: As mentioned previously, the ground state is annihilated by all non-zero

oscillator modes and so it satisfies,

$$\begin{aligned}\alpha_n^i |0, k\rangle_{NS} &= b_r^i |0, k\rangle_{NS} = 0 \quad \forall n, r > 0, \\ \alpha_0^\mu |0, k\rangle_{NS} &= \sqrt{2\alpha'} k^\mu |0, k\rangle_{NS}.\end{aligned}\tag{2.43}$$

Using the mass formula on the ground state then yields,

$$\alpha' M^2 |0, k\rangle_{NS} = N |0, k\rangle_{NS} - \frac{1}{2} |0, k\rangle_{NS} = -\frac{1}{2} |0, k\rangle_{NS}$$

which implies that the NS ground state is tachyonic with mass $m = -\frac{1}{2\alpha'}$ and is identified as a non-degenerate bosonic ground state. The first excited state can be found by applying the creation operators, $b_{-1/2}^i$, on the ground state which raises the eigenvalue by a factor 1/2 and the other excited states follow consecutively from the first. Therefore, the first excited state in the NS-sector is,

$$(\alpha' M^2) b_{-1/2}^i |0, k\rangle_{NS} = b_{-1/2}^i |0, k\rangle_{NS} \left(-\frac{1}{2}\right) = \left(\frac{1}{2} - \frac{1}{2}\right) \left|\frac{1}{2}, k\right\rangle_{NS} = 0.$$

The first excited state describes 8 polarization modes of the massless photon field in 10 spacetime dimensions. Furthermore, all states in the NS-sector are spacetime bosons since they transform in appropriate irreducible representations of $SO(8)$ [27].

- *R-sector*: As before, the ground state is annihilated by the non-zero mode oscillators.

From the second condition in Eq.(2.35) we get the Dirac-Ramond equation,

$$\begin{aligned} \left(\alpha_0^i d_0^i + \sum_{n=1}^{\infty} (\alpha_{-n}^i d_n^i + d_{-n}^i \alpha_{-n}^i) \right) |0, k\rangle_R = 0 \\ \implies \Gamma_{\mu} k^{\mu} |0, k\rangle_R = 0, \end{aligned} \tag{2.44}$$

which is the massless Dirac equation in the momentum representation. The ground state however is degenerate since the zero mode oscillators satisfies the 10-D Dirac algebra and so we obtain a ground state which is a $Spin(9,1)$ spinor. Since Dirac matrix in 10-D is a 32×32 matrix, the ground state is thus a 32 component spinor. However, imposing Majorana and Weyl conditions simultaneously reduces the number of independent components to 8. As a result the R-sector ground state is a spinor in an irreducible $Spin(8)$ representation. The excited states can be obtained by acting on the ground state with α_{-n}^i or d_{-n}^i and since these operators are spacetime vectors acting on the spinor ground states, the resulting R-sector spectrum comprises of spacetime spinors [24].

Closed String Spectra Since the closed string can be thought of as a superposition of a left-moving and a right-moving open string, the closed string spectrum can be obtained by taking tensor products of left-movers and right-movers. In contrast to the open string case, one now need to consider four distinct sectors that was mentioned previously when discussing the boundary conditions for the closed string: R-R, NS-NS, NS-R and R-NS. Similar to the open string case in the NS-sector, the NS-NS sector of the closed string is plagued by the presence of a tachyon and here again the GSO projection can be implemented to remove the tachyonic ground state.

Therefore, we see that the NS-sector encompasses spacetime bosons while the R-sector is comprised entirely of spacetime fermions hinting at a possible spacetime unbroken SUSY between the two sectors. However, the NS-sector ground state is tachyonic which needs to be remedied before we can establish a consistent theory. Heuristically, this maybe done if we could shift the first excited state of the NS-sector to be its ground state which will then pair up with the corresponding fermionic degrees of freedom in the R-sector. This is carried out by implementing the GSO projection mentioned early in our discussion.

2.1.4 GSO Projection

One starts by defining a *G-parity* operator, which in the NS-sector is given by,

$$G = (-1)^{F_{NS}+1} = (-1)^{\sum_{r=1/2}^{\infty} b_{-r}^i b_r^i + 1} \quad (2.45)$$

where F denotes the number of b -oscillator excitations which corresponds to the worldsheet fermion number. Correspondingly in the R-sector the G-parity operator is given as,

$$G = \Gamma_{11}(-1)^{F_R} = \Gamma_{11}(-1)^{\sum_{n=1}^{\infty} d_{-n}^i d_n^i} \quad (2.46)$$

where $\Gamma_{11} = \Gamma_0 \Gamma_1 \dots \Gamma_9$ is the 10-D analogue of the 4-D γ_5 matrix and satisfies the relations,

$$(\Gamma_{11})^2 = 1 \quad \text{and} \quad \{\Gamma_{11}, \Gamma^\mu\} = 0.$$

Chirality of a spinor is determined by how the spinor transforms under the action of Γ_{11} such that spinors with positive chirality satisfy $\Gamma_{11}\psi = +\psi$ while spinors with negative chirality

satisfy $\Gamma_{11}\psi = -\psi$. Furthermore, we have the chirality projection operator,

$$P_{\pm} = \frac{1}{2}(1 \pm \Gamma_{11}) \quad (2.47)$$

that will be crucial to establish spacetime SUSY in the physical superstring spectrum.

Open String Case Imposing the GSO projection on the NS-sector states means projecting out the states with negative G-parity and keeping only those states with positive G-parity i.e. the states $|\text{phys}\rangle_{NS}$ that satisfies,

$$G|\text{phys}\rangle_{NS} = (-1)^{F_{NS}+1}|\text{phys}\rangle_{NS} = |\text{phys}\rangle_{NS}, \quad (2.48)$$

which is only true when F_{NS} is odd. Thus, in the NS-sector we keep the states with an odd number of b oscillators and project out those states with even F which includes the tachyonic ground state. This means that post GSO projection, the new ground state in the NS-sector is the first-excited state which is a massless boson and this matches up well with the ground state in R-sector which is a massless spinor. Thus, in the ground state we now have a massless boson with 8 physical polarizations attributed to the NS-sector and a massless Weyl-Majorana spinor with 8 physical polarizations as well; they form the $\mathbf{8}_v \oplus \mathbf{8}_s$ vector supermultiplet in the $D = 10, N = 1$ SUSY algebra [27]. The massive states also respect unbroken SUSY, as extensively shown in Ref. [24]. In the R-sector, one can project on states with positive or negative G -parity depending on the chirality of the spinor ground state.

Closed String Case As before, the NS-sector is rid of the tachyonic ground state by projecting onto states with a positive G -parity. Moreover, in the R-sector the GSO projection can be on states with either positive or negative G -parity depending on the chirality of the ground state but now there are essentially two strings to be accounted for, a left-mover and a right mover; this leads to two different superstring theories namely: *Type IIA* and *Type IIB* superstring theories. Type IIB theory consists of left and right-moving R-sector ground states having the same chirality, chosen to be positive, which implies the same G -parity of the two R-sectors. Since both left and right-movers have the same chirality, it admits a left-right asymmetry thereby making Type IIB theories chiral. Conversely then, the Type IIA theory has left and right-moving R-sector ground states with opposite chiralities and hence opposite G -parity which leads to it being a non-chiral theory. The resulting spectrum of the two theories are pretty similar with the difference between them being that the IIA theory has fermionic states with two different chiralities. In the massless spectrum of both theories, we have two Majorana-Weyl gravitinos and as a result the closed superstring sector is said to endow us with $N = 2$ supergravity. The massless closed superstring spectrum is summarized in the table below [27].

Sector	Boson / Fermion?	$SO(8)$ representation	Massless Fields
NS-NS	boson	$\mathbf{8}_v \otimes \mathbf{8}_v = \mathbf{35} \oplus \mathbf{28} \oplus \mathbf{1}$	$g_{\mu\nu}, B_{\mu\nu}, \Phi$
NS-R	fermion	$\mathbf{8}_v \otimes \mathbf{8}_s = \mathbf{8}_s \oplus \mathbf{56}_s$	ψ_μ, λ
R-NS	fermion	$\mathbf{8}_s \otimes \mathbf{8}_v = \mathbf{8}_s \oplus \mathbf{56}_s$	ψ'_μ, λ'
R-R	boson	$\mathbf{8}_s \otimes \mathbf{8}_s =$ p - forms	Ramond-Ramond fields

Table 2.1: The massless states of the closed superstring. The fields ψ_μ, ψ'_μ are identified as the spin- $\frac{3}{2}$ gravitino fields and λ, λ' as the spin- $\frac{1}{2}$ dilatino fields.

2.2 Types of Superstring Theories

We have briefly mentioned two types of superstring theories arising from the distinct GSO projection choice. In fact, there exists five consistent, perturbative superstring theories in ten spacetime dimensions that we briefly discuss for completeness.

- *Type II Superstrings:* As already mentioned, type II theories possess local $N = 2$ spacetime SUSY after GSO projection. Additionally, these theories are built off strings with oriented worldsheets such as a torus. Type II theories are split into IIA and IIB theories on account of their different GSO projection choices that result in distinct chiral structure of the two ground states.
- *Type I Superstrings:* Type I superstring theory can be obtained by invoking the worldsheet parity operator on Type IIB theory. The resulting effect of this operation is to yield a theory of unoriented strings because for any given string orientation the parity operator also retains the orientation-reversed state, unlike the IIB theory. Doing so removes one of the two gravitinos from the IIB spectrum such that we are left with a theory with $N = 1$ SUSY in ten dimensions which we term as Type I superstring theory.
- *Heterotic Strings:* Another consistent choice in implementing boundary conditions on closed string theory is to consider the left-moving sector separately to be bosonic and the right-moving sector to be fermionic or vice versa. This results in two $N = 1$ heterotic string theories namely, the $SO(32)$ heterotic string and the $E_8 \times E_8$ heterotic string.

Furthermore, the five theories discussed above are interrelated by various *dualities* and can be shown to be different limits of an underlying 11 – D theory known as *M-theory* [28].

Chapter 3

String Compactifications

In our discussion of superstring theory in the previous chapter, it was mentioned that consistent superstring theory frameworks necessitate the existence of 6 (or 7 for M-theory) spacetime dimensions in addition to the observed four. Thus, given string theory is the fundamental theory that describes our universe, one needs to explain the “hidden” dimensions. Therein enters the idea of *compactifications* which imply that the extra dimensions evade detection because they are curled up into extremely tiny undetectable volumes. The idea of extra compact dimensions is not new however, and was first postulated by Kaluza and Klein in the 1920’s in an attempt to unify electromagnetism with gravitation which required a fifth spacetime dimension [29, 30]. Later this idea was extended to include more compact dimensions and applied to string theory. Increasing the number of compact dimensions obviously introduces more nuanced geometrical and topological complexities which means that any discussion on compactifications can quite easily become highly technical. Since our main results rely only on the phenomenology of string theory and string compactifications, the purpose of this section will be to provide the big picture behind the idea in a qualitative manner with no pretence of completeness or mathematical rigour.

3.1 The General Construct

In superstring theories, a geometric solution requires a $10 - D$ spacetime \mathcal{M}_{10} , that includes the usual $4 - D$ spacetime \mathcal{M}_4 and the extra spatial dimensions compactified on a

six-manifold X_6 , which can be expressed as,

$$\mathcal{M}_{10} = \mathcal{M}_4 \times X_6.$$

The best understood string solutions are those configurations for which the compact manifold X_6 is a Calabi-Yau *threefold* having 3 complex dimensions with unbroken SUSY on \mathcal{M}_4 . Additionally, one imposes the Ricci-flatness condition i.e. the CY manifold has locally zero curvature. This restriction is phenomenologically well-motivated for a number of reasons; one, a non-zero curvature introduces internal stress-energy contributions which lead to non-vacuum solutions. Secondly, a negative curvature seem to violate positive energy requirement [31] while a positive Ricci curvature results in a negative cosmological constant Λ_{cc} [32] which is a direct contradiction to observation. Thus, a Ricci flat CY threefold is the only choice that leads to interesting solutions with either $N = 1$ or $N = 2$ unbroken SUSY on \mathcal{M}_4 , depending on which of the five superstring theories one decides to start with. While, non-SUSY preserving solutions have been proposed [33], such solutions run into instabilities thereby resulting in complications to build a consistent low-energy EFT with the SM gauge group and its matter content. An interesting low-energy EFT must result in a $4 - D$ theory with unified gravity which can be extended to include the SM from a single theory with zero free parameters.

3.2 Moduli Stabilization

Even after choosing the most promising compactification manifold with intrinsic properties as described in the previous section, one is left with another problem that is a generic feature

of any theory built on the original Kaluza-Klein (KK) idea of extra dimensions. In the KK construct, general relativity (GR) is extended to five dimensions by taking a $5 - D$ metric tensor $g_{\mu\nu}$ depending on the corresponding $5 - D$ indices $\mu = 0, 1, 2, 3, 4$ with the extra dimension compactified on a circle of radius R . Such an extension of GR leads to an unrealistic $5 - D$ Minkowski spacetime as a solution but also includes other solutions due to the extra degrees of freedom $g_{\mu 5}$ introduced in the metric tensor. The components of the metric tensor are recognized as massless scalar fields in $4 - D$ which can lead to new long-range forces or time-dependent parameters [34]; such phenomena are ruled out by observation. Such massless scalar fields are termed as *moduli* and not only do these persist in more robust higher dimensional compactifications of superstring theories, typical superstring solutions generally introduce hundreds or thousands of moduli. Moreover, in interacting string theory, the coupling strength between strings is characterized by another massless scalar field called the *dilaton*. Thus, in the superstring framework there is a proliferation of these unobserved massless scalar fields and a long-standing issue in string phenomenology, known as the *moduli stabilization problem*, is to develop mechanisms via which these can become massive by gaining non-zero VEV's. The VEV's of the moduli then determine many properties of the low-energy EFT such as coupling constants and scale of the SUSY breaking.

3.2.1 Promising Solutions to the Moduli Stabilization Problem

In chapter 2 we discussed at length how SUSY, if in fact present in nature, must be broken at an energy scale above observational limits. In the context of superstring theories, a realistic model breaks $4 - D$ SUSY at some scale $m_{SUSY} \geq 1$ TeV. A possible solution to the moduli problem proposes that following breaking of supersymmetry, the moduli may gain

mass of order $m \sim \left(\frac{m_{SUSY}}{M_P}\right)m_{SUSY}$ where M_P is the Planck mass. This leads to very light moduli however leading to the Polonyi problem [35] in cosmology wherein such light moduli in the early universe results in *overclosure* [36, 37]. Therefore, any realistic mechanism that is touted to solve the moduli problem need not only generate massive scalar fields but must also respect cosmological constraints on how light these fields can be.

Flux Compactifications A particularly promising moduli stabilization mechanism arises in Type IIB theory from the existence of generalized background magnetic fields in the extra dimensions called *flux*. To investigate solutions in string theory, one needs to first decide on a possible CY 3-fold from a choice of thousands of topologically distinct ones. Having chosen a CY 3-fold topology (for instance, a hollow donut with one or multiple holes), one may thread the manifold with units of magnetic flux lines, as in Figure 3.1. Similar to magnetic flux

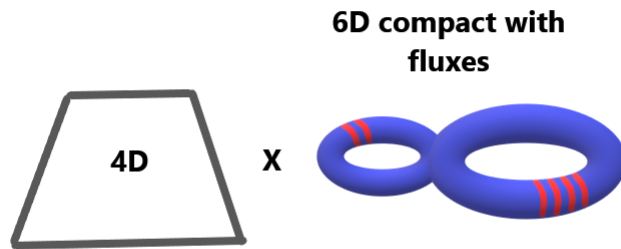


Figure 3.1: An example of a compact topology with fluxes shown in red.

through a solenoid, this flux contributes positive energy to the effective potential V_{eff} , which contain all classical and quantum contributions to the total potential energy. Introduction of fluxes therefore allows the moduli to have a non trivial scalar potential paving the way

for them to become massive. However, Einstein equations impose severe constraints on the existence of fluxes in compact manifolds and in fact non-vanishing fluxes violate the Einstein equations in $10 - D$ leading to well-known no-go theorems [38]. This can be understood semi-technically by looking at the following ansatz for vacuum configurations [39],

$$ds^2 = g_{\mu\nu} dx^\mu dx^\nu + g_{IJ} dy^I d\bar{y}^J \quad (3.1)$$

where $g_{\mu\nu}, x$ and g_{IJ}, y, \bar{y} are the metrics and coordinates of the $4 - D$ Minkowski spacetime and the internal CY manifold respectively. Including fluxes modifies the measure as,

$$ds^2 = e^{2A(y)} g_{\mu\nu} dx^\mu dx^\nu + e^{-2A(y)} g_{IJ} dy^I d\bar{y}^J. \quad (3.2)$$

where $A(y)$ is termed as the *warp* factor. The no-go theorem forbids any non-trivial warp factors and hence would rule out warped compactifications in string theory. This was a big stumbling block that hindered progress of building a realistic superstring compactification until Polchinski's discovery of higher dimensional objects called *D-branes* [40]. These objects can be thought of as hyperplanes with p -dimensions satisfying Dirichlet boundary conditions as depicted in Figure 3.2. The Dp -branes serve as local sources of the fluxes as they can carry gauge and matter fields and also make positive contributions to V_{eff} . One need further incorporate non-dynamical objects with negative energy contribution to V_{eff} to counteract the positive energy contributions from the Dp -branes and flux units. These are known as *orientifold planes* or more generally Op -planes where p is taken in analogy to dimensions of the branes. To summarize, inclusion of Op -planes in addition to Dp -branes allow us to

augment the compact dimensions with p -form fluxes that originate as p -form fields in the NS-NS and R-R sectors of superstring theories, while obeying Einstein equations of gravity in $10 - D$.

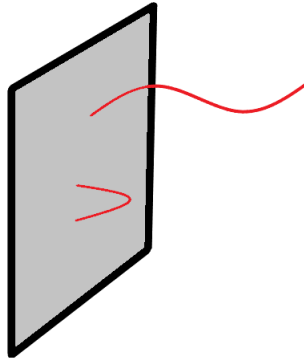


Figure 3.2: A D2-brane with a string with one-end attached to it and another string with both ends attached to it.

The presence of fluxes, branes and Op -planes deform the background metric on the CY manifold. Such deformations are allowed as long as they still preserve SUSY and the topology and obey the Ricci flatness condition. The moduli parameterize changes of size and shape of the CY manifold without changing its topology. This yields two types of moduli fields namely, the *complex structure* moduli related to changes in shape of the manifold, U^α , and the *Kähler structure* moduli related to the size or volume changes of the manifold, T^β . The complex structure and the dilaton moduli are fixed by choice of fluxes and gain masses of order the Kaluza-Klein (KK) scale, $m_{KK} \sim 10^{17}$ GeV, but the Kähler moduli are not. Currently, the best understood Kähler moduli stabilization methods that yield realistic solutions and roughly reproduce the SM in the low energy limit is in the context of Type IIB superstring theory on a CY 3-fold with fluxes and branes that results in models with $N = 1$ SUSY. Two noteworthy stabilization approaches based on this are:

- **KKLT:** This mechanism, proposed in the seminal paper by Kachru-Kallosh-Linde-Trivedi [41], achieves moduli stabilization by considering all non-perturbative contributions to the superpotential in the presence of 3-form fluxes and D-branes. In their construct all Kähler moduli are stabilized via such non-perturbative superpotential contributions that generate scalar potentials for the moduli and results in a supersymmetric AdS vacuum with a negative cosmological constant. However, they go on to show that via introduction of anti-D3-branes on a CY O3/O7-plane one is able to break SUSY and also lift the cosmological constant to be small and positive, thus yielding a metastable dS vacuum with broken SUSY.
- **LVS:** LVS refers to the *Large Volume Scenario* that achieves moduli stabilization by considering both perturbative corrections to the Kähler (or scalar) potential along with the non-perturbative corrections to the superpotential. In this construct, one assumes the volume of the compactification manifold to be exponentially large such that the leading string scale corrections in α' to the Kähler potential in perturbation theory compete against non-perturbative superpotential terms. Following this approach one ends up with a non-supersymmetric AdS vacuum unlike in KKLT. However, one can lift this to a dS vacuum depending on the SUSY breaking mechanism in other sectors of the theory characterized by anti-branes and O_p -planes as before.

We will analyze both of these phenomenologically later in the dissertation.

3.2.2 Vacuum Multiplicity

Even after appropriate moduli stabilization via flux compactifications that potentially

leads to low-energy theories roughly resembling the SM, one is left wondering if there exists any one particular vacuum solution that would explain observable phenomena. The answer would be a negative since there is no unique choice of CY manifold, nor is there any unique number of fluxes that one can incorporate to reproduce the one true low-energy theory. Rather, a huge number of distinct topological and geometric choices may lead to a plethora of consistent solutions. This vacuum multiplicity was problematic since it could lead one to believe that the predictability of string theory with regards to testable observations is highly speculative. However, this issue can be resolved by employing statistical methods based on Weinberg's anthropic arguments, pioneered by Bousso & Polchinski [42], Douglas [43] and others.

The configuration space containing all possible string compactifications that result in a discretuum of vacua was termed the *string theory landscape* [44]. The number of vacuum solutions in the landscape is enormous with the estimated number ranging from $N_{vac} \sim 10^{500} - 10^{272000}$. These ingredients are sufficient to implement Weinberg's anthropic solution to the cosmological constant [45, 46]. In this scenario, it is envisaged that Λ_{cc} scans uniformly on the landscape and can assume a multitude of values which then may lead to various *pocket universes* in an eternally inflating *multiverse*; however, only those pocket universes with strictly positive and tiny Λ_{cc} are hospitable to galaxy condensation and therefore can lead to observers like us. This idea will serve as the cornerstone of this dissertation and we will henceforth discuss comprehensive phenomenological implications of the string landscape with regards to particle physics and cosmology.

Chapter 4

Naturalness and the Anthropic Landscape

Naturalness has served as a guiding principle in the exploration of physics beyond the SM. In fact, it has been successfully implemented in critical new discoveries in particle physics, notably when Gaillard and Lee [47] used naturalness notions to predict the mass of the charm quark to a precision of $m_c \sim 1.5 \pm 0.5$ GeV before its eventual discovery. Since then, naturalness has also enjoyed considerable success in explaining new physics, for instance the realization that the smallness of the electron mass arises from chiral symmetry of the Dirac Lagrangian [48]. Following this discovery, 't Hooft famously defined (technical) naturalness as: *a quantity is allowed to be small ($\mathcal{O}(1)$) only if there is an enhancement in symmetry of the underlying theory as the quantity tends to zero* [49]. 't Hooft's notion also helps to understand why the proton mass does not blow up to the Planck scale since the smallness of the proton mass results in an enhancement of *conformal* symmetry in QCD [48]. However, as discussed in chapter 1, for the Higgs mass to be stabilized at its measured value, one needs to tune the Higgs mass parameters to huge opposite sign numbers to cancel out the divergent contributions. There is no reason for such fine-tuning to ensure the smallness of the Higgs mass as compared to m_P since there is no resulting enhancement of symmetry in the SM, therefore 't Hooft's notion fails in this instance. Even stronger challenges to naturalness come from Weinberg's anthropic principle [45] which points to an *environmental selection* of parameters rather than them being determined from an underlying theory such that Λ_{cc} would appear to be fine-tuned to a value just right to support life. Similar reasoning holds in analyzing the string theory landscape of vacua that arise from flux compactifications as

studied in the previous chapter. Thus it may seem that naturalness has reached an impasse and maybe nature is indeed fine-tuned. In this chapter, we will study how the string landscape coupled with anthropics lead to a more nuanced notion of naturalness.

4.1 Anthropic Resolution of the Cosmological Constant Problem

The cosmological constant, Λ_{cc} , appears in the Einstein's field equation of GR,

$$R_{\mu\nu} - \frac{1}{2}Rg_{\mu\nu} + \Lambda_{cc}g_{\mu\nu} = 8\pi GT_{\mu\nu} \quad (4.1)$$

but its value is ambiguous and cannot be attributed to any fundamental construct of the theory. Einstein famously referred to it as his “greatest blunder” since the magnitude of Λ_{cc} needed to be artificially tuned and substituted into Eq.(4.1) to yield a static universe. In fact, it was later observed by Hubble that the universe was not static but rather seemed to be expanding outwards which seemed to suggest $\Lambda_{cc} = 0$ for an expanding, homogeneous and flat universe devoid of matter i.e. $T_{\mu\nu} = 0$ (Einstein - de Sitter universe). However, a vanishing Λ_{cc} term was unsettling because $T_{\mu\nu}$ contributes to the energy density of vacuum and as such behaves as a cosmological constant [46]. As we have mentioned earlier, observational bounds indicate that $\Lambda_{cc} \simeq 10^{-122}m_P^2$ which, although small, is importantly non-zero. In contrast, if one assumes that GR is correct all the way up to the Planck scale and include quantum loop contributions to the vacuum energy then, $\Lambda_{cc} \simeq m_P^2$ in astonishing disagreement between theory and experiment. To avert this crisis, Weinberg in his seminal paper [45] made one of the great predictions of the 20th century: *given a multiverse which includes a vast assortment of pocket-universes (PU) with varying cosmological constants, then it may not be surprising*

to find $\Lambda_{cc} \sim 10^{-122} m_P^2$ since if it was much bigger, then galaxy condensation would not occur and we would not even be here to discuss the issue. This is known as Weinberg's structure principle and using such reasoning he was able to successfully calculate the value of Λ_{cc} to within a factor of a few nearly a decade before it was experimentally measured. Weinberg argued that Λ_{cc} should scan over the decades uniformly on a logarithmic scale and it should be as big as possible subject to the constraint that observers exist to measure it, as depicted in Figure 4.1 [3].

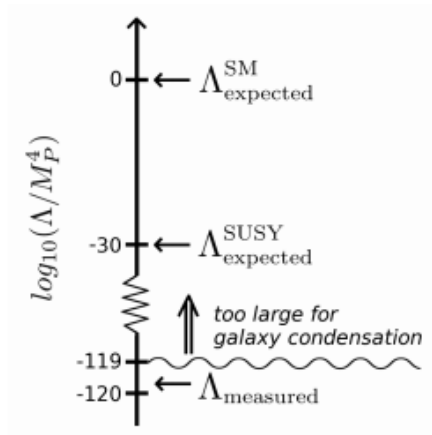


Figure 4.1: Distribution of Λ_{cc} on a log scale.

Weinberg's idea of an eternally inflating multiverse containing $\gg 10^{120}$ PU's, each with its unique value of Λ_{cc} , implies that our universe (OU) is a PU in this huge ensemble of bubble universes with its unique laws of physics. This construct, as identified by Bousso and Polchinski in their remarkable paper in 2000 [42], naturally aligns with the landscape of vacua that emerges upon flux compactifications in string theory. In the discretuum of string flux vacua, each *metastable* minimum of the string theory scalar potential would have a different value of Λ_{cc} , different $4 - D$ laws of physics and perhaps even different spacetime dimensions. The vacua are termed as metastable due to their non-zero probability to randomly quantum

tunnel to another vacua, a process that can happen over and over again. The tunneling

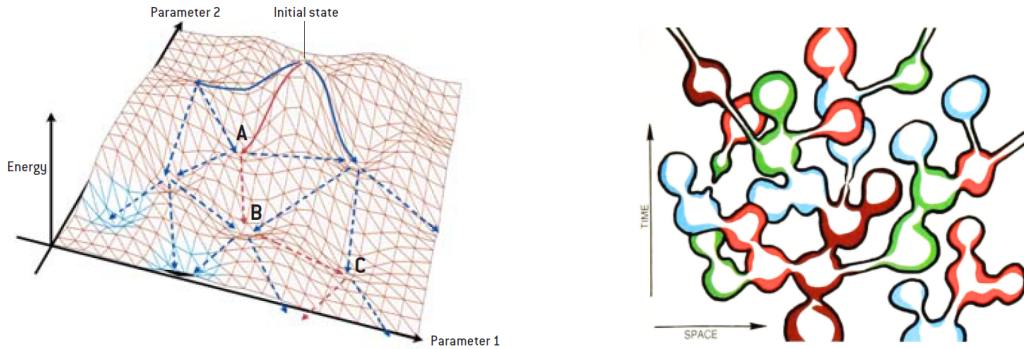


Figure 4.2: (a) Simplified depiction of a landscape with local minima identified as valleys and initial state identified by hills. Any state can tunnel to any local minima infinitely many times. [50] (b) Colored bubbles correspond to different universes which may have had shared origins from decay of parent universes. Our local universe is a tiny portion of this complex global multiverse. [51]

process can be visualized as shown in Figure 4.2 frame (a) that depicts a simplified $2 - D$ landscape of hills and valleys (local minima): any vacua can start at a hill and randomly tunnel to a valley with lower energy which can again tunnel to another even lower valley and so on. There is even a non-zero probability to tunnel from a lower valley to a higher one. This process can occur at different regions of the landscape simultaneously with each tunneling following a different path to a lower vacuum which implies that all possible valleys are visited. This means that all possible Λ_{cc} values are sampled from $\mathcal{O}(1) \sim +\Lambda_P$ (at the highest hills) to $-\Lambda_P$ (say, at the bottom of the sea) where the label P is identified with Planck energy, resulting in a highly dense distribution of possible vacuum energies. As a result, in a landscape of $\sim 10^{500}$ flux vacua, only a small fraction of the total vacua will have $\Lambda_{cc} \sim 0 - 10^{-120}\Lambda_P$ which explains how such small vacuum energy values come about [50]. On the other hand, if the universe had $\Lambda_{cc} < 0$, it would lead to a ‘big crunch’ and this can

be seen by considering the Friedmann equation in units of $c = 1$,

$$\left(\frac{\dot{R}}{R}\right)^2 = \frac{8\pi G\rho}{3} - \frac{k}{R^2} + \frac{\Lambda_{cc}}{3} \quad (4.2)$$

where R is the Friedmann-Robertson-Walker (FRW) scale factor, ρ is the matter density, k describes the curvature of space, while Λ is the cosmological constant. The solutions to this equation can be viewed as in the Figure 4.3 from which we notice the impact of the different values for the cosmological constant term. Therefore, it should not be surprising if many of the

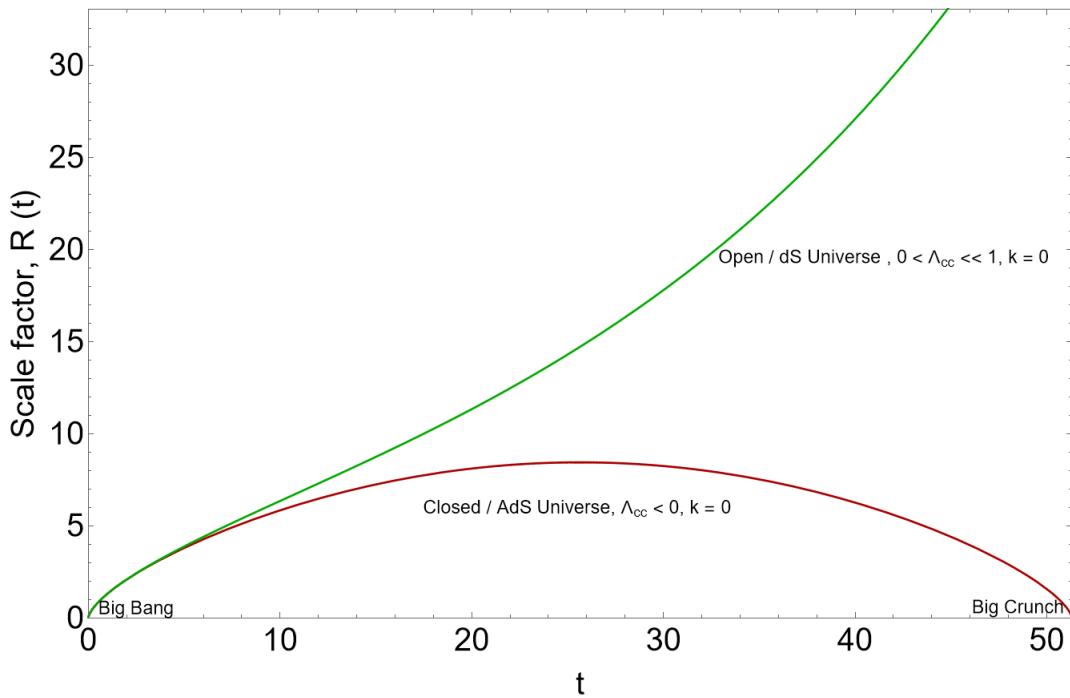


Figure 4.3: Solutions to the Friedmann equation for different values of Λ_{cc} .

constants of nature take on environmentally determined values rather than being determined by fundamental underlying principles. In the context of our observed $4 - D$ universe then, we find ourselves in a fertile patch of the string landscape of vacua that is anthropically favored on account of a small positive Λ_{cc} which allows structure formation necessary for life

as we know it. Thus, each anthropically favored flux vacua then corresponds to a habitable PU in the multiverse, remaining oblivious to the existence of the others in the ensemble. However, each PU can decay to form daughter universes while itself undergoing eternal expansion, as shown in Figure 4.2 frame (b). The expansion and decay rate is determined by the value of the vacuum energy Λ_{cc} and too large of a value would lead to extremely vigorous expansion inhospitable to structure formation while a negative value would lead to a big crunch with the universe collapsing onto itself [50], as can be seen by the red curve in Figure 4.3. This implies that PU's can go in and out of existence in many different places in the multiverse analogous to an initial state flux vacuum tunneling through to different vacua in the landscape. Thus, an observer in a PU similar to ours will find the universe to be expanding facilitated by a small positive value of Λ_{cc} which acts like an *anti-gravity* source that counters the gravitational attraction of baryonic matter and causes the visible dimensions to accelerate outwards. Consequently, Λ_{cc} is identified as the source of the mysterious *dark energy* which constitute $\sim 68\%$ of the visible universe according to observations. Thus, Weinberg's anthropic view serves multiple purposes: it is the only compelling explanation for the observed value of Λ_{cc} available while successfully merging with the landscape of flux vacua in string theory enabling a predictive framework to emerge, as will be shown shortly. Moreover, it also culminates in the only plausible framework to explain the observed dark energy content in cosmology.

4.2 Anthropic Origin of the Weak-Scale

One of the most attractive features of $10 - D$ string theory is the existence of one length

scale i.e. the string scale $l_s \sim l_P$, where l_P is the Planck length. Associated to the length scale is the mass scale, $m_s = 1/l_s$. This is the scale at which quantum gravitational effects become noticeable. Observation tells us that the weak-scale is, however, very much smaller than the Planck or string scale $M_P \simeq 10^{19}$ GeV $\gg m_{weak} \sim m_{W,Z,h} \simeq 100$ GeV and this astonishing hierarchy is termed as the BHP of the SM, as discussed earlier in Chapter 1. Agrawal, Donoghue *et.al* [52, 53] applied anthropic arguments similar to what Weinberg did for the cosmological constant, to address this issue. Based on nuclear physics calculations, they observed that in order for complex nuclei to form and hence for atoms to exist, which are necessary for life as we know it to emerge, the weak-scale magnitude should not be too much bigger than what we measure it to be. This is known as the atomic principle. As such, they identified a narrow range of allowed weak-scale values that are hospitable to atom formation, which we would refer to as the *ABDS window*, and lead to habitable pocket universes in the multiverse. From their calculation, the ABDS window extends roughly from $m_{weak}^{PU} \sim 0.5m_{weak}^{OU} - (2 - 5)m_{weak}^{OU}$ with m_{weak}^{OU} being the measured value of the weak-scale in our universe; the ABDS window is shown in the Figure 4.4. If $m_{weak}^{PU} \gtrsim (2 - 5)m_{weak}^{OU}$, then

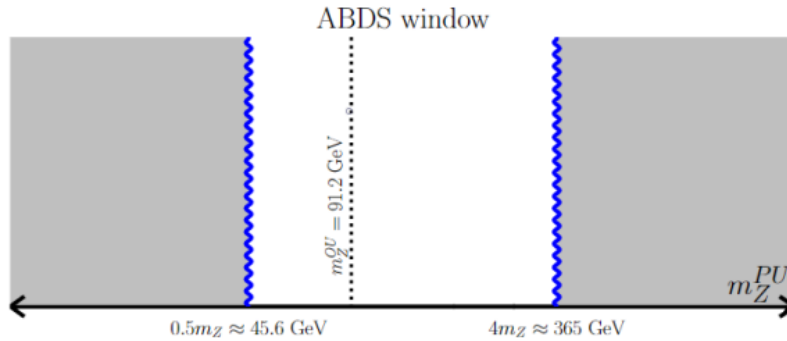


Figure 4.4: A simplified picture of the ABDS window [54]. Any habitable PU must have m_{weak} located within this window as required by the atomic principle.

the up-down quark mass hierarchy would be so large that neutrons will no longer be stable

within nuclei. Consequently, the Coulomb repulsion would dominate rendering formation of multi-proton nuclei impossible, thereby leading to a chemically sterile universe with only single-proton states [54]. We will see how this anthropic notion plays a crucial role in the phenomenological study of the string landscape in the following section.

4.3 Naturalness Re-examined

We have motivated the existence of a string theory landscape of vacua resulting from appropriate flux compactification of Type IIB superstring theory and discussed how an anthropic selection of parameters like Λ_{cc} seem inevitable. The next logical question one needs to ask is how can the string landscape framework lead to testable predictions and is naturalness still a valid argument? Since Type IIB superstring theory exhibits $N = 1$ SUSY that is broken at some scale in the hidden sector, one inevitably is led to search for supersymmetric particles. While non-supersymmetric constructs are possible, it has been argued that such vacua likely give rise to *Witten bubble of nothing* instabilities [55]. Thus far however, supersymmetric particles have evaded detection at the Large Hadron Collider (LHC) or at Dark matter direct detection experiments [56] leading many to abandon SUSY altogether. In fact current search limits from LHC Run 2 has pushed the gluino masses as high as $m_{\tilde{g}} \gtrsim 2.25$ TeV while the top-squark masses are expected to be $m_{\tilde{t}_1} \gtrsim 1.1$ TeV. More worrisome signals come from the supposed failure of naturalness which has conventionally predicted sparticles around the weak-scale with $m_{\tilde{g}} \lesssim 0.4$ TeV [57, 58, 59, 60]. This seemingly implies that the soft SUSY breaking scale, m_{soft} , lie in the multi-TeV range, far removed from the weak-scale. Thus, one ends up with a *Little Hierarchy Problem* (LHP) [61]: why

does the weak-scale not blow up to the energy scale associated with soft SUSY breaking i.e. why is $m_{weak} \ll m_{soft}$? In this section we contextualize the naturalness notion in light of the discovery of the string landscape of vacua and argue that the pessimism surrounding SUSY mainly stem from misleading naturalness measures. The following discussion is derived from two of our published work which can be found in Ref.[2, 54]. Before getting into the main aspects of the discussion however, it is instructive to briefly elucidate the salient features of two gravity-mediated SUSY models on which the rest of the chapter heavily relies on.

4.3.1 CMSSM / mSUGRA and NUHM n models

CMSSM / mSUGRA: CMSSM is an abbreviation of *Constrained* MSSM and is the simplest class of models with SUSY breaking effects in the hidden sector communicated to the observable sector via gravity mediation. This framework is built on the hypothesis of *universality* which implies all soft SUSY breaking terms have mass degeneracy at the GUT scale, $m_{GUT} \simeq 2 \times 10^{16}$ GeV. Universality of scalar masses can be obtained by choosing a flat Kähler metric while universal gaugino masses may arise due to grand unification of gauge interactions at m_{GUT} [17]. Universality then implies,

$$m_0^2 \equiv m_{Q_i}^2 = m_{U_i}^2 = m_{D_i}^2 = m_{L_i}^2 = m_{E_i}^2 = m_{H_u}^2 = m_{H_d}^2, \quad (\text{scalar masses})$$

$$m_{1/2} \equiv M_1 = M_2 = M_3, \quad (\text{gaugino masses})$$

$$A_0 \equiv A_t = A_b = A_\tau \quad (\text{trilinear scalar coupling terms})$$

$$g_{GUT} \equiv g_1 = g_2 = g_3 \quad (\text{gauge couplings}).$$

Further, it is phenomenologically advantageous to replace the high-scale soft SUSY breaking

B -parameter from the MSSM RGE's with $\tan\beta \equiv \frac{v_u}{v_d}$ is the ratio of the Higgs VEV's. Additionally, the magnitude of the superpotential μ term is fixed by REWSB effects but not its sign and thus the CMSSM parameter space is completely characterized by the parameter set [17],

$$m_0, m_{1/2}, A_0, \tan\beta, \text{sign}(\mu). \quad (4.3)$$

NUHMn: The universality hypothesis for soft SUSY breaking scalar mass, m_0 , is phenomenologically motivated for matter scalars due to the fact that such universality notion guarantees suppression of flavor changing neutral currents (FCNCs) via a super Glashow-Iliopoulos -Maiani (GIM) mechanism [62]. However, this is not quite true for the case of the Higgs scalars in that there is no such motivation for these to have common GUT scale mass m_0 . In fact, for the case of SUSY $SO(10)$ GUTs, which are highly motivated from increasing evidence for non-zero neutrino masses, the matter multiplets of each of the three generations live in the $16 - D$ spinorial representation of $SO(10)$ with a singlet neutrino superfield while the Higgs multiplets belong to one $10 - D$ fundamental representation which imply unrelated masses. Thus, we dub these models as *Non-universal Higgs Model* (NUHM). In the simplest scenario, one assumes $m_{H_u}^2 = m_{H_d}^2 \neq m_0^2$ such that this is a one parameter extension from the CMSSM model and is so known as NUHM1 model [63] which is completely defined by the parameter set,

$$m_0, m_\phi, m_{1/2}, A_0, \tan\beta, \text{sign}(\mu), \quad (4.4)$$

where $m_\phi = \text{sign}(m_{H_u, d}^2) \cdot \sqrt{|m_{H_u, d}^2|}$. The more general NUHM2 model, that we will extensively use for our phenomenological studies, has two independent mass parameters for the MSSM Higgs scalars i.e. $m_{H_u}^2 \neq m_{H_d}^2$. Furthermore, another generalization of this framework

is the NUHM3 model wherein the third generation matter scalars are split from the first and second generations i.e. $m_0(3) \neq m_{1,2}$. For phenomenological studies, typically the high scale parameters m_{H_u} and m_{H_d} are traded for weak-scale parameters μ and the pseudoscalar Higgs mass, m_A . As such, the NUHM2 model parameter space is fully characterized by,

$$m_0, m_{1/2}, A_0, \tan \beta, \mu, m_A. \quad (4.5)$$

and the parameter space for NUHM3 is completely specified by [64, 65, 66, 67, 67, 68, 69],

$$m_0(1,2), m_0(3), m_{1/2}, A_0, \tan \beta, \mu, m_A. \quad (4.6)$$

4.3.2 Practical Naturalness Measures

Traditionally, upper bounds on sparticle masses derived from naturalness were computed using the EENZ/BG log-derivative measure [57, 58]: for an observable \mathcal{O} ,

$$\Delta_{BG}(\mathcal{O}) \equiv \max_i \left| \frac{\partial \log \mathcal{O}}{\partial \log p_i} \right| = \max_i \left| \frac{p_i}{\mathcal{O}} \frac{\partial \mathcal{O}}{\partial p_i} \right| \quad (4.7)$$

where the p_i are fundamental parameters of the underlying theory. For an observable depending linearly on model parameters, $\mathcal{O} = a_1 p_1 + \dots + a_n p_n$, then $\partial \mathcal{O} / \partial p_i = a_i$ and $\Delta_{BG}(\mathcal{O})$ just selects the maximal RHS contribution to \mathcal{O} and compares it to \mathcal{O} . In the case where one contribution $a_i p_i \gg \mathcal{O}$, then some other term(s) will have to be fine-tuned to large opposite-sign values such as to maintain \mathcal{O} at its measured value. Such fine-tuning of fundamental parameters are deemed unnatural absent some symmetry or parameter selection

mechanism. Thus, we infer that the log-derivative is a measure of *practical naturalness* [3] defined as: *An observable \mathcal{O} is natural if all independent contributions to \mathcal{O} are comparable to or less than \mathcal{O} .* In the context of the LHP then, the observable \mathcal{O} is conventionally taken to be m_Z^2 and the p_i are taken to be the MSSM μ and soft SUSY breaking terms. As a result, practical naturalness then demands all independent contributions to m_Z^2 to be comparable to m_Z^2 : this is the basis for expecting sparticles to occur around 100 GeV (weak-scale). However, determining the correct choice of p_i is ambiguous in computing Δ_{BG} [70, 71, 72, 73]. The ambiguity arises because soft terms are expected to be correlated with one another in fundamental supergravity/superstring theories (in our universe) but they may also be introduced as independent parameters in an effective 4 – D SUSY theory to parameterize one’s ignorance of the SUSY breaking sector. Depending on one’s choice of parameter co-dependence or lack thereof, Δ_{BG} yields significantly different values.

Another measure of practical naturalness that is common in the literature is the *High-Scale* measure or Δ_{HS} defined as,

$$\Delta_{HS} \equiv \frac{\delta m_{H_u}^2}{m_h^2}, \quad (4.8)$$

which is applied in context of the Higgs mass,

$$m_h^2 \simeq m_{H_u}^2(\text{weak}) + \mu^2(\text{weak}) + \text{mixing} + \text{rad. corr.} \quad (4.9)$$

where the mixing and radiative corrections are both comparable to m_h^2 . Also, $m_{H_u}^2(\text{weak}) = m_{H_u}^2(\Lambda) + \delta m_{H_u}^2$ where it is common to estimate $\delta m_{H_u}^2$ using its renormalization group

equation (RGE)

$$\frac{dm_{H_u}^2}{dt} = \frac{1}{8\pi^2} \left(-\frac{3}{5}g_1^2 M_1^2 - \dots + 3f_t^2 X_t \right), \quad (4.10)$$

(with $t = \log Q^2$) by setting several terms in Eq.(4.9) to 0 so as to integrate in a single step,

$$\delta m_{H_u}^2 \sim -\frac{3f_t^2}{8\pi^2} (m_{Q_3}^2 + m_{U_3}^2 + A_t^2) \ln (\Lambda^2/m_{soft}^2). \quad (4.11)$$

Taking $\Lambda \sim m_{GUT}$ and requiring $\Delta_{HS} \lesssim 1$ implies a natural SUSY framework. This measure has been used in the past to predict three third generation squarks lighter than 500 GeV [74, 75] (now highly constrained by LHC top-squark searches) along with small Higgs trilinear coupling terms, A_t , (whereas $m_h \simeq 125$ GeV typically favors A_t to multi-TeV values [76, 77] due to large mixing, notably in the stop sector, as we will examine shortly). The shortcomings of Δ_{HS} measure of naturalness is rooted in assuming several terms to vanish in Eq. (4.9) resulting in an oversimplification. A closer look at the X_t term in Eq.(4.9) for instance, highlights this: $X_t = m_{Q_3}^2(Q) + m_{U_3}^2(Q) + m_{H_u}^2(Q) + A_t^2(Q)$ [17]; in calculating $\delta m_{H_u}^2$, the $m_{H_u}^2(Q)$ term in X_t is set to 0 (Eq.(4.10)). Doing so, ignores the fact that $\delta m_{H_u}^2$ is highly dependent on $m_{H_u}^2(Q)$. In fact, the larger one makes $m_{H_u}^2(Q)$, then the larger becomes the cancelling correction $\delta m_{H_u}^2$ meaning that these terms are *not independent*: one cannot tune $m_{H_u}^2(\Lambda)$ against a large contribution $\delta m_{H_u}^2$ [2]. Thus, weak-scale top squarks and small A_t are not required by naturalness.

To ameliorate these glaring issues in calculating naturalness, a more robust model-independent measure Δ_{EW} was introduced [78, 79]. In calculating this measure one employs

the weak-scale SUSY Higgs potential minimization condition [17],

$$\begin{aligned} \frac{m_Z^2}{2} &= \frac{m_{H_d}^2 + \Sigma_d^d - (m_{H_u}^2 + \Sigma_u^u) \tan^2 \beta}{\tan^2 \beta - 1} - \mu^2 \\ &\simeq -m_{H_u}^2 - \mu^2 - \Sigma_u^u(\tilde{t}_{1,2}), \end{aligned} \quad (4.12)$$

which relates the measured value of the Z -boson mass, that characterizes the weak-scale, with various SUSY contributions. Then,

$$\Delta_{EW} = |(\text{max RHS contribution})| / (m_Z^2/2) \quad (4.13)$$

is low provided all weak-scale contributions to $m_Z^2/2$ are comparable to or less than $m_Z^2/2$. In Eq.(4.12), μ is the superpotential parameter, $m_{H_d}^2, m_{H_u}^2$ are the soft breaking Higgs terms, $\tan \beta \equiv v_u/v_d$ is the ratio of the Higgs VEV's and the Σ_u^u and Σ_d^d contain over 40 radiative corrections which are listed in the Appendix of [79]. Model independence of this measure means that one obtains exactly the same fine-tuning value whether the spectrum is generated from multi- or few parameter model or whether calculations are done at the weak-scale or at much higher scales. This feature is what distinguishes Δ_{EW} from the older measures Δ_{BG} and Δ_{HS} . A conservative estimate for a natural SUSY model is taken to be $\Delta_{EW} < 30$ which requires $|\mu| \lesssim 350$ GeV to offset negative contribution from $m_{H_u}^2$ and radiative corrections at the weak-scale such that the cancellations do not become too severe [80]. On the other hand, with respect to the other measures of naturalness discussed, a value of $\Delta_{BG}, \Delta_{HS} \leq (10-100)$ has been considered in the literature for natural models depending on how much fine-tuning is permitted. The implications of these measures of practical naturalness can be studied

in Figure 4.5 [2] where we analyze practical naturalness in the unified scalar (m_0) and gaugino ($m_{1/2}$) mass plane by comparing two popular classes of gravity-mediated SUSY models. The SUSY spectrum generator, Isajet [81], that uses a Monte Carlo program to simulate high-energy $pp, p\bar{p}, e^+e^-$ collisions, was employed for the analysis. Isajet is pre-programmed to do the naturalness calculations that we are investigating, for a choice of input parameters. In Figure 4.5 frame a) we plot naturalness contours in the m_0 vs. $m_{1/2}$ plane

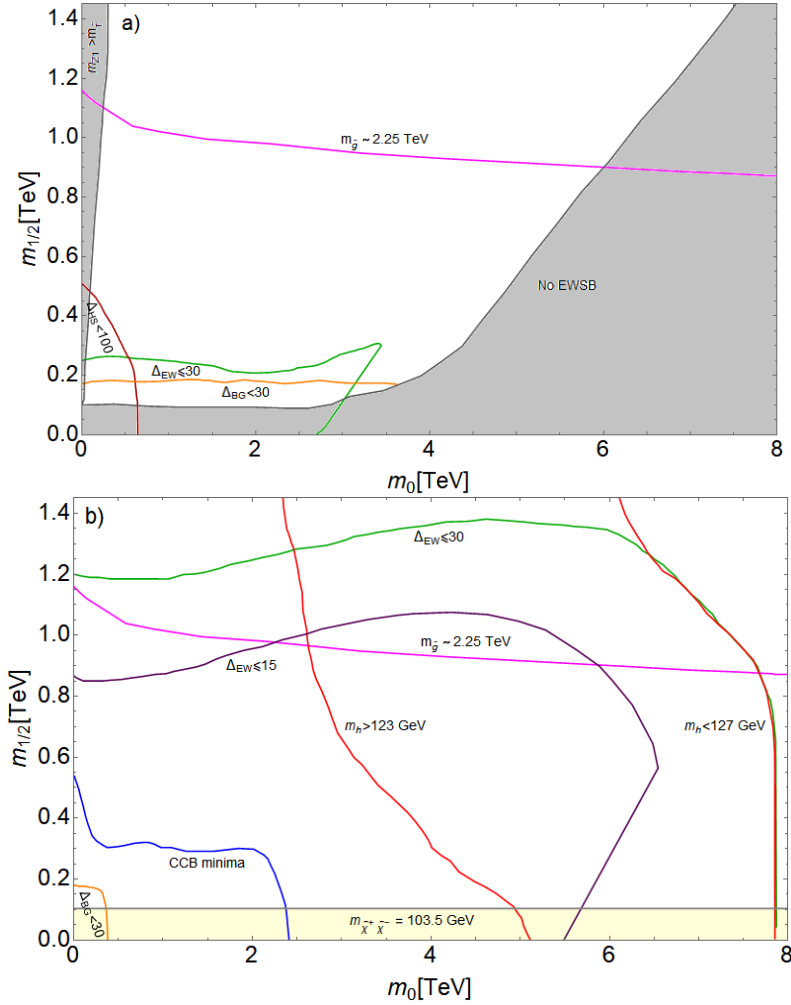


Figure 4.5: The m_0 vs. $m_{1/2}$ plane of (a) the mSUGRA/CMSSM model with $A_0 = 0$ and (b) the NUHM2 model with $A_0 = -1.6m_0, \mu = 200$ GeV, $m_A = 2$ TeV. For both cases, we take $\tan\beta = 10$. We show contours of the various fine-tuning measures along with Higgs mass contours and LEP2 and LHC Run 2 search limits.

of the CMSSM/mSUGRA model [82] for $A_0 = 0$, $\tan\beta = 10$ and $\mu > 0$. The $\Delta_{HS} < 100$ contour shows the region of the lighter top squarks for small A_0 parameter in the low m_0 , low $m_{1/2}$ region. The orange contour denotes where $\Delta_{BG} < 30$ while the green contour denotes where $\Delta_{EW} < 30$ and the LHC limit on $m_{\tilde{g}} \gtrsim 2.25$ TeV is shown as the magenta contour. This plane may result in a premature dismissal of weak-scale natural SUSY since the LHC bounds seem to have covered most of the parameter space beyond the predicted naturalness bounds. Moreover, in this plane the light Higgs mass m_h is always below 123 GeV, in direct conflict with observation. The crucial point from practical naturalness in the CMSSM plane then is that *more* natural regions occur at the lowest m_0 and $m_{1/2}$ values, where the various measures are smallest, and the sparticle masses are closest to the measured weak-scale. For comparison, we show the same plane in Figure 4.5 frame b) for the NUHM2 model where $\mu = 200$ GeV, $m_A = 2$ TeV, $A_0 = -1.6m_0$ and with the same $\tan\beta$. In this case, Δ_{HS} is not calculable since the lower left parameter space lead to CCB minima (blue contour) while Δ_{BG} , although still calculable, the contour has shrunk to a tiny region in the lower left region due to large A_0 term contributions. However, we now see that the Δ_{EW} values have expanded out to much larger m_0 and $m_{1/2}$ values since it is largely determined by the $\Sigma_u^u(\tilde{t}_{1,2})$ values, as μ is fixed to be near the measured weak-scale. Noticeably a substantial amount of natural SUSY parameter space remains unprobed beyond LHC gluino bounds. Nonetheless, practical naturalness would still prefer the lower portions of the plane since those yield smaller Δ_{EW} values. Additionally, the allowed Higgs mass contours of $m_h = 123$ GeV and $m_h = 127$ GeV and the bounded region overlaps nicely with the natural SUSY region with plenty of parameter space left to be explored but the further one is pushed towards the outer edges of the Δ_{EW} contours, less natural the model becomes. Therefore, $\Delta_{EW} \leq 15$ is more natural

than $\Delta_{EW} \leq 30$ which implies that the most natural region is currently just beyond the LHC gluino bound but not too far removed from present LHC reach.

4.3.3 Stringy Naturalness

Thus far we have seen how naturalness measures developed over the years allow us to predict upper bounds to sparticle masses in our search for SUSY, which could hint at an underlying string theory. We have also seen how naturalness has come under increasing stress from stronger bounds from LHC results. Moreover, the discovery of the discretuum of flux vacua in string theory posed difficult questions about the predictive power of the string landscape framework - how are we to identify one unique vacuum that fits observations in our universe out of a choice of $\sim 10^{500}$? This led Douglas and collaborators [83] to introduce a *statistical program* for determining BSM physics that altered the perception of naturalness. They proposed the notion of *stringy naturalness*: “the value of an observable \mathcal{O}_2 is more natural than a value \mathcal{O}_1 if more *phenomenologically viable* vacua lead to \mathcal{O}_2 than to \mathcal{O}_1 ”. This places Weinberg’s anthropics on a more agreeable setting with the idea of naturalness in that if one contextualize this definition to Λ_{cc} , then *phenomenologically viable* implies only those vacua to be habitable that allows galaxy condensation while vetoing all others. Among the allowed vacua in the landscape then, Λ_{cc} is expected to be as large as possible as anthropically allowed since now one is left with a distribution in Λ_{cc} space that is skewed toward larger values. The next question that inevitably arises is what are the implications of stringy naturalness for SUSY searches?

Soft term distribution and anthropic selection criteria for landscape SUSY The distribution of string vacua in terms of SUSY breaking scales m_{hidden}^2 is given by the ansatz,

$$dN_{vac}[m_{hidden}^2, m_{weak}, \Lambda_{cc}] = f_{SUSY}(m_{hidden}^2) \cdot f_{EWFT} \cdot f_{cc} \cdot dm_{hidden}^2, \quad (4.14)$$

where the soft breaking scale, $m_{soft} = m_{hidden}^2/m_P$ for gravity mediated SUSY breaking and m_P is the reduced Planck mass. It is instructive to analyze these distributions separately.

- f_{cc} : This is the distribution related to the cosmological constant fine-tuning penalty. In a 4 – D SUGRA EFT emerging upon flux compactification, the cosmological constant is given by,

$$\Lambda_{cc} = m_{hidden}^4 - 3e^{K/m_P^2}|W|^2/m_P^2$$

where $m_{hidden}^4 = \Sigma_i |F_i|^2 + \frac{1}{2}\Sigma_\alpha D_\alpha^2$ is the hidden sector mass scale, which in SUGRA-mediated models is assumed to be $m_{hidden} \sim 10^{12}$ GeV such that the gravitino gets a mass $m_{3/2} \sim m_{hidden}^2/m_P$. However, Susskind [1] and Denef and Douglas [84] observed that the second term in the above expression is not correlated with the distribution of the soft SUSY breaking terms F_i and D_α , rather W was distributed uniformly as a complex variable at the minima. Hence, setting $\Lambda_{cc} = 0$ has no effect on the SUSY breaking scale distribution and as a result one can easily replace m_{hidden}^4 with m_{string}^4 in effect decoupling f_{cc} from having any influence on the distribution of m_{soft} in the landscape.

- f_{SUSY} : Douglas, *et al.* also observed that flux compactification in II-B string theory leads to a uniform distribution of the soft breaking F_i and D_α terms. The F_i terms are expected to be distributed as complex numbers while the D_α terms are distributed as

real numbers. Then, the soft SUSY breaking distribution scale expected is,

$$f_{SUSY}(m_{hidden}^2) \sim (m_{hidden}^2)^{2n_F+n_D-1} \quad (4.15)$$

where, n_F is the number of F -breaking fields and n_D is the number of D -breaking fields while the factor of 2 is the volume factor in the space of SUSY breaking field values. Consequently, if one assumes SUSY breaking via a single F – *term* then one yields a *linear* statistical draw towards large soft terms as $f_{SUSY} \sim m_{soft}^n$ where $n = 2n_F + n_D - 1$ and in this case $n = 1$. More complicated SUSY breaking contributions from various hidden sectors are expected in string theory which implies the draw to large soft terms can be even stronger that would lead to heavier sparticles, in contrast to practical naturalness expectations.

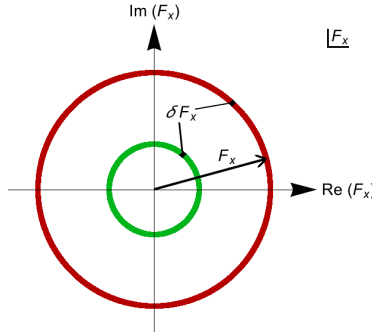


Figure 4.6: Annuli of soft SUSY breaking F-terms in the complex plane. Soft terms enjoy a mild statistical draw to larger values towards the outer (red) annulus [85].

- f_{EWFT} : This is the anthropic fine-tuning factor which traditionally was assumed to be m_{weak}^2/m_{soft}^2 which would penalize soft terms too far beyond the measured weak-scale. However, we have seen how some parameter values may lead to CCB minima (Figure 4.5) which must be forbidden for a PU that is hospitable to life as we know it.

To determine a viable f_{EWFT} function one needs to consider various phenomenologically significant phenomena. Firstly, f_{EWFT} must require that electroweak symmetry is properly broken, like in our universe, which is accommodated by the RGE running of the Higgs mass parameter $m_{H_u}^2$ to negative values at the weak-scale (REWSB). The landscape statistical draw to large values pull $m_{H_u}^2(\Lambda)$ as large as possible at the high scale (such as the GUT scale) provided it just barely runs negative at the weak-scale and does not make too big of a contribution to m_Z^2 in Eq.(4.12). This phenomenon

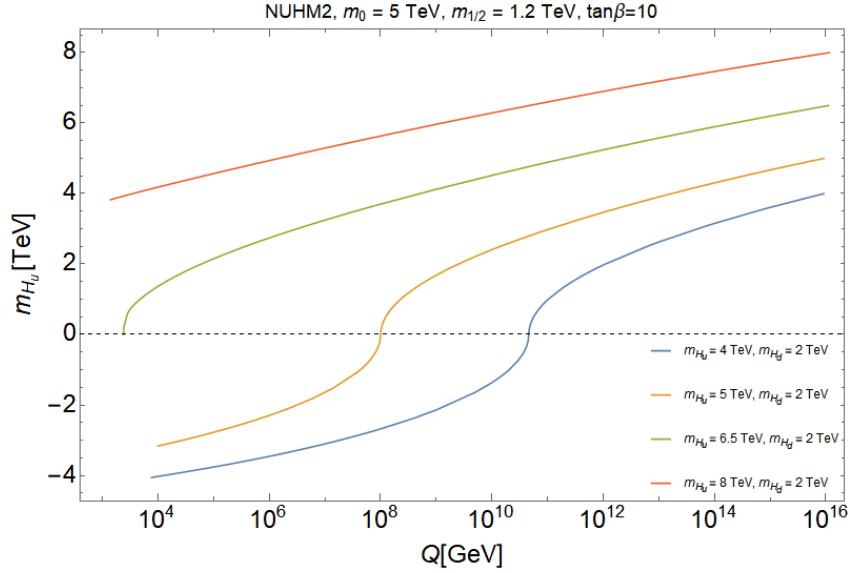


Figure 4.7: RG Evolution of $m_{H_u}^2$ vs. Q for several choices of $m_{H_u}^2(\Lambda)$ for a given benchmark point for the NUHM2 model [2].

is illustrated by the green curve in Figure 4.7 for a NUHM2 model benchmark point with unified scalar mass parameter, $m_0 = 5$ TeV, unified gaugino mass parameter, $m_{1/2} = 1.2$ TeV, the trilinear coupling term, $A_0 = -8$ TeV, for a selection of $m_{H_u}^2(\Lambda)$ values at the high scale Λ . One can notice that $m_{H_u}(\Lambda)$ cannot be too big since then $m_{H_u}^2$ is not even driven negative, denoted as the red curve, at the weak-scale ($Q \sim 100$ GeV). Such unphysical vacua with no REWSB must be vetoed. Thus, we find ourselves

in a habitable vacuum of the landscape where electroweak symmetry is barely broken radiatively - exactly what is required to gain a natural value of the weak-scale. This predicament that we happen to find ourselves in has been dubbed as *living dangerously* by Arkani-Hamed *et.al* [86, 87] since the selection of the soft terms is as large as possible but stopping barely short of being drawn too big that would result in a violation of a crucial feature of our low-energy world. This paradigm is known as radiatively-driven naturalness, or *radiative natural SUSY* [78, 80]. If on the other hand, $m_{H_u}^2(\Lambda)$ were too small then $m_{H_u}^2$ runs deeply negative at the weak-scale which results in too large a contribution to the weak-scale which are signified by the blue and yellow curves.

Radiative Corrections, $\Sigma_u^u(\tilde{t}_{1,2})$: The largest cancellations takes place as a result of large mixing in the top squark (*stop*) sector, provided that the trilinear coupling term A_t is big enough. This happens to be the dominant contributions in $\Sigma_u^u \sim \Sigma_u^u(\tilde{t}_{1,2})$. Large stop mixing then renders the radiative correction terms in Eq.(4.12), $\Sigma_u^u(\tilde{t}_{1,2}) \sim m_{weak}^2$ facilitated by large A_t terms. The situation is illustrated in Figure 4.8, where we plot $\Sigma_u^u(\tilde{t}_{1,2})$ vs. A_t at the weak-scale for the same NUHM2 parameter choices as in Figure 4.7 but with fixed $\mu = 200$ GeV, $m_A = 2$ TeV and with A_t varied over its allowed range. The dotted lines at ± 355 GeV denote the ABDS window of allowed contributions to m_{weak} . Here, we see that for small $A_t \sim 0$ TeV, the $\Sigma_u^u(\tilde{t}_{1,2})$ contributions are large negative with $\text{sign}(\Sigma_u^u(\tilde{t}_{1,2})) \cdot \sqrt{|\Sigma_u^u(\tilde{t}_{1,2})|} \sim -400$ GeV. As A_t becomes increasingly negative, the radiative correction $\Sigma_u^u(\tilde{t}_1)$ become smaller and at around $A_t \sim -5$ TeV one gets radiative contributions comparable to m_{weak}^{OU} . However, much larger negative A_t beyond ~ -5 TeV rapidly drives us into the CCB region since the stop squared-mass

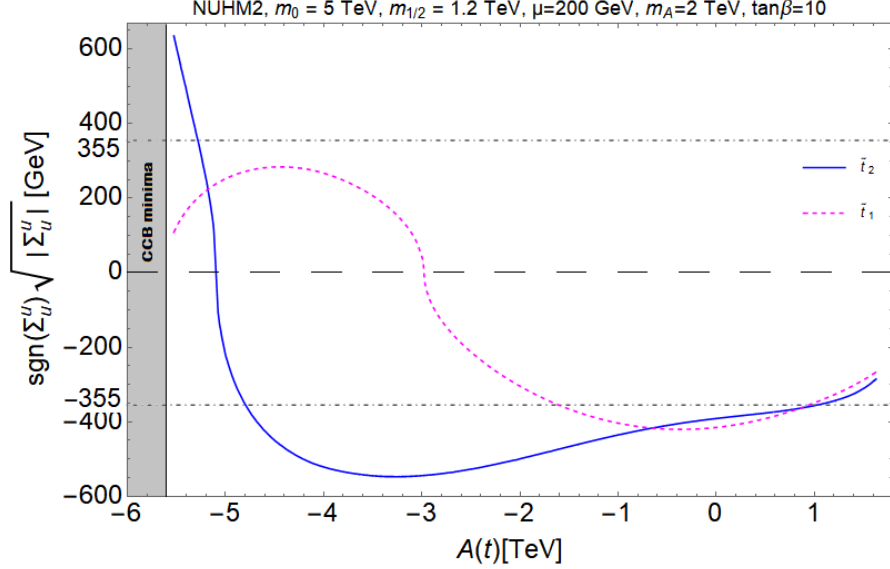


Figure 4.8: Contributions of $\text{sgn}(\Sigma_u^u(\tilde{t}_{1,2})) \cdot \sqrt{|\Sigma_u^u(\tilde{t}_{1,2})|}$ to the weak-scale vs. $A_t(\text{weak})$ for the given NUHM2 model benchmark point [2].

soft terms are RG evolved to negative values which must be subject to anthropic veto. As a result we see another instance of living dangerously in the string landscape: A -terms are statistically preferred to be large (negative) values but not too large as to land us in dangerous CCB minima. A testable consequence of this scenario is depicted in Figure 4.9. Large mixing in the stop sector generated by large A_t results in maximization of the Higgs mass peaking around its measured value of $m_h \sim 125$ GeV, as can be seen from the plot. For smaller $A_t \rightarrow 0$, one expects $m_h \sim 119$ GeV which is evidently too light. In summary, the landscape prefers a statistical draw of soft terms to large values. However, for a habitable PU one must temper this draw by imposing anthropic conditions which entail vetoing vacua with no EWSB, those that exhibit CCB giving rise to tachyonic particles and those vacua that generate a weak-scale value in excess of the ABDS allowed range. Taking all this into account, we employ $f_{EWFT} = \Theta(30 - \Delta_{EW})$ which corresponds to a conservative naturalness

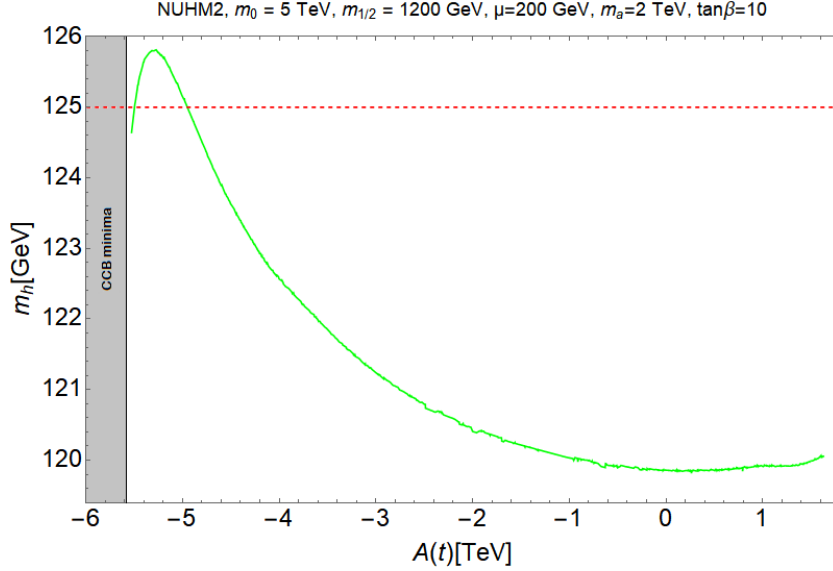


Figure 4.9: m_h vs. A_t for the given NUHM2 model benchmark point [2].

measure $\Delta_{EW} \lesssim 30$.

4.4 Naturalness versus Stringy Naturalness

We are now ready to examine how the notion of stringy naturalness compares to conventional naturalness expectations. When we studied Figure 4.4 in the context of practical naturalness alone, the most natural region of parameter space arose for smaller values of $m_0, m_{1/2}$. In contrast, the stringy naturalness draw to large soft terms would pick off the largest possible $m_0, m_{1/2}$ values subject to anthropic veto on no EWSB and CCB vacua. As such, more stringy natural parameter space would be pushed towards the edge of the Δ_{EW} contours. To illustrate this, we choose the NUHM2 model with the same parameter choice as in Figure 4.7 and plot the $m_0 - m_{1/2}$ plane in Figure 4.10, but now the soft SUSY terms scan as Douglas' power law with $n = 2n_F + n_D - 1$ for $n = 1, 2, 3, 4$ in accord with the expected landscape distribution given by Eq.(4.14). The more stringy natural region of

parameter space is then identified by the higher density of sampled points. In all frames,

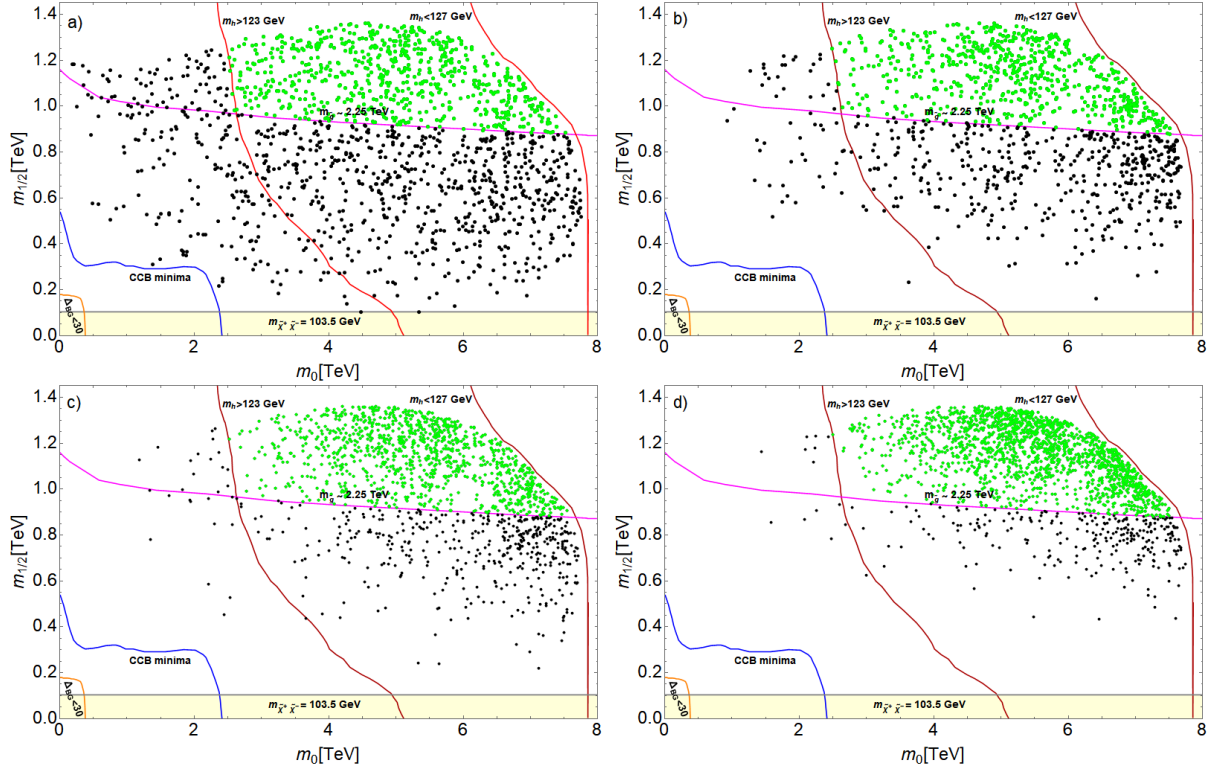


Figure 4.10: m_0 vs. $m_{1/2}$ plane for the given NUHM2 model with $A_0 = -1.6m_0$, $\mu = 200$ GeV, $m_A = 2$ TeV. The four frames (a, b, c, d) elucidate landscape expectations of soft terms for $n = 1, 2, 3, 4$ draws respectively [2].

there are no points below the lower left CCB contour since those vacua are anthropically vetoed as discussed. Beyond the CCB region, the allowed solutions fill-up the parameter space. A characteristic trend can be observed: the density of points *increases* with increasing $m_0 - m_{1/2}$. This trend becomes increasingly noticeable with stronger power-law draws in frames $b - d$ so much so that only a few solutions lie below the LHC gluino search limit shown by the magenta contour. An upper bound to how large the values m_0 and $m_{1/2}$ can assume in the landscape is inferred from the density of points dropping to zero in accordance with ABDS constraints. The conclusion from stringy naturalness is then as follows: *stringy naturalness with $n \geq 1$ power-law draw on soft terms favors the largest soft terms tempered by*

the requirement that m_Z^{PU} is not too far from m_Z^{OU} . This stands in sharp contrast to practical naturalness expectations of lower values of soft terms. Thus, from the perspective of stringy naturalness, one would expect to observe a Higgs mass around 125 GeV with sparticles beyond current LHC reach [2]. Hence, while conventional naturalness notions would put increasing doubt on the existence of natural SUSY, stringy naturalness paradigm actually re-invigorates SUSY prospects since the detectors are just starting to probe the stringy natural parameter space.

4.5 The Triumph of Natural SUSY in the Landscape

In this section, we compare different SUSY models in light of the emergent landscape from string compactifications. The goal here is to identify the most likely SUSY scenarios that are preferred by the string landscape, out of the numerous paradigms that have been proposed in the literature.

4.5.1 Fate of the SM and CMSSM in the Landscape

To determine the likelihood of the SM being the low-energy EFT of an underlying string theory in the landscape, we take a closer look at EWSB in the SM. The Higgs potential that facilitates EWSB via the Higgs mechanism in the SM can be written as [2],

$$V_{SM} = -\mu_{SM}^2 \phi^\dagger \phi + \lambda_{SM} (\phi^\dagger \phi)^2, \quad (4.16)$$

which, upon minimization ultimately yields the physical Higgs mass including quadratically

divergent radiative corrections,

$$m_H^2 \simeq m_H^2(\text{tree}) + \delta m_H^2 \quad (4.17)$$

where $m_H^2(\text{tree}) = 2\mu_{SM}^2$ and $\delta m_H^2 = \frac{3}{4\pi^2} \left(-\lambda_t^2 + \frac{g^2}{4} + \frac{g^2}{8\cos^2\theta_W} + \lambda_{SM} \right) \Lambda_{SM}^2$, with Λ_{SM} denoting the mass scale cut-off beyond which the SM ceases to be a valid low-energy EFT. As was discussed in chapter 1, to obtain the measured Higgs mass, $m_H \simeq 125$ GeV, one needs to tune $m_H^2(\text{tree})$ against the large corrections δm_H^2 . Enabling such tuning of $m_H^2(\text{tree})$ for $\Lambda_{SM} \gg m_H$, we check the required value of μ_{SM} , which is the SM Higgs mass parameter, to gain $m_H = 125$ GeV, as shown in Figure 4.11. We assume a uniform distribution of μ_{SM} in the

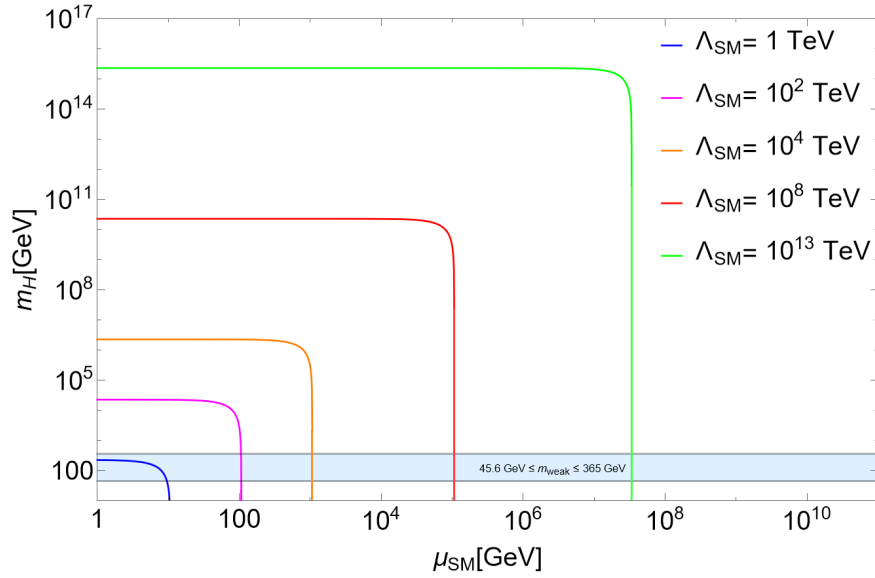


Figure 4.11: m_H vs. μ_{SM} for various theory cut-off values Λ_{SM} . The ABDS window is shown shaded as blue. [2].

landscape, since no particular value of μ is favoured in the SM. Additionally, we highlight the ABDS anthropic bound on the weak-scale by the blue shaded region in Figure 4.11. From the figure, it is evident that for $\Lambda_{SM} = 1$ TeV, a significant range of μ_{SM} values lie in the ABDS

allowed region. As Λ_{SM} increases such that $\Lambda_{SM} \gg m_{weak}$, extremely tiny fine-tuned ranges of μ_{SM} values lead to a viable weak-scale. Thus, in the string landscape, for an anthropic weak-scale to arise, the SM is likely an extremely rare occurrence as a low-energy EFT since for $\Lambda_{SM} \gg 1$ TeV the anthropically allowed μ_{SM} becomes increasingly constrained [2]. This is an instance where conventional naturalness is in agreement with stringy naturalness - large fine-tuning is required to stabilize the Higgs mass which is considered unnatural even in the conventional sense.

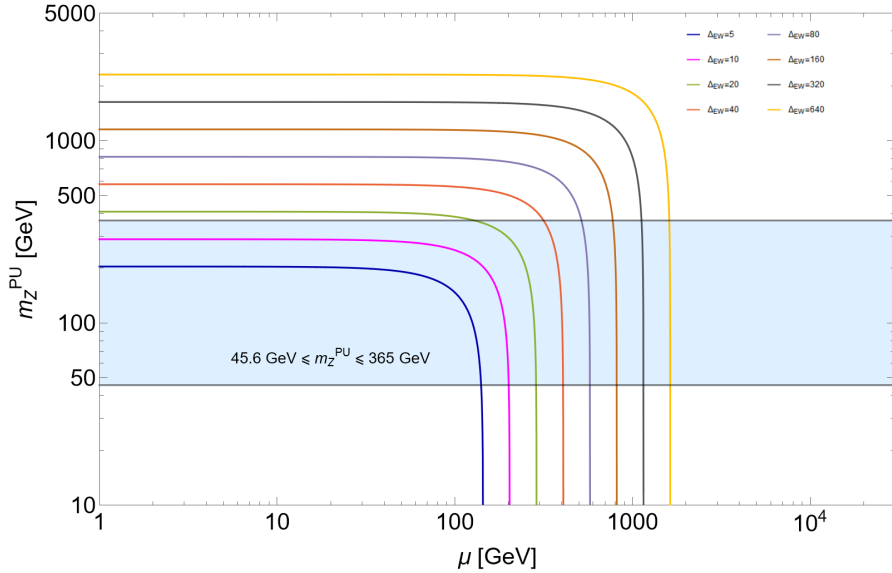


Figure 4.12: m_Z^{PU} vs. μ for various values of naturalness measure Δ_{EW} . The ABDS window is shown shaded as blue. [2]

One can also test for the frequency of PU with vacua that exhibit a 4-D low energy physics described by the CMSSM framework. We have already seen how this model is increasingly under stress from LHC bounds on sparticle and Higgs mass measurements. Certainly CMSSM falls under the umbrella of unnatural models since one of its key features is the requirement of universal scalars which usually means $m_{H_u}^2$ is driven to deep unnatural values. Consequently, in lifting the Higgs mass up to $m_h \simeq 125$ GeV, the model-independent Δ_{EW} assumes values

in the range $100 \leq \Delta_{EW} \leq 10^4$ for detailed scans over CMSSM parameter space [72], in gross violation of ABDS anthropic window. As such, we investigated the prospects of models like the CMSSM with high Δ_{EW} values in Ref.[2]. For simplicity, we take the limit of Eq.(4.13) wherein the radiative corrections are small such that Eq.(4.12) becomes

$$m_Z^2 \simeq -2m_{H_u}^2 - 2\mu^2,$$

and then consider SUSY models where $m_{H_u}^2$ is driven to large negative values at the weak-scale. Then, one can happily replace $-m_{H_u}^2$ (*weak*) by $\Delta_{EW} \cdot m_Z^{OU}/2$ using Eq.(4.13) to calculate the derived value of m_Z^{PU} which is expected in SUSY models within the landscape, in terms of Δ_{EW} and μ . We show our results in Figure 4.12 wherein we plot m_Z^{PU} versus μ for an assortment of Δ_{EW} values which ranges from natural values $\sim 5 - 20$ to unnatural values up to ~ 640 . The ABDS anthropic window is depicted as before by the light blue shaded region. From the figure it is evident that, for μ distributed uniformly on the landscape, low, natural values of Δ_{EW} yield significantly larger range of μ values that lead to habitable values of m_Z^{PU} . In contrast, as Δ_{EW} gets larger, one is increasingly restricted to tinier (fine-tuned) ranges of μ for which the derived m_Z^{PU} lead to habitable PU's. Thus, we would expect that SUSY frameworks like the CMSSM/mSUGRA, for which Δ_{EW} cannot attain natural values to allow for $m_h \sim 125$ GeV, to be rare occurrences in our *fertile patch of the landscape* which, by parsimony, contain the MSSM as the low energy EFT.

4.5.2 Radiative Natural SUSY emergent from the Landscape

In Ref.[54], we contrasted the prospects of natural and fine-tuned SUSY paradigms in

a more robust manner. Thus far we have employed the SUSY spectra generator Isajet to test various models and artificially imposed the ABDS constraints using the value of Δ_{EW} as calculated in Isajet. Since all popularly available SUSY spectra generators carry out their calculations with respect to a fixed weak-scale at $m_Z^{OU} = 91.2$ GeV, accidental fine-tuning of parameters conspiring to generate $m_Z^{PU} \neq m_Z^{OU}$ that nonetheless fall within the ABDS window is impossible. For instance, one can estimate a value for m_Z^{PU} from Isajet by the following approximation resulting from Eq.(4.12) and Eq.(4.13) where m_{weak} is determined by the maximal contribution on the RHS such that,

$$m_Z^{PU} \simeq \sqrt{\Delta_{EW}/2} m_Z^{OU}. \quad (4.18)$$

This then implies for $\Delta_{EW} \sim 30$ one obtains $m_Z^{PU} \sim 360$ GeV $\sim 4m_Z^{OU}$ which happily sits within the ABDS anthropic bound. To illustrate the general idea, by setting the radiative corrections to zero in Eq.(4.12) for simplicity, we generate the plot, shown in Figure 4.13, of the possible outcome we expect from the multiverse where the parameters are free to tune and derive a weak-scale value that respects the ABDS criterion. In Figure 4.13, to generate an anthropically allowed weak-scale, one must live between the the red and green curves. Statistically speaking, one is most likely to occupy such a PU when the area between the curves is largest. Immediately then we can appreciate the largest such area occurs for the smallest values of μ^{PU} and $\sqrt{-m_{H_u}^2(weak)}$ i.e. when both values are $\lesssim 360$ GeV at the derived weak-scale. Alternatively, as both these parameters become $\gtrsim 360$ GeV, the area between the curves become increasingly smaller. This highlights the fact that it is expected to be highly unlikely in a statistical sense, for habitable PU's, with ABDS allowed weak-scale,

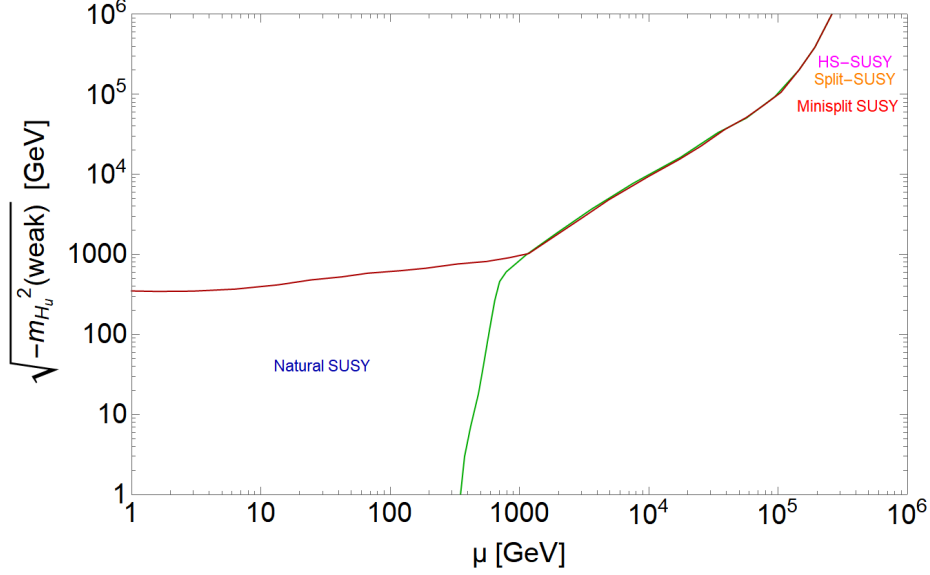


Figure 4.13: The expected $\sqrt{-m_{H_u}^2(weak)}$ vs. μ^{PU} parameter space in a toy model ignoring radiative corrections to the Higgs potential. The region between red and green curves satisfies the atomic principle since there $m_{weak}^{PU} \lesssim 4m_{weak}^{OU}$ [54].

to form wherein the low energy EFT happens to be fine-tuned SUSY models like High-Scale (HS) SUSY [88, 89], Split SUSY [90, 91] and Minisplit SUSY [92, 93] (models that have been promoted in the literature). Moreover, the region above the red curve produces too big a weak-scale that violates the atomic principle while for regions below the green curve we generate PU's with no EWSB or with CCB minima. However, this plot is an approximation since radiative corrections are in fact non-zero and are often the dominant contributions to the RHS of Eq.(4.12); additionally, $m_{H_u}^2(weak)$, μ^{PU} are not fundamental scale-invariant parameters and as such it is not obvious that they should be distributed uniformly on a log-scale as shown here. Rather $m_{H_u}^2(weak)$, μ^{PU} are determined from their RGE running from the GUT scale and even though μ^{PU} barely evolves, $m_{H_u}^2(weak)$ is highly distorted from its RGE evolution and the requirement of REWSB. As a result, in an effort to explore these connections more completely, we opted to write a computer code that could serve as a toy

simulation of the multiverse. The goal of the model is to simulate what is thought to occur within the multiverse restricted to a subset of vacua containing the MSSM as the low energy EFT. Our toy simulation is capable of solving the set of 26 coupled RGE's via Runge-Kutta method, listed in Chapter 9 of Ref.[17], by taking in input boundary conditions at the GUT scale, $m_{GUT} \simeq 2 \times 10^{16}$ GeV, and evolving them down to a low scale, Q , which is determined by the energy scale at which $m_{H_u}^2$ first runs negative provided that $m_{weak}^{OU} \leq Q \leq m_0(3)$ where $m_0(3)$ is the third generation unified scalar mass. Altogether, the GUT scale parameters that are used as input boundary conditions are: $m_0(1, 2, 3)$, m_{H_u} , m_{H_d} , $m_{1/2}$, A_0 , $\tan \beta$, and μ . We use the one-loop RGE's but augmented by the two-loop terms from Eq. 11.22 of Ref.[17] needed to set the upper bounds on the first/second generation scalar masses. If proper REWSB occurs, we then employ Eq.(4.12) including radiative corrections, to calculate m_Z^{PU} . If, on the other hand, there is no REWSB or if the RGE running generates negative weak-scale values for charged or colored scalar squared masses such that we encounter CCB vacua, we anthropically veto such solutions. To determine the input boundary conditions at m_{GUT} the parameters scan over the ranges:

$$m_0(1, 2) : 0 - 60 \text{ TeV}$$

$$m_0(3) : 0.1 - 10 \text{ TeV}$$

$$m_{H_u} : m_0(3) - 2m_0(3) \text{ TeV}$$

$$m_{H_d} (\sim m_A) : 0.3 - 10 \text{ TeV}$$

$$m_{1/2} : 0.5 - 3 \text{ TeV}$$

$$- A_0 : 0 - 50 \text{ TeV}$$

$$\mu_{GUT} : 1 - 10^4 \text{ GeV}$$

$$\tan \beta : 3 - 60$$

The soft terms scan according to $f_{SUSY} \sim m_{soft}^1$ as expected for SUSY breaking from a single F -term in the landscape, μ scan as $f_\mu \sim 1/\mu$ (scale invariant choice) while $\tan \beta$ scan uniformly. The result of this simulation is depicted in Figure 4.14 by using the same plane as Figure 4.13. The plot is generated for the NUHM2 model with fixed choices for $m_{H_u} = 1.3m_0$, $A_0 = -1.6m_0$ and $\tan \beta = 10$, while $m_0, m_{1/2}$ and μ are allowed to scan. In

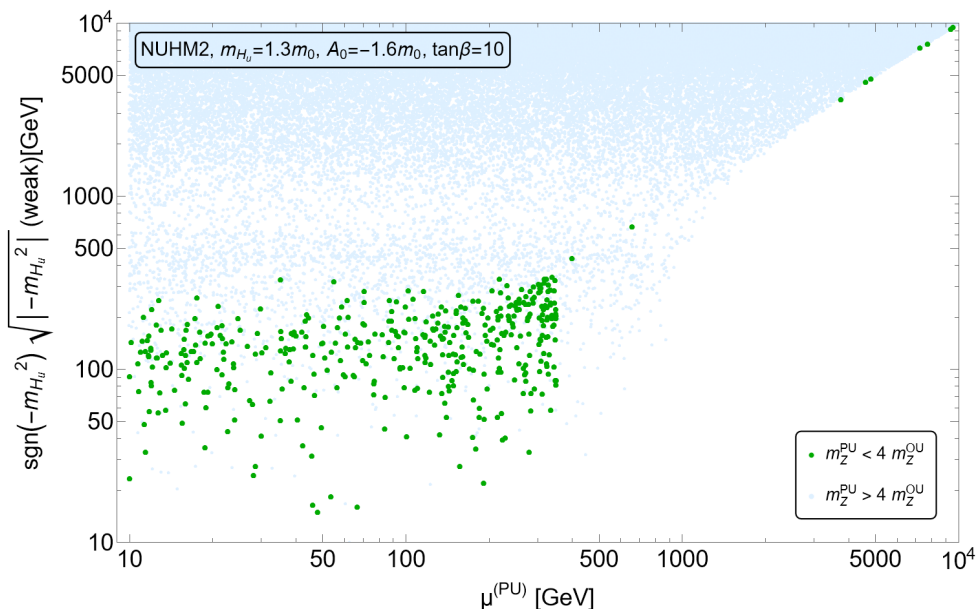


Figure 4.14: The $\sqrt{-m_{H_u}^2(weak)}$ vs. μ^{PU} parameter space wherein the green points denote vacua with appropriate EWSB within ABDS constraints. The blue points denote the vacua that generate $m_{weak}^{PU} > 4m_{weak}^{OU}$ [54].

the figure, the green points are the ABDS allowed points with proper EWSB for which $m_Z^{PU} \leq 4m_Z^{OU}$, while the light blue ones are anthropically disfavored on account of yielding too big a weak-scale value. We notice that the bulk of the allowed points live in the lower left corner of p -space, in agreement with the expected parameter hypercube in Figure 4.13.

Additionally, we also notice that the toy model simulation yield a few green points in the tiny hypercube ranging up to high values for μ^{PU} and $\sqrt{-m_{H_u}^2(weak)}$. These points can be inferred as accidental fine-tuning of parameters to yield a habitable weak-scale. One can surmise from the figure that natural SUSY models, represented by numerous green points in the lower left corner of p -space, are much more prevalent than fine-tuned models, in the landscape with the MSSM as low energy EFT. We can analyze this more closely by contrasting natural SUSY model NUHM2 with the unnatural CMSSM framework, for specific benchmark parameter choices. To this end, we plot the value of m_Z^{PU} as generated with our natural SUSY parameter choice but with varying μ^{PU} using the usual distribution $f_\mu \sim 1/\mu^{PU}$. The results are shown in Figure 4.15 for three sets of parameter and model choices. In the top-most frame, we adopt a set of natural SUSY benchmark parameter values with variable μ^{PU} . We notice a large selection of μ^{PU} values in the range $\sim 100 - 210$ GeV which yield $m_Z^{PU} \leq 4m_Z^{OU}$, as denoted by the green points. For larger values of μ^{PU} , m_Z^{PU} drops below the ABDS window lower bound and then hits the boundary where electroweak symmetry is not properly broken. By contrast, in the middle frame we show a stringy unnatural parameter choice with $m_{H_u}(GUT) < m_0$ which causes $m_{H_u}^2$ to run deeply negative at the weak-scale. This yields an extremely fine-tuned range at $\mu^{PU} \sim 4$ TeV that results in anthropically allowed vacua. Thus, compared to the natural parameter choice as in the top frame, we see that, given a uniform distribution of μ parameters on the landscape, the unnatural model - while logically possible - is highly improbable. Furthermore, in the bottom frame, we analyze the scenario in the CMSSM/mSUGRA framework which, as has been discussed, is a notable example of a fine-tuned model occurring, albeit rarely, in the string landscape. Here again, for typical benchmark parameter values, we find an extremely tiny

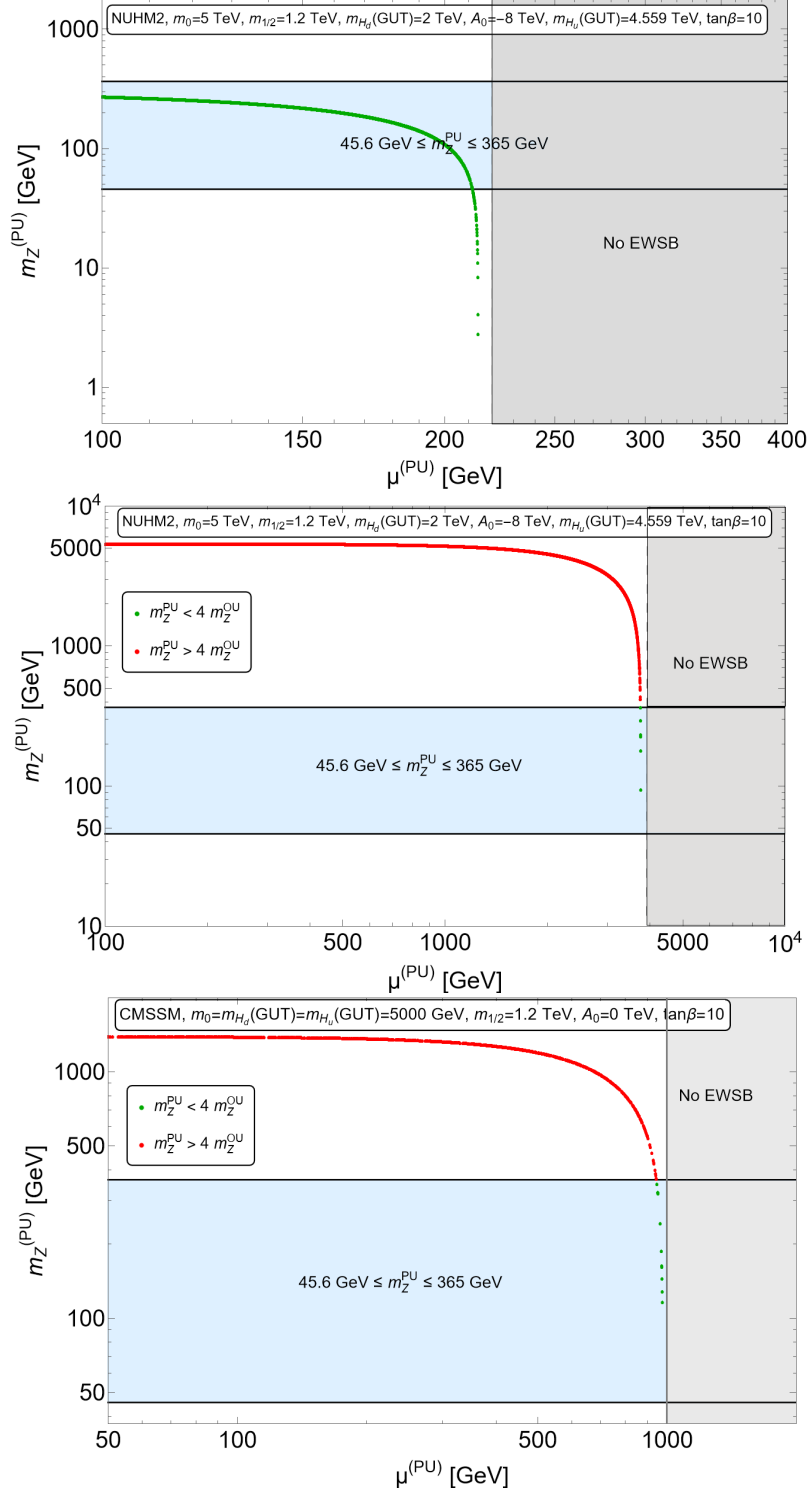


Figure 4.15: $m_Z^{(PU)}$ vs. $\mu^{(PU)}$ parameter space wherein the green points denote vacua with appropriate EWSB within ABDS constraints. The red points have $m_{weak}^{(PU)} > 4m_{weak}^{(OU)}$ [54].

hypercube at $\mu^{PU} \sim 2$ TeV that yields $m_Z^{PU} \leq 4m_Z^{OU}$. This reinforces our arguments in the previous subsection in that vacua exhibiting CMSSM as the low energy EFT are extremely rare in the landscape as compared to natural SUSY models with non-universal scalar masses and $m_{H_u}(GUT) \sim 1.3m_0$ which accommodates REWSB.

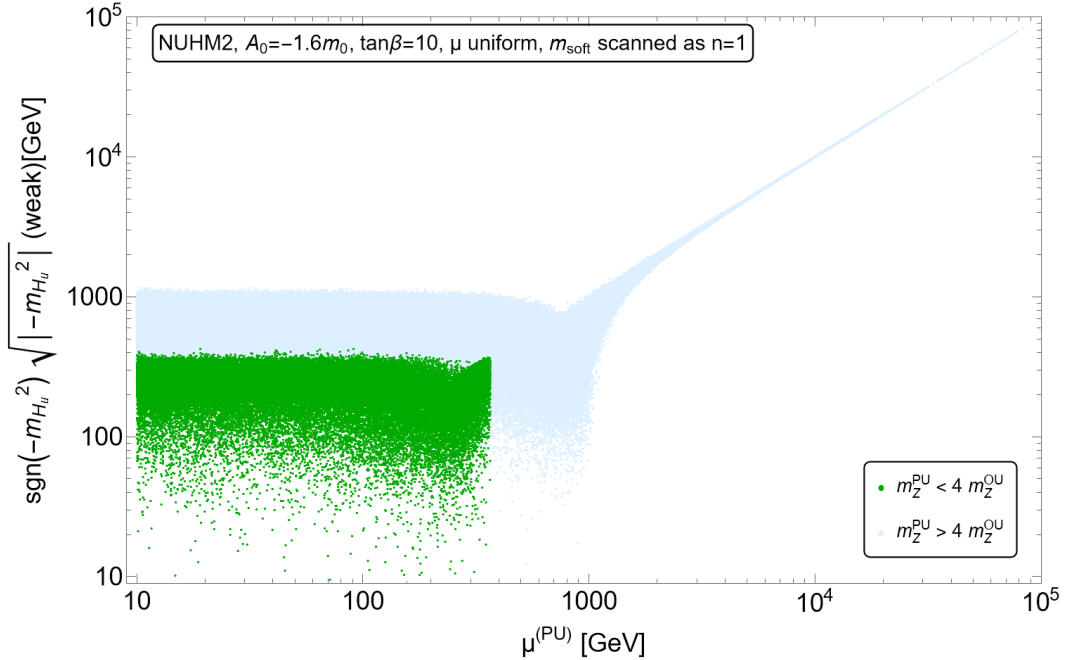


Figure 4.16: The $\sqrt{-m_{H_u}^2(weak)}$ vs. μ^{PU} parameter space from Isajet wherein the green points denote vacua with appropriate EWSB within ABDS constraints. The blue points denote the vacua that generate $m_{weak}^{PU} > 4m_{weak}^{OU}$. This run implements $m_Z^{PU} = \sqrt{\Delta_{EW}/2}m_Z^{OU}$ [54].

To compare our results, we used Eq.(4.18) to compute the approximate weak-scale from Δ_{EW} value generated by Isajet using NUHM2 model parameters as input with parameters scanning as before. The main difference in this approach is that we have no accidental fine-tuning of parameters since the weak-scale is derived from the maximal RHS contribution in Eq.(4.12). We plot our results in Figure 4.16 in the same p -space as before. The results are evidently in agreement with Figure 4.13 and Figure 4.14 with the most populous region

of allowed weak-scale being the region of natural SUSY. Furthermore, since no allowance for fine-tuning is made, we see the green points that were generated along the diagonal stretch to the top right corner of the plane, has vanished. This plot emphasizes why event generators like Isajet with $f_{EWSB} = \Theta(30 - \Delta_{EW})$ produce good representations of expected sparticle and Higgs mass spectra in scans over the landscape of string vacua, that we will explore further in the following chapter.

Chapter 5

String landscape guide to SUSY and DM searches

In this chapter, we aim to make comprehensive predictions from the string landscape. We start by investigating different ways soft SUSY breaking terms may statistically scan on the landscape. In the previous chapter, we assumed a mild statistical draw wherein all soft terms are drawn as m_{soft}^n with $n = 1, 2, 3, 4$. In the current chapter we study different statistical scans for the gaugino masses, scalar masses and trilinear soft terms. To present our results, we require stringy naturalness wherein the likelihood of values for the observables is proportional to their frequency within a fertile patch of landscape including the parsimonious choice of the MSSM as the low energy EFT. Thereafter, several numerical results for Higgs and sparticle mass predictions for various SUSY models are presented. The contents of this chapter are reliant on the following published papers in Refs. [3, 4, 5, 6, 94].

5.1 Soft terms in the low energy EFT

To motivate the topic to be discussed, we begin by briefly recalling the discussion on string compactifications in Chapter 3. In string theory, we start with a $10/11-D$ UV-complete string theory and then write the corresponding $10/11-D$ effective SUGRA theory by integrating out the KK modes and other super heavy states. Then one compactifies the $10/11-D$ SUGRA on a CY manifold that, as we have seen in our discussion of compactifications, preserves $N = 1$ SUSY in the ensuing $4-D$ theory containing visible sector fields along with a plethora of gravitationally coupled moduli fields grouped according to complex structure moduli, U_j , and Kähler moduli, T_i , along with the dilaton field S . For the best understood Type IIB

constructions, the U_j are stabilized by fluxes while the T_i has been shown to be stabilized by various non-perturbative effects, for instance by the KKLT stabilization mechanism [41]. Realistically, of order ~ 100 moduli are expected but for simplicity one assumes only a single or a few T_i in explicit constructions. In principle, moduli stabilization allows for determination of their VEV's from which one obtains the parameters of the EFT. We want to be able to identify which MSSM soft terms should scan independently within the landscape. To that end, we assume C_α to be the visible sector fields which consist of the usual MSSM fields. The S, T_i, U_j together form the hidden sector of the $4 - D$ theory and provide the required arena for SUSY breaking. The following discussion is presented in units of $m_P = M_P/\sqrt{8\pi} = 1$.

We start our discussion by taking a closer look at the SUSY breaking sector, the dynamics of which determines the resulting soft SUSY breaking terms. To that end, we note that the $4 - D, N = 1$ SUGRA Lagrangian is determined by just two functions that depend on the chiral superfields ϕ_M of the model: the real gauge invariant Kähler function,

$$G(\phi_M, \phi_M^*) = K(\phi_M, \phi_M^*) + \log |W(\phi_M)|^2$$

and the holomorphic gauge kinetic function $f_a(\phi_M)$. The chiral superfields are distinguished according to visible sector fields C_α and the hidden sector fields h_m . Following [41, 95, 96] we begin by expanding the superpotential as a power series in terms of the visible sector fields:

$$W = \hat{W}(h_m) + \frac{1}{2}\mu_{\alpha\beta}(h_m)C^\alpha C^\beta + \frac{1}{6}Y_{\alpha\beta\gamma}(h_m)C^\alpha C^\beta C^\gamma + \dots \quad (5.1)$$

followed by the expansion of the Kähler potential as,

$$K = \hat{K}(h_m, h_m^*) + \tilde{K}_{\bar{\alpha},\beta}(h_m, h_m^*) C^{*\bar{\alpha}} C^{*\beta} + \left[\frac{1}{2} Z_{\alpha\beta}(h_m, h_m^*) C^\alpha C^\beta + h.c. \right] + \dots \quad (5.2)$$

wherein the various coefficients are functions of the hidden sector fields h_m which are to-be-determined. Here, the Greek indices represent the visible sector fields and the lower-case Latin indices correspond to hidden sector fields while the general chiral superfields are denoted with upper case Latin indices. Additionally, the F -part of the scalar potential is,

$$V(\phi_M, \phi_M^*) = e^G \left(G_M K^{M\bar{N}} G_{\bar{N}} - 3 \right) = \left(\bar{F}^{\bar{N}} K_{\bar{N}M} F^M - 3e^G \right) \quad (5.3)$$

from which one notes that if some of the h_m fields develop VEV's such that at least one of the auxiliary fields $F^m = e^{G/2} \bar{K}^{m\bar{n}} G_{\bar{n}} \neq 0$, then SUGRA is spontaneously broken. Thereafter, the gravitino gains a mass $m_{3/2} = e^{G/2}$ while the soft terms are generated by replacing the h_m and their F_M terms by their nonzero VEV's in the 4 - D , $N = 1$ SUGRA Lagrangian derived in Ref. [97] and taking the so-called flat limit $m_P \rightarrow \infty$, keeping $m_{3/2}$ fixed. One is then left with the low-energy EFT which includes a renormalizable global SUSY Lagrangian augmented by soft SUSY breaking terms. From the fermionic part of the SUGRA Lagrangian [97], the canonically normalized gaugino masses are obtained as [98],

$$M_a = \frac{1}{2} (\text{Re } f_a)^{-1} F^M \partial_M f_a \quad (5.4)$$

along with the unnormalized Yukawa couplings,

$$Y'_{\alpha\beta\gamma} = \frac{\hat{W}^*}{|\hat{W}|} e^{\hat{K}/2} Y_{\alpha\beta\gamma} \quad (5.5)$$

and the superpotential μ contribution,

$$\mu'_{\alpha\beta} = \frac{\hat{W}^*}{|\hat{W}|} e^{\hat{K}/2} \mu_{\alpha\beta} + m_{3/2} Z_{\alpha\beta} - \bar{F}^{\bar{M}} \partial_{\bar{M}} Z_{\alpha\beta}. \quad (5.6)$$

On the other hand, the scalar potential is expanded as,

$$V_{soft} = m_{\alpha\beta}^{\prime 2} C^{r*\bar{\alpha}} C^\beta + \left(\frac{1}{6} A'_{\alpha\beta\gamma} C^\alpha C^\beta C^\gamma + \frac{1}{2} B'_{\alpha\beta} C^\alpha C^\beta + h.c. \right) \quad (5.7)$$

from which one obtains the unnormalized scalar soft terms as,

$$m_{\bar{\alpha}\beta}^{\prime 2} = (m_{3/2}^2 + V_0) \tilde{K}_{\bar{\alpha}\beta} - \bar{F}^{\bar{M}} \left(\partial_{\bar{M}} \partial_N \tilde{K}_{\bar{\alpha}\beta} - \partial_{\bar{M}} \tilde{K}_{\bar{\alpha}\gamma} \tilde{K}^{\gamma\bar{\delta}} \partial_N \tilde{K}_{\bar{\delta}\beta} \right) F^N \quad (5.8)$$

and the trilinear parameter,

$$A'_{\alpha\beta\gamma} = \frac{\hat{W}^*}{|\hat{W}|} e^{\hat{K}/2} F^M \left[\hat{K}_M Y_{\alpha\beta\gamma} + \partial_M Y_{\alpha\beta\gamma} - \left(\tilde{K}^{\delta\bar{\rho}} Y_{\delta\beta\gamma} + (\alpha \leftrightarrow \beta) + (\alpha \leftrightarrow \gamma) \right) \right] \quad (5.9)$$

while the rather lengthy expression for the bilinear B -term is left out since it is not required in the discussion that follows. The next step is to analyze the equations and study their implications for the string landscape.

Gaugino masses In Eq.(5.4), $Re(f_a) = 1/g_a^2$ where f_a is the gauge kinetic function. For non-zero gaugino masses, f_a must be a non-trivial function of the moduli fields and often in

most $4 - D$ string constructs f_a is taken as $k_a S$ where the k_a is the Kac-Moody level of the gauge factor. Gauge kinetic function of this form results in universal gaugino masses which require SUSY breaking in the dilaton field S . The rest of the moduli can enter f_a at the loop level and lead to non-universal gaugino masses. Consequently, one possibility is that the moduli contribution to M_a can be comparable to the dilaton contribution, in which case non-universal gaugino masses are expected and the gaugino masses scan as m_{soft}^n where the precise value of n depends on the number of contributing moduli fields. Otherwise, when the dilaton is the dominant contribution to M_a then only a single hidden sector field contributes and non-universality is expected to be negligible. In this case, $f_{SUSY} \sim m_{soft}^1$ i.e. a *linear scan*, is the expected distribution function for the gaugino masses. Shortly, we will see that the landscape actually prefers gaugino masses to be smaller than scalar masses i.e. $F^S \ll F^M$ where F^S refers to SUSY breaking by the dilaton while F^M denotes the collective SUSY breaking scale from all the moduli fields. This is another instance wherein non-universality of gaugino masses maybe expected as a result of the loop-suppressed moduli-mediated terms becoming comparable to the dilaton-mediated contribution. However, even if the moduli-mediated contributions are suppressed, the anomaly-mediated contributions (arising from anomalous violation of superconformal invariance [99]) might be as dominant as the universal contribution. To address this issue, we will introduce the *generalized* [100] *Mirage Mediation* [101] (gMM') scheme for soft term masses wherein substantial non-universality of gaugino masses are expected. Such non-universality leads to gaugino mass unification at a scale, μ_{mir} (mirage scale) such that $\mu_{mir} \ll m_{GUT} \simeq 2 \times 10^{16}$ GeV where m_{GUT} is the scale at which the gauge couplings unify [100]. As such, gaugino masses are expected to scan independently of other soft terms and so hereafter $n_{1/2}$ will be used to denote the value of n in the f_{SUSY}

distribution to distinguish gauginos from other soft terms.

Soft scalar masses The soft SUSY breaking scalar masses are obtained from Eq.(5.8). Upon proper normalization, the first part of the equation gives the canonical kinetic terms which lead to diagonal and universal scalar masses. This universality was an attractive feature in the past since it offered a *universality* solution to the SUSY flavor problem [102]. The second term in Eq.(5.8) involving the partial derivatives of the visible sector Kähler metric, leads to non-universal scalar masses. Specifically, non-universality is expected in the two Higgs doublets $m_{H_u}^2$ and $m_{H_d}^2$ in addition to non-universal masses $m_0(1), m_0(2)$ and $m_0(3)$ for each of the generations. Lately, non-universality has emerged as a *desired* feature in SUGRA models since they accommodate RNS [78, 79] via RG running from large high scale values to natural contributions at the weak-scale. The RNS framework finds a natural home in the string landscape [103] and has been discussed in the previous chapter and how it results in a scenario in which we are *living dangerously* close to violating a fragile but crucial feature of the low-energy world in proper EWSB. This expected non-universality of soft scalar masses for each generation in gravity-mediation was problematic for many years, as surveyed in Ref. [102] and in fact provided strong motivation for flavor-independent SUSY mediation schemes like gauge-mediation [104, 105] and anomaly-mediation [106, 107, 108, 109]. However, in the face of LHC measurement of the Higgs mass at $m_h \simeq 125$ GeV, the original incarnations of these models has become highly disfavored due to their inability to reproduce the rather large Higgs mass. As an aside, we briefly review the SUSY flavor and CP problems to gain some insight on why these are significant model-building constraints to be considered.

- *SUSY flavor problem*: Qualitatively, flavor changing neutral currents (FCNC)'s are

possible particle interactions that results in fermions changing flavor without altering their electric charge. Such processes are extremely constrained in nature [110] and so consistent models are required to provide suppression mechanisms for FCNC's. In the MSSM, FCNC sources arise from the many new parameters of the theory, especially in the soft SUSY breaking sector. These include sfermion mass squared matrices of the form [111],

$$\mathcal{L}_{soft} \ni -\tilde{f}_i^\dagger(\mathbf{m}_f^2)\tilde{f}_j^\dagger$$

where $i, j = 1 - 3$ are generation indices and the sfermion index \tilde{f} runs over the various matter superfields $\hat{Q}, \hat{U}^c, \hat{D}^c, \hat{L}^c, \hat{E}^c$, using notation of Ref. [17]. Additional contributions to FCNC can arise from trilinear soft terms,

$$\mathcal{L}_{soft} \ni (\mathbf{a}_u)_{ij\epsilon ab}\tilde{Q}_i^a H_b^u \tilde{u}_{Rj}^\dagger + (\mathbf{a}_d)_{ij\epsilon ab}\tilde{Q}_i^a H_{da} \tilde{d}_{Rj}^\dagger + (\mathbf{a}_e)_{ij\epsilon ab}\tilde{L}_i^a H_{da} \tilde{e}_{Rj}^\dagger + \text{h.c.} .$$

In gravity-mediated SUSY breaking, the trilinear terms are expected to be proportional to the corresponding Yukawa couplings such that these contributions are small for the first/second generations. However, for the sfermion squared mass matrices \mathbf{m}_f^2 , no FCNC occurs only in the case when the squared sfermion mass matrices are diagonalized by the same transformation that diagonalize the corresponding fermion mass matrices [17]. In gravity-mediation though, no principle enforces such a mechanism and the large off-diagonal mass matrix elements may lead to FCNC effects [111].

- *SUSY CP Problem:* Many soft SUSY breaking parameters happen to be, in general, complex valued which raises the possibility of TeV scale imaginary components to

these which would give rise to large Charge (C) and Parity (P) (CP) violating phases. Limits have been placed on these complex valued soft terms from measurements of CP-violating decays of the kaon, $K_L \rightarrow \pi\pi$, and experimental upper limits from *electric dipole moments* (EDMs) [17]. These constrain the CP-violating mass terms to be extremely small and determining the physical principle behind the smallness of such phases is known as the SUSY CP problem. Thus, a crucial element of consistent SUSY models must include an explanation as to why SUSY contributions to CP violation are small. As a result, a common feature of traditional SUSY models was to assume *reality* and *universality* of the soft masses and that the trilinear \mathbf{a} terms are proportional to their corresponding Yukawa matrices; together these assumptions render FCNC effects to be below experimental bounds while all CP-violating phases vanish save the CP-violating phases in the CKM mixing matrix [17].

The string landscape provides its own solution to both the SUSY flavor and CP problems arising from non-universal generations [111]. In the landscape, as has been discussed, soft terms are statistically pulled to values *as large as possible such that their contributions to the weak-scale remain of order the weak-scale*. The first/second generation squarks have smaller Yukawa couplings while the third generation squarks e.g. the *stops*, have larger Yukawa couplings. As such, the landscape pull on the first/second generation squarks is expected to be stronger which results in their masses to be pulled into the 20 - 40 TeV regime while the third generation squarks are more mildly pulled up to the few TeV regime. The upper bounds on the first/second generation squarks are in fact a relic of two-loop RG effects which restricts the third generation soft masses to smaller values (aiding naturalness by suppressing

$\Sigma_u^a(\tilde{t}_{1,2})$) until these run tachyonic. Therefore, the first and second generation soft masses are pulled to large values but to a common, flavor independent upper bound. This provides a *quasi-degenerate*, decoupling solution to the SUSY flavor and CP problems [4]. Hereafter, the landscape selection of scalar masses are denoted by n_0 to distinguish them from landscape selection for gauginos, which one expects to scan independently on the landscape.

Trilinears The soft breaking trilinear terms, also called the A -terms, are given in Eq.(5.9). All SUSY breaking moduli fields contribute to the A -terms and are of order m_{soft} . Consequently they scan as $f_{SUSY} \sim m_{soft}^{n_0}$ in the landscape, same as for the scalar masses. As such, the A -terms enjoy a statistical draw to large values and this leads to maximal mixing in the top squark sector thereby lifting the Higgs mass to $m_h \sim 125$ GeV. However, the A -terms are only drawn to as large (negative) values as possible subject to anthropic veto of CCB minima of the scalar potential that results if the A -terms get too large, as was discussed in Figure 4.9 [2] as another instance of living dangerously on the landscape.

μ parameter The bilinear term $\frac{1}{2}\mu_{\alpha\beta}(h_m)C^\alpha C^\beta$ in Eq.(5.1) is forbidden for all matter superfields of the MSSM to ensure gauge invariance, save the vector-like pair of Higgs doublets $\mu H_u H_d$ due to their opposite hypercharges [4]. Since μ is a superpotential SUSY preserving term, dimensional analysis would indicate $\mu \sim m_P$; on the other hand, in the context of string theory being scale invariant, no mass terms are allowed for massless states such that one then gets $\mu = 0$ [112]. Furthermore, proper EWSB in SUSY models require $\mu \sim m_{weak}$, which is phenomenologically crucial. This conflict amongst the above issues pertaining to the value for the μ -term is known as the *SUSY μ problem*. Notably, $\mu \sim m_{weak}$ is also motivated by stringy

naturalness with proper EWSB but this also introduces a little hierarchy problem that has to do with the large gap that opens up between μ and m_{soft} , as discussed in the previous chapter. Analysis of soft terms reveals two possible resolutions of the μ problem, which could potentially act simultaneously. The possible solutions rely on the mixing between observable sector fields H_u, H_d with hidden sector fields h_m . In Eq.(5.6), if $Z_{\alpha\beta} \sim \lambda h_m/m_P$ gains a VEV $\lambda m_{hidden}^2/m_P$ upon SUSY breaking, then a $\mu \sim m_{soft}$ is generated [113]. Alternatively, a value for the μ parameter can also be generated from Eq.(5.1) if the hidden sector fields h_m gain a VEV since $\mu_{\alpha\beta}$ is a function of the hidden sector fields. The Kim-Nilles (KN) mechanism [114] provides another solution in the context of the MSSM [115], wherein one adds a singlet observable sector superfield X and upon SUSY breaking it gains a VEV and generates a μ term. If $\mu_{\alpha\beta}$ contains non-renormalizable terms such as $\lambda_\mu X^2/m_P$ then one obtains $\mu \sim \lambda_\mu m_{hidden}^2/m_P$ upon SUSY breaking such that $\mu \sim m_{weak} - m_{soft}$. The KN mechanism originally relied on a Pecce-Quinn (PQ) symmetry to forbid the initial $\mu \sim m_P$ term which also solves the strong CP problem via a supersymmetrized [116, 117] DFSZ axion [118, 119]. However, a global PQ symmetry is inconsistent with gravity/string theory [120, 121, 122, 123] and to get around this issue one might invoke a (gravity-compatible) discrete gauge symmetry [124] \mathbb{Z}_N or a discrete R -symmetry \mathbb{Z}_N^R where the latter might originate as a discrete remnant of $10 - D$ Lorentz symmetry breaking after compactification [125]. Then the global PQ symmetry emerges as a result of the underlying discrete gauge or R -symmetry. For the discrete R -symmetry case, Ref. [126] showed that in the NMSSM, various \mathbb{Z}_N^R are anomaly-free and consistent with grand unification for $N = 4, 6, 8, 12$ and 24. Moreover, \mathbb{Z}_{24}^R symmetry is able to suppress non-renormalizable contributions to the scalar potential up to powers of $(1/m_P)^8$, which consequently solves the strong CP problem

while maintaining the strong CP angle $\bar{\theta} \lesssim 10^{-10}$. Thus, by invoking a discrete \mathbb{Z}_{24}^R symmetry one is able to solve the strong CP problem and the SUSY μ problem by restricting μ to natural values, while conserving R -parity and suppressing dangerous dimension-5 proton decay operators [127].

In the rest of the chapter, we will study these various terms in the context of several SUSY models with both gravity-mediated and generalized mirage-mediated SUSY breaking schemes. The results of the study will be analyzed against current data from SUSY searches and will serve as general predictions from the string landscape.

5.2 Results from gravity mediated SUSY breaking schemes

We have already examined some landscape implications in the context of mSUGRA and NUHM2 models when distinguishing between practical and stringy naturalness (see Figure 4.5 and Figure 4.10). Here, we employ the more general NUHM3 model wherein $m_0(1, 2)$ and $m_0(3)$ obtain independent masses in addition to independent Higgs MSSM scalars. Such a setup is partially motivated from investigations of the *mini-landscape* picture of heterotic string models compactified on an orbifold [128]. The first/second generation multiplets are located near orbifold fixed points and obey localized grand unification [129] forming a $16 - D$ spinor representation of $SO(10)$. On the other hand, the third generation matter scalars, Higgs multiplets and gauginos live in the bulk of the compactified orbifold and thus live in the usual SM split multiplets [3]. To explore the NUHM3 parameter space and generate the corresponding mass spectra, we employ the Monte Carlo event generator program Isajet 7.88 [81]. We choose a mild statistical draw for the soft terms such that $m_{soft}^{n=1}$ to scan over the

parameter space with the following ranges:

$$m_0(1, 2) : 0 - 55 \text{ TeV},$$

$$m_0(3) : 0 - 20 \text{ TeV},$$

$$m_{1/2} : 0 - 3.2 \text{ TeV},$$

$$-A_0 : 0 - 25 \text{ TeV and}$$

$$m_A : 0 - 10 \text{ TeV}.$$

Moreover, the parameter ranges

$$\tan \beta : 3 - 60 \text{ and}$$

$$\mu : 100 - 360 \text{ GeV}$$

are scanned over uniformly since these are not soft SUSY breaking terms. The lower limit for the μ term arises from the LEP2 limit in the lightest chargino mass, $\tilde{\chi}_1^\pm > 103.5 \text{ GeV}$. These are then input into Isajet as the NUHM3 parameters augmented by the requirement that ABDS anthropic condition is satisfied (i.e. $\Delta_{EW} < 30$) and that EWSB occurs radiatively.

The first set of results are displayed in Figure 5.1 and Figure 5.2 where we show the locus of $n = 1$ landscape scan points in the $m_0(3)$ vs. A_0 and the $m_{1/2}$ vs. $m_0(3)$ planes for the NUHM3 model with $\mu = 100 - 360 \text{ GeV}$, respectively. We divide our scan points into three sets. The yellow points are excluded by recent LHC Run 2 search limits:

- $m_{\tilde{g}} \gtrsim 2.25 \text{ TeV}$ for $\tilde{g} \rightarrow t\bar{t} + \tilde{\chi}_1^0$ [130],

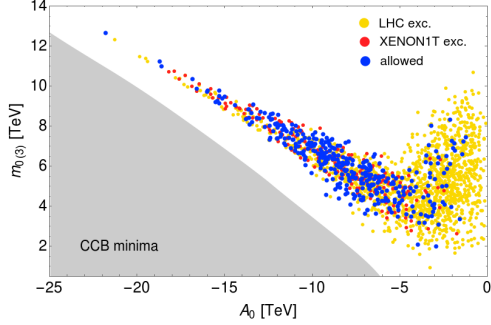


Figure 5.1: Regions of $\Delta_{EW} > 30$ (blank) and CCB minima (lower left) in the scalar potential. The blue points are LHC Run 2 and DM-allowed. [3]

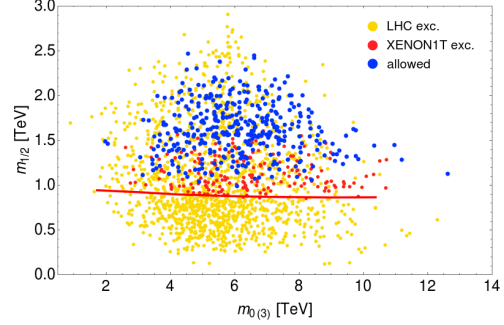


Figure 5.2: LHC Run 2 limit for $m_{\tilde{g}} \geq 2.25$ TeV is shown by the red contour. [3]

- $m_{\tilde{t}_1} \gtrsim 1.1$ TeV for $\bar{t} \rightarrow t^* + \tilde{\chi}_1^0$ [131]
- bounds from $H/A \rightarrow \tau^+\tau^-$ in the $\tan\beta$ vs. m_A plane [132],
- higgsino pair production [133]: points are beyond the recent LHC soft dilepton + jets + Missing transverse energy, \cancel{E}_T constraints.
- $m_h = 125 \pm 2$ GeV (to account for the theory error of the calculation).

Next we have the blue shaded points which denote those parameter points that have acceptable vacua and obey both LHC and WIMP search constraints. The red shaded points are allowed by LHC search limits but excluded by XENON1T spin-independent (SI) direct WIMP detection (DD) searches [56]. The takeaway lesson from Figure 5.1 is that the acceptable (blue) points lie in a very restricted regions where $m_{h_0(3)}$ and $-A_0$ are correlated: if A_0 gets too large (negative), then the model is forced into CCB minima (gray) which is anthropically vetoed. Likewise, for fixed A_0 , if $m_{h_0(3)}$ gets too large, then the third generation contributions to the weak-scale $\Sigma_u^u(\tilde{t}_{1,2})$ increase beyond a factor four allowed by ABDS bounds and we run into blank regions of the parameter space. In Figure 5.2 the $m_{1/2}$ vs. $m_{h_0(3)}$ plane is

depicted where the LHC Run 2 limit $m_{\tilde{g}} \gtrsim 2.25$ TeV is shown by the red contour. Here, we see that bulk of the allowed points occur for $m_{1/2} \sim 1 - 2.5$ TeV range which correspond to $m_{\tilde{g}} > 2.25$ TeV, well beyond current search limits. We note that there are few surviving scan points for $m_0(3) \lesssim 2$ TeV since the landscape $n = 1$ scan prefers linearly increasing soft terms. However, the linear draw to large terms dies down due to the $\Sigma_u^u(\tilde{t}_{1,2})$ contributions to the weak-scale getting too big such that fine-tuning starts setting in. This situation is exemplified by very few allowed points for $m_0(3) \gtrsim 12$ TeV [3].

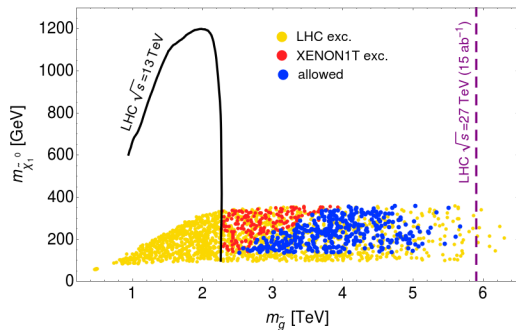


Figure 5.3: Locus of $n = 1$ landscape scan points for the NUHM3 model with $\mu = 100 - 360$ GeV in the $m_{\tilde{\chi}_1^0}$ vs. $m_{\tilde{g}}$ plane versus recent LHC Run2 constraints. [3]

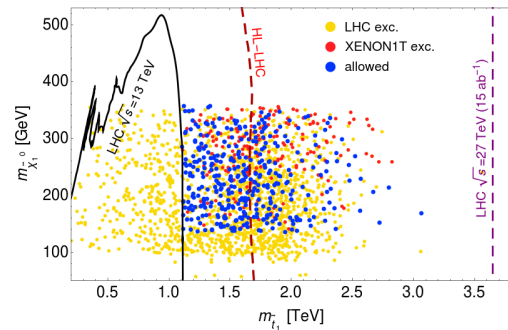


Figure 5.4: Locus of $n = 1$ landscape scan points for the NUHM3 model with $\mu = 100 - 360$ GeV in the $m_{\tilde{\chi}_1^0}$ vs. $m_{\tilde{t}_1}$ plane versus recent LHC Run2 constraints. [3]

The next set of results from $n = 1$ landscape scan is shown in Figure 5.3 and Figure 5.4. In Figure 5.3 the results are presented in the $m_{\tilde{\chi}_1^0}$ vs. $m_{\tilde{g}}$ plane which is the usual simplified model plane used to present LHC gluino search results. The current LHC Run 2 exclusion contour based on 80 fb^{-1} of integrated luminosity is shown as the black contour while the projected search limit for the High Energy - LHC (HE-LHC) with $\sqrt{s} = 27$ TeV and 15 ab^{-1} computed to 95% CL is also shown by the purple dotted line. From the figure we note that the XENON1T DM search also excludes significant regions of the lighter LSP masses for gluino masses of order 2 - 3.5 TeV. The High Luminosity - LHC (HL-LHC) is expected to

cover points with gluinos only up to 2.8 TeV via the gluino pair production search channel [134] while the HE-LHC reaches up to 6 TeV. Evidently, a complete examination of the $n = 1$ landscape points in the $\tilde{g}\tilde{g}$ search channels will require HE-LHC.

In Figure 5.4 on the other hand, we examine the $n = 1$ landscape in the $m_{\tilde{\chi}_1^0}$ vs. $m_{\tilde{t}_1}$ simplified model plane with current LHC limit shown by the black contour while the projected HE-LHC limit is shown in purple as before. Additionally we include the projected HL-LHC search limit with $\sqrt{s} = 14$ TeV and 3 ab^{-1} , by the red dotted line. Notably, there is a high density of LHC-allowed (blue) points in the range $m_{\tilde{t}_1} \sim 1.1 - 2.7$ TeV, which is significantly explored by the HL-LHC. Nevertheless, to exhaust the complete set of $n = 1$ landscape points in this search plane, an upgrade to HE-LHC is required [3].

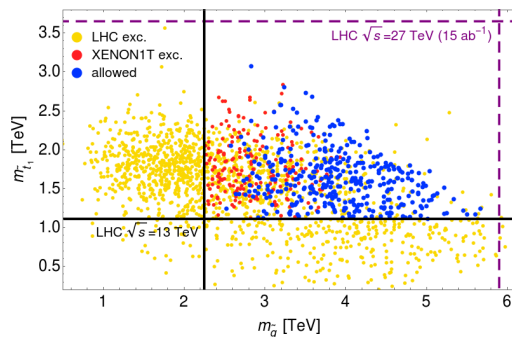


Figure 5.5: Locus of $n = 1$ landscape scan points for the NUHM3 model with $\mu = 100 - 360$ GeV in the $m_{\tilde{t}_1}$ vs. $m_{\tilde{g}}$ plane versus recent LHC Run2 constraints (black) and projected HE-LHC 95% CL reach contours (purple-dashed). [3]

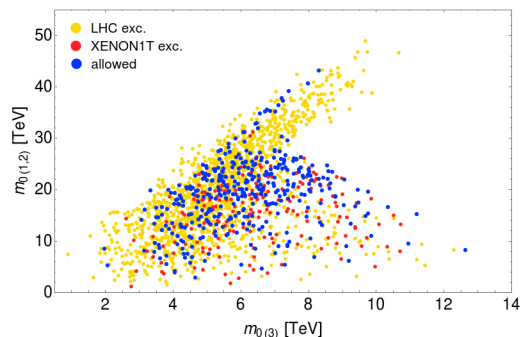


Figure 5.6: Locus of $n = 1$ landscape scan points for the NUHM3 model in the $m_0(1,2)$ vs. $m_0(3)$ plane for $\mu = 100 - 360$ GeV. [3]

In Figure 5.5 we examine the $m_{\tilde{g}} - m_{\tilde{t}_1}$ plane with the landscape $n = 1$ statistical draw on soft terms. The crucial feature that this plane exhibits is that points with the largest values of $m_{\tilde{g}}$ have the smaller range of $m_{\tilde{t}_1}$ and vice-versa. Therefore if, for example, gluinos were able to evade LHC detection on account of being too heavy, the top squarks would

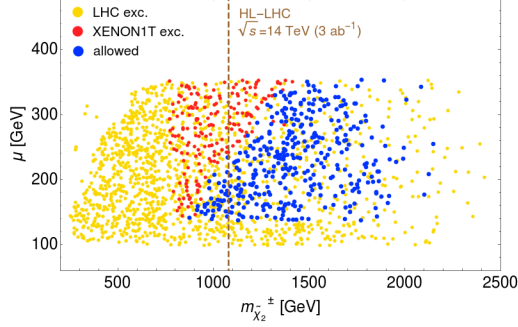


Figure 5.7: Locus of $n = 1$ landscape scan points for the NUHM3 model with $\mu = 100 - 360$ GeV in the μ vs. $m_{\tilde{\chi}_2^0}$ plane versus projected HL-LHC 95% CL search limits. [3]

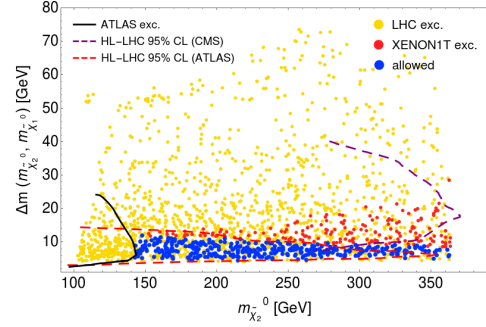


Figure 5.8: Locus of $n = 1$ landscape scan points for the NUHM3 model with $\mu = 100 - 360$ GeV in the $m_{\tilde{z}_2} - m_{\tilde{z}_1}$ vs. $m_{\tilde{z}_2}$ plane versus projected HL-LHC 95% CL search limits. [3]

most likely be detected since they are expected to be much lighter (and vice-versa). The LHC energy reach appear to stop just short of the landscape allowed points (blue) in this parameter plane and a complete coverage of the $n = 1$ landscape parameter space will require an upgrade to the HE-LHC [3].

Additionally, in Figure 5.6 we show the $m_0(1,2) - m_0(3)$ plane of the NUHM3 model for the $n = 1$ landscape. Evidently from this plane, one can see that the landscape picture prefers first/second generation matter scalars at the 10 – 30 TeV range while third generation scalars happen to be much lighter, typically below 10 TeV. RG running and mixing effects then cause the third generation squarks/sleptons to lie in the few TeV range so that their loop-contributions (Σ_u^u 's) are suppressed to be near the weak-scale, while the first/second generation squarks and sleptons masses ($m_{\tilde{q}}, m_{\tilde{l}} \sim m_0(1,2)$) can be pulled much higher into the tens of TeV range which results in a partial decoupling solution to the SUSY flavor and CP problems. They can be so heavy because the first/second generation sfermion contributions to the weak-scale are D -term contributions which largely cancel [135, 3].

A further plane of interest for LHC searches is the $\mu - m_{\tilde{\chi}_2^\pm}$ plane shown in Figure 5.7, which

presents results from same-sign diboson (SSdB) production arising from wino pair production in SUSY models with light higgsinos. The reaction is $pp \rightarrow \tilde{\chi}_2^\pm \tilde{\chi}_4^0$ where $\tilde{\chi}_2^\pm \rightarrow W^\pm \tilde{\chi}_{1,2}^0$ and $\tilde{\chi}_4^0 \rightarrow W^\mp \tilde{\chi}_1^\pm$ so that half the time the resultant final state consists of two same-sign W bosons plus large \cancel{E}_T . This decay channel is illustrated in Figure 5.9. Another possibility occurs for leptonically-decaying W bosons wherein the final state consists of same-sign dilepton + \cancel{E}_T signature which is relatively jet free with rather tiny SM backgrounds [136, 137, 138] as compared to same-sign dileptons originating from gluino and squark pair production. Thus far, no search results have been presented by ATLAS or CMS. From Figure 5.7, one can notice that LHC-allowed points only start appearing at wino masses $m_{\tilde{\chi}_2^\pm} \sim 800$ GeV and then extend out to $m_{\tilde{\chi}_2^\pm} \sim 2300$ GeV which is mostly beyond even HL-LHC reach shown by the brown contour [138].

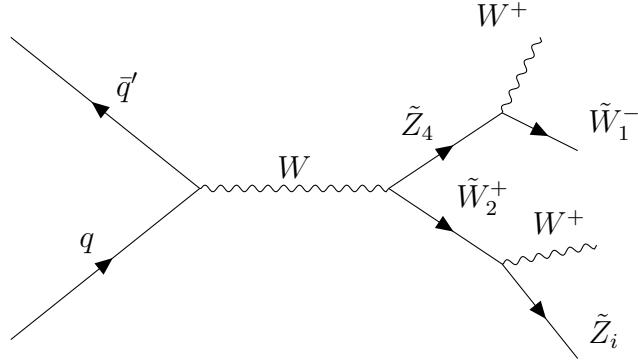


Figure 5.9: The SSdB decay signature. Here, $\tilde{Z}_4 = \tilde{\chi}_4^0$ and $\tilde{W}_{1,2}^\pm = \tilde{\chi}_{1,2}^\pm$.

In Figure 5.8 we present our $n = 1$ landscape scan results in the $\Delta m \equiv m_{\tilde{\chi}_2^0} - m_{\tilde{\chi}_1^0}$ against $m_{\tilde{\chi}_2^0}$ plane which is another significant plane of interest for light higgsino searches. The corresponding reaction is $pp \rightarrow \tilde{\chi}_2^0 \tilde{\chi}_1^0$ (and $\tilde{\chi}_2^0 \tilde{\chi}_1^\pm$) where $\tilde{\chi}_2^0 \rightarrow l^+ l^- \tilde{\chi}_1^0$ which gives rise to a soft opposite-sign dilepton pair + jet + \cancel{E}_T (OSDLJMET) whose invariant mass is bound by $m_{\tilde{\chi}_2^0} - m_{\tilde{\chi}_1^0}$ [139, 140, 141]. The Feynman diagram for this decay channel is depicted in

Figure 5.10. The hard jet radiation from the initial state recoiling against the soft dileptons provides a trigger for such events inside the detector. Recent LHC search limits and projected search limits for the HL-LHC [142] for both the ATLAS and CMS detectors are labelled in Figure 5.8. The main result we infer from this plane is that the $n = 1$ landscape scan favors heavier gauginos while μ must not be too far from the weak-scale [3]. This combination squeezes down the inter-higgsino mass gap $\Delta m \equiv m_{\tilde{\chi}_2^0} - m_{\tilde{\chi}_1^0}$, such that in this case all the LHC-allowed points have $\Delta m \lesssim 10$ GeV. The HL-LHC ATLAS contour (dashed red) appears to be a very promising avenue for SUSY searches since it seemingly covers almost all of the parameter space in this plane. The OSDLJMET is the only channel which is expected to be completely examined by the HL-LHC since, as has been discussed above, gluino and top squark masses are likely pulled to heavier values in the string landscape that possibly draws them beyond HL-LHC projected limits. Thus, we would expect a SUSY signal in this channel to emerge slowly but conclusively in the next 15 years as LHC acquires its full complement of 3 ab^{-1} of integrated luminosity [3]. We will explore this search plane in more detail when discussing search prospects for DM from the string landscape.

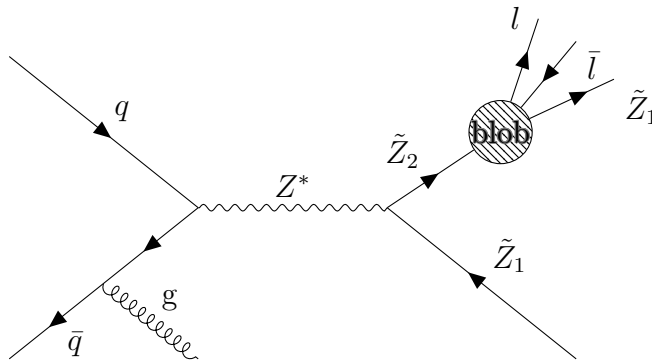


Figure 5.10: Feynman diagram for the OSDLJMET decay signature.

Another natural SUSY search channel occurs in the Higgs sector by examining $pp \rightarrow$

$A, H \rightarrow \tau^+\tau^-$ events. The results of these searches are typically presented in the $\tan\beta$ against m_A plane, as shown in Figure 5.11. Following our earlier plots, here too we show the LHC excluded region is labelled by the black contour [131]. This contour assumes only SM decay modes for the A and H but in the string landscape decay modes like $H, A \rightarrow higgsinos$ should almost always be present as well, which might lead to $4l + \cancel{E}_T$ signatures [143]. However, the latter decay modes barely affect the search limits since a diminution of Higgs to SM branching fractions can be offset by increasing the Higgs production cross sections by choosing somewhat larger $\tan\beta$ [144]. Evidently, Figure 5.11 shows that the LHC-allowed points lie typically well beyond current LHC search limits and the highest density of landscape points occur in the region $m_A \sim 2 - 5$ TeV and at lower values of $\tan\beta$ for which the dominant Higgs production cross section contribution from $b\bar{b}$ fusion is not too big [3]. Thus, we expect the likelihood of a SUSY signal emerging in this channel to be quite small.

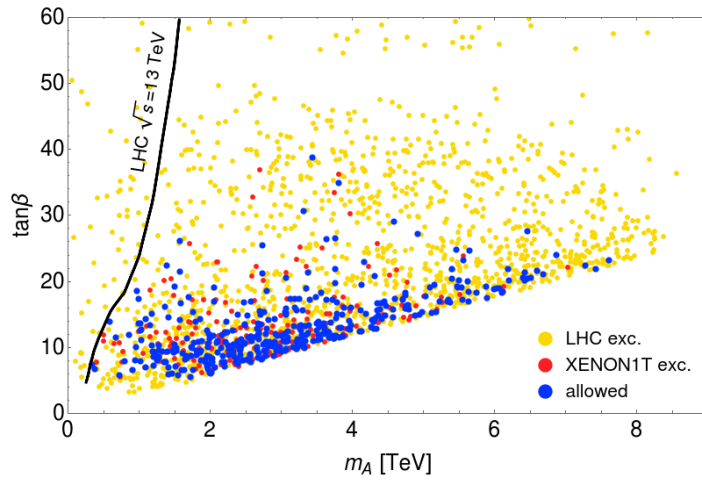


Figure 5.11: Locus of $n = 1$ landscape scan points for the NUHM3 model with $\mu = 100 - 360$ GeV in the $\tan\beta$ vs. m_A plane versus recent LHC Run2 constraints. Blue points are LHC Run 2 and DM-allowed while red points are LHC-safe but excluded by XENON1T WIMP search limits. [3]

5.3 Results from Generalized Mirage-Mediation (GMM')

We begin this section by giving a brief outline of the salient features of the GMM' model. Then we go on to discuss what outcomes can manifest in the low energy EFT via such SUSY breaking scheme from string landscape arguments.

5.3.1 GMM' model and parameter space

The mirage-mediation (MM) model is built out of comparable contributions from moduli- and anomaly-mediated SUSY breaking terms. The anomaly-mediation arises from one-loop contributions to the soft SUSY breaking parameters which always accompany the tree-level gravitational interactions in SUGRA models. Such corrections to the leading tree-level soft SUSY breaking parameters originate in the super-Weyl anomaly, thus named anomaly mediated SUSY breaking (AMSB) [17]. Furthermore, moduli/gravity-mediation effects on soft SUSY breaking masses are believed to be communicated via the moduli. The earliest rendition of mirage mediation grew out of the KKLT moduli stabilization construct [41]. As previously discussed, stabilization of the Kähler modulus, T , requires non-perturbative effects such as gaugino condensation with $m_T \sim m_{3/2} \log(m_P/m_{3/2})$ which results in a supersymmetric AdS vacuum which is then uplifted to a dS vacuum by introducing an anti-D3 brane [145]. The complex structure moduli and the dilaton, on the other hand, could be stabilized by introducing three-form fluxes, obtaining masses near the string scale. A little hierarchy was expected in the KKLT scheme such that [101, 146],

$$m_T \sim (4\pi^2)m_{3/2} \sim (4\pi^2)^2 m_{soft}$$

wherein m_{soft} is the expected scale of moduli-mediated soft terms while $\log(m_P/m_{3/2}) \sim 4\pi^2$. Here, m_{soft} is suppressed relative to $m_{3/2}$ while AMSB contributions to m_{soft} are also suppressed by a loop factor of $1/16\pi^2$ relative to $m_{3/2}$ [17], which justifies the comparability of the two contributions. The model derives its name from the distinctive feature that RGE running of non-universal gaugino and scalar masses at $m_{GUT} \simeq 2 \times 10^{16}$ GeV to ultimately unify at some intermediate scale,

$$\mu_{mir} = m_{GUT} e^{-8\pi^2/\alpha}$$

known as the *mirage* scale, where α parameterize the relative moduli- to anomaly-mediated contributions to the soft terms [4]. One can then note that $\alpha \rightarrow 0$ yields pure AMSB and moduli-mediation is recovered with $\alpha \rightarrow \infty$. Thus, the smoking gun signature of mirage mediation is that gaugino masses unify at this intermediate μ_{mir} scale rather than at m_{GUT} [4] and this can be tested at e^+e^- colliders operating at collision energy, $\sqrt{s} > 2m(\text{higgsino})$ [147, 148].

Integrating out the heavy dilaton and the complex structure moduli results in an effective theory with broken SUGRA consisting of the observable sector fields \hat{Q} and the Kähler modulus \hat{T} . The location of the matter and the Higgs superfields in the compactified dimensions influence the Kähler potential via their modular weights $n_i = 0$ (1) for the matter fields living on $D7$ ($D3$) branes, or $n_i = 1/2$ for chiral multiplets located on the brane intersections. Additionally, the gauge kinetic function $f_a = \hat{T}^{l_a}$, where a labels the gauge group, is determined by the corresponding location of the gauge supermultiplets, since $l_a = 1$ (0) for gauge fields living on $D7$ ($D3$) branes [145, 149, 150]. Thus, the parameter space for

the MM model is specified by,

$$m_{3/2}, \alpha, \tan \beta, \text{sign}(\mu), n_i, l_a \quad (5.10)$$

and grand unification implies that modular weights for the matter fields in the same GUT multiplet are common which means the l_a are universal. Defining $c_i = 1 - n_i$, for simplicity one can therefore assume, $c_m = c_{m3}$ for the matter scalars but the modular weights for the two Higgs doublets c_{H_u} and c_{H_d} are necessarily different, as motivated by, for instance, $SO(10)$ SUSY GUT models. Recent studies of the MM phenomenology by scanning over the MM parameter space with the added requirement of $m_h = 125 \pm 2$ GeV deem these models to be highly fine-tuned according to the Δ_{EW} measure [72]. A more robust generalization of the MM framework is the GMM' model, discussed below.

The soft SUSY breaking parameter expressions have been calculated in Ref's [149, 150, 151, 152] for simple flux compactifications of II-B string theory with only a single Kähler modulus. In realistic compactifications however, numerous Kähler moduli can be present and in that case the discrete-valued modular weights are generalized to be continuous parameters constituting the *generalized* or GMM' model [100]. Thus, in the GMM' framework the set of soft SUSY breaking gaugino, scalar and Higgs masses are given by,

$$\begin{aligned} M_a &= \frac{m_{3/2}}{16\pi^2} (\alpha + b_a g_a^2), \\ m_i^2(1, 2) &= \left(\frac{m_{3/2}}{16\pi^2} \right)^2 (c_m \alpha^2 + 4\alpha \xi_i - \dot{\gamma}_i), \\ m_j^2(3) &= - \left(\frac{m_{3/2}}{16\pi^2} \right)^2 (c_{m3} \alpha^2 + 4\alpha \xi_j - \dot{\gamma}_j), \\ m_{H_u}^2 &= \left(\frac{m_{3/2}}{16\pi^2} \right)^2 (c_{H_u} \alpha^2 + 4\alpha \xi_{H_u} - \dot{\gamma}_{H_u}), \\ m_{H_d}^2 &= \left(\frac{m_{3/2}}{16\pi^2} \right)^2 (c_{H_d} \alpha^2 + 4\alpha \xi_{H_d} - \dot{\gamma}_{H_d}), \end{aligned} \quad (5.11)$$

while the set of soft breaking A parameters are,

$$\begin{aligned}
A_\tau &= \frac{m_{3/2}}{16\pi^2} (-a_3\alpha + \gamma_{L_3} + \gamma_{H_d} + \gamma_{E_3}), \\
A_b &= \frac{m_{3/2}}{16\pi^2} (-a_3\alpha + \gamma_{Q_3} + \gamma_{H_d} + \gamma_{D_3}), \\
A_t &= \frac{m_{3/2}}{16\pi^2} (-a_3\alpha + \gamma_{Q_3} + \gamma_{H_u} + \gamma_{U_3}),
\end{aligned}
\tag{5.12}$$

Here, the index i runs over the first/second generation MSSM scalars $i = Q_{1,2}, U_{1,2}, D_{1,2}, L_{1,2}$ and $E_{1,2}$ while j runs over third generation scalars $j = Q_3, U_3, D_3, L_3$ and E_3 . Due to quasi-degeneracy, wherein first/second generations can be mass degenerate at the mirage scale while the third generation is separate, we choose independent values for c_m and c_{m3} for first/second and third generation scalars respectively. Moreover, the independent values of $c_{m_{H_u}}$ and $c_{m_{H_d}}$ which set the moduli-mediated contribution to the Higgs mass-squared soft terms, can be traded for weak-scale values of μ and m_A akin to what we generally do for the NUHM2 model. Doing so enables a more direct exploration of stringy natural SUSY parameter space where most landscape solutions fall within $\mu \sim 100 - 360$ GeV in anthropically-allowed pocket universes [2]. Therefore, the GMM' parameter space can be defined by

$$\alpha, m_{3/2}, c_m, c_{m3}, a_3, \tan\beta, \mu, m_A.
\tag{5.13}$$

5.3.2 Results in the m_0^{MM} vs. $m_{1/2}^{MM}$ plane

Before we do a thorough scan of the GMM' model parameter space, we opt to present some of the main results in the m_0^{MM} against $m_{1/2}^{MM}$ plane analogous to the $m_0 - m_{1/2}$ plane we examined previously in the context of the CMSSM or NUHM2, 3 models. To display our

results we define the following parameters which outline the moduli-mediated contributions to soft terms in terms of mirage mediation parameters,

$$\begin{aligned}
m_0^{MM} &\equiv \frac{m_{3/2}}{16\pi^2} \sqrt{c_m} \alpha, \\
m_{1/2}^{MM} &\equiv \frac{m_{3/2}}{16\pi^2} \alpha, \\
a_3 &= 1.6 \sqrt{c_m}, \\
c_m &= c_{m3}.
\end{aligned}
\tag{5.14}$$

We employ the Monte Carlo event generator program Isajet 7.88 [81] to generate the corresponding mass spectra using the defined parameter set as inputs. The main objective here is to investigate how the $m_0 - m_{1/2}$ plane compares between gravity mediated SUSY breaking with all soft terms having a common statistical draw m_{soft}^n with $n = 1, 2, 3, 4$ and mirage mediated SUSY breaking with gauginos and scalars scanning with different statistical draws (i.e. $n_{1/2} \neq n_0$) in the landscape. Our results are displayed in four frames of Figure 5.12 with all four frames produced with $n_{1/2} = 1$ but with $n_0 = 1, 2, 3, 4$ in frames *a*, *b*, *c*, *d* respectively. Here, the dots denote the expected statistical result of scanning the landscape and larger density of dots correspond to greater stringy naturalness. The lower-left yellow region in all frames depict the parameter space for which $m_{\tilde{\chi}_1^\pm} < 103.5$ GeV in violation of LEP2 constraints while the orange box shows regions of parameter space for which the older naturalness measure $\Delta_{BG} < 30$. Additionally we indicate by the blue contour, regions of CCB which must be anthropically vetoed and the magenta contour denotes $m_{\tilde{g}} = 2.25$ TeV below which is excluded by LHC gluino pair searches [153, 154]. In plane *a*), bulk of the low $m_{1/2}$ region here leads to tachyonic top squark soft terms due to large trilinear terms

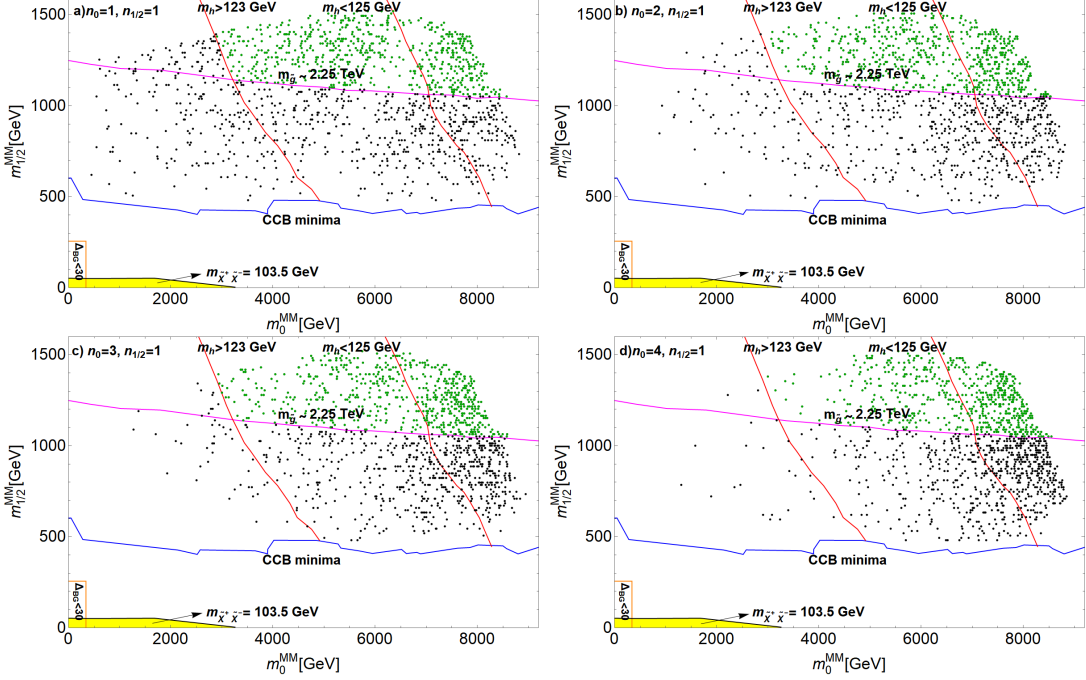


Figure 5.12: m_0^{MM} vs. $m_{1/2}^{MM}$ plane of the GMM' model for a value of $n_{1/2} = 1$ but with a) $n_0 = 1$, b) $n_0 = 2$, c) $n_0 = 3$, d) $n_0 = 4$. For all frames, we take $m_{3/2} = 20$ TeV, $\mu = 200$ GeV, $m_A = 2$ TeV, $\tan \beta = 10$ and $a_3 = 1.6\sqrt{c_m}$ and require $m_Z^{PU} < 4m_Z^{OU}$. [4]

$A_0^{MM} \equiv -a_3 \left(\frac{m_{3/2}}{16\pi^2} \right)$. This region is almost flat with increasing m_0 mainly because the larger one makes the GUT scale top-squark squared mass soft terms, the larger is the cancelling contribution from RG evolution. As $m_{1/2}^{MM}$ gets bigger, we obtain phenomenologically viable electroweak vacua since large M_3 enhance top squark squared mass running to large positive values. We also show on the figure LHC Higgs mass constraints: $m_h \simeq 125 \pm 2$ GeV, indicated by the red contours. The green points are consistent with LHC sparticle search limits and the Higgs mass measurements. We can infer from all four frames that the regions of high stringy naturalness remain safely beyond current LHC sparticle search limits while at the same time yields the proper Higgs mass $m_h \simeq 125$ GeV. Thus we can see, while early naturalness measures preferred smaller values for m_0 and $m_{1/2}$ [57, 58, 59, 60], stringy naturalness prefers

the opposite [2]: as large as possible values of m_0^{MM} and $m_{1/2}^{MM}$ subject to the anthropic condition that m_{weak}^{PU} is within a factor four of our measured value (lest the atomic principle be violated) [4]. This then implies the most stringy natural parameter space statistically prefers a light Higgs mass $m_h \sim 125$ GeV while sparticles are pulled beyond LHC Run 2 search limits. As comparison, as n_0 is increased to 2, 3, 4 in frames b, c, d respectively (which corresponds to more moduli fields contributing to SUSY breaking in the scalar sector), we note a shift of the stringy natural region to higher values of m_0^{MM} and $m_{1/2}^{MM}$ and a sharpening of the Higgs mass prediction that $m_h \simeq 125$ GeV. In fact, as seen in frame d) for $n_0 = 4$ there are only a handful of dots with $m_h < 123$ GeV. This fact is emphasized in Figure 5.13 where we show the Higgs mass probability distribution for the same scan of the GMM' parameter space. An anti-intuitive conclusion that can be drawn from our calculations is that a 3 TeV gluino is more stringy natural than a 300 GeV gluino [4].

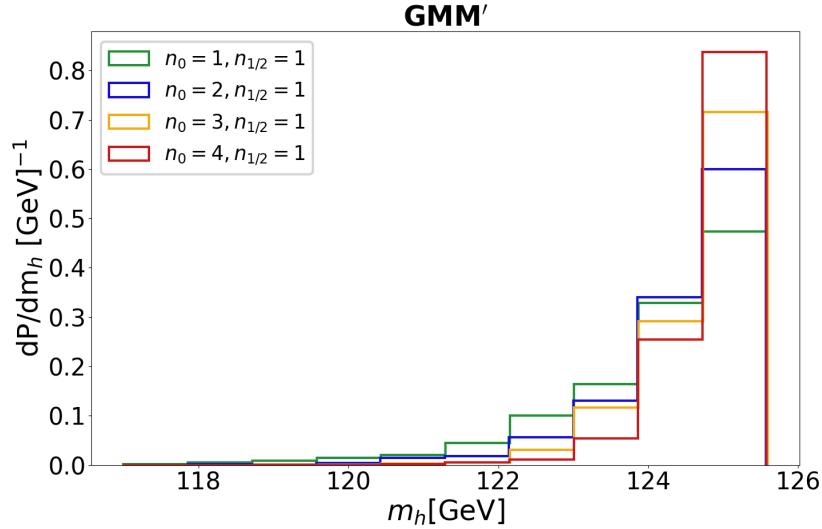


Figure 5.13: Probability distribution dP/dm_h vs. m_h for $n_{1/2} = 1$ and $n_0 = 1, 2, 3, 4$ for scans of the GMM' model for $m_{3/2} = 20$ TeV, $\mu = 200$ GeV, $m_A = 2$ TeV, $\tan \beta = 10$ and $a_3 = 1.6\sqrt{c_m}$ while enforcing $m_Z^{PU} < 4m_Z^{OU}$. [4]

5.3.3 Higgs and sparticle mass distributions in the GMM' model for varying n_0

Using Isajet, we scan the GMM' parameter space as follows:

- Fix $m_{3/2} = 20$ TeV which fixes the AMSB contribution to SSB terms.
- Fix $\mu = 200$ GeV for a natural solution to the SUSY μ problem. Doing so enables for arbitrary values of m_Z^{PU} to be generated but disallows any possibility of fine-tuning μ to gain the measured value of the weak-scale in our universe, i.e. m_Z^{OU} .

Then we invoke Douglas *et al*'s power law selection [1, 86, 155] of moduli-mediated SSB terms relative to AMSB contributions within the GMM' model. Therefore, for assumed values of $n_{1/2}$ and n_0 we generate

- $\alpha^{n_{1/2}}$ with α : 3-25, corresponding to a power-law draw for moduli/dilaton mediated gaugino masses M_a ($a = 1 - 3$ over the gauge groups),
- $(a_3\alpha)^{n_0}$: 3-100, which corresponds to a power-law draw of moduli mediated A -terms,
- $(\sqrt{c_{m_3}\alpha^2})^{n_0}$: 3-80, corresponding to a power-law draw on third generation scalar masses $m_0(3)$,
- $(\sqrt{c_m\alpha^2})^{n_0}$: $(\sqrt{c_{m_3}\alpha^2})^{n_0}$ -320 which corresponds to a power-law draw on first/second generation scalar masses $m_0(1, 2)$,
- a power-law statistical selection on $m_{H_d}^2$ via $m_A^{n_0}$ with m_A : 300-10,000 GeV,
- a uniform selection on $\tan\beta$: 3-50 since it is not a soft term.

Furthermore, similar to all other scans presented thus far, the statistical preference to large soft terms is tempered with the ABDS anthropic bound on the weak-scale such that in any

PU, $m_Z^{PU} \lesssim 4m_Z^{OU}$ and that any livable PU must exhibit proper EWSB. Thus, the soft terms can be as big as possible but not too big which would result in a violation of the ABDS condition or lead to no EWSB at all.

To begin exploring our results, we first analyze the probability distribution for the light Higgs mass dP/dm_h vs. m_h generated by a general landscape scan with fixed $n_{1/2} = 1$ but with $n_0 = 1$ (blue) $n_0 = 2$ (red), as depicted in Figure 5.14. We see that both distributions

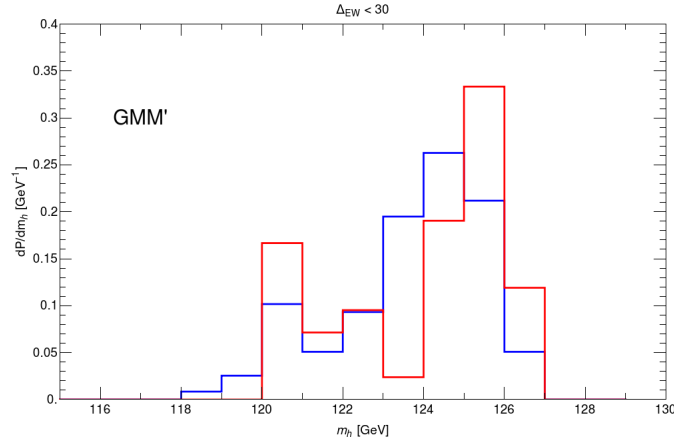


Figure 5.14: Probability distribution dP/dm_h vs. m_h for $n_{1/2} = 1$ and $n_0 = 1$ blue, 2 red for general statistical scans over the GMM' model for $m_{3/2} = 20$ TeV, $\mu = 200$ GeV. [4]

peak at around $m_h \sim 125$ GeV but the general scan with the stronger statistical draw $n_0 = 2$ on scalar and trilinear soft terms peaks more sharply than with the milder draw of $n_0 = 1$. This reaffirms our results for the case $n_0 = 1$ and 2 from the more restricted scan as depicted in Figure 5.13. General scans were also performed with $n = 3, 4$ but these tend to become increasingly inefficient since with such strong power-law draws, one almost always gets pushed into no EWSB or CCB minima or with minima which are vetoed by the ABDS condition, thereby yielding poor statistics to generate reliable distributions [4]. In Figure 5.15 we present mass distributions for a) $dP/dm_{\tilde{g}} vs. m_{\tilde{g}}$, b) $dP/dm_{\tilde{t}_1} vs. m_{\tilde{t}_1}$, c) $dP/dm_{\tilde{t}_2} vs. m_{\tilde{t}_2}$,

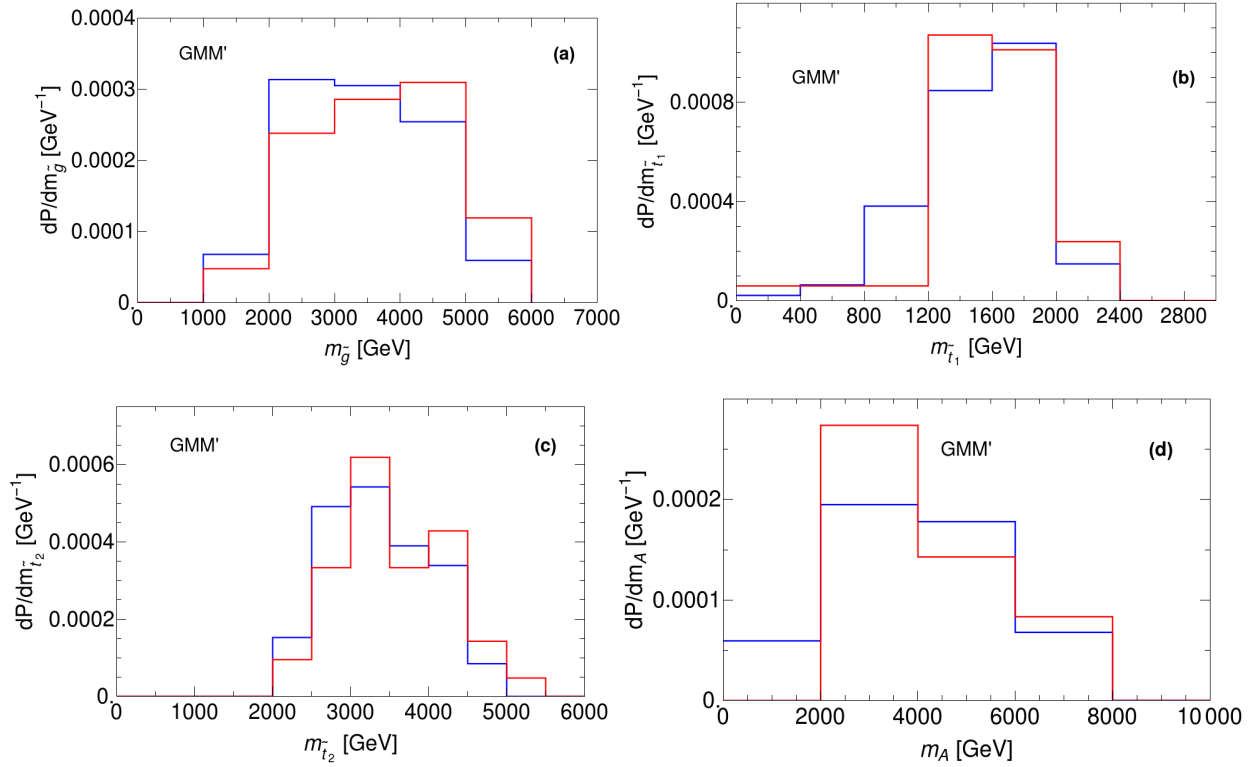


Figure 5.15: Probability distributions of *a)* $m_{\tilde{g}}$, *b)* $m_{\tilde{t}_1}$, *c)* $m_{\tilde{t}_2}$, *d)* m_A for a general landscape scan over the GMM' model for a value of $n_{1/2} = 1$ but with *a)* $n_0 = 1$ (blue), *b)* $n_0 = 2$ (red). For all frames, we take $m_{3/2} = 20$ TeV, $\mu = 200$ GeV and $n_0 = 1$ selection is denoted by blue while $n_0 = 2$ selection is denoted by red. [4]

and *d)* dP/dm_A vs. m_A . In frame *a)*, we observe that for the case with $n_0 = 1$ the landscape prediction for $m_{\tilde{g}}$ is that it most likely lie in the fairly broad 1.5 – 5 TeV range with a peak at ~ 2.5 TeV. For the $n_0 = 2$ case, the landscape prediction exhibits a peak at ~ 4.5 TeV while the broader prediction range is still pretty similar. Thus, contrary to conventional naturalness which would favor much lighter values for $m_{\tilde{g}}$, stringy naturalness seem to favor gluinos to be heavier and beyond current LHC reach and even possibly beyond (5σ) HL-LHC reach which has been computed to be capable of reaching $m_{\tilde{g}} \sim 2.8$ TeV. Thus, an energy upgrade to the HE-LHC ¹, with reach computed with 95% CL to be $m_{\tilde{g}} \lesssim 6$ TeV, may well

¹while this dissertation was being written, CERN decided to abandon the HE-LHC concept and proceed with the Future Circular Collider (FCC) which could operate at $\sqrt{s} = 50 - 100$ TeV.

be required to discover SUSY in the $pp \rightarrow \tilde{g}\tilde{g}X$ channel. The distributions for $m_{\tilde{g}}$ are hardly changed if n_0 is varied since the gaugino mass distribution depends on $n_{1/2}$ instead [4]. In frame b), we see that the landscape probability distribution lies in the 1 – 2 TeV range with a common peak probability around $m_{\tilde{t}_1} \sim 1.5$ TeV for both $n_0 = 1$ and $n_0 = 2$ cases. Current limit from LHC Run 2 is $m_{\tilde{t}_1} \geq 1.1$ TeV [131, 7] which implies that we have just only began to explore the stringy natural parameter space via stop pair production. For comparison, the HE-LHC possibly reaches stop masses up to $\sim 3 - 3.5$ TeV based on 5σ (95% CL) predictions. Thus, again an energy upgrade to the LHC is likely required to encompass the full range of stop masses in landscape SUSY. These distributions are barely influenced by altering n_0 since for fixed $\mu \sim m_{weak}$, the largest contribution to m_{weak} typically comes from $\Sigma_u^u(\tilde{t}_1, \tilde{t}_2)$ which determines the upper bound on $m_{\tilde{t}_1}$ [4]. From frame c) we observe that the landscape prediction for $m_{\tilde{t}_2}$ lies in the 2 – 5 TeV range. Assuming similar reaches of HL- and HE-LHC for $m_{\tilde{t}_2}$ as that for $m_{\tilde{t}_1}$, we would expect the HE-LHC to cover only about half the expected mass range for the heavier top squark eigenstate, \tilde{t}_2 . With larger value of n_0 we notice, in this frame, that the predicted statistical distribution for $m_{\tilde{t}_2}$ shifts to higher $m_{\tilde{t}_2}$ values, as might be expected [4]. Lastly, in frame d), we find the distribution for m_A to lie between $m_A \sim 1 - 8$ TeV with a peak around $m_A \sim 3$ TeV for both $n_0 = 1$ and $n_0 = 2$. The upper bound on m_A arises from the $m_{H_d}^2/(\tan^2 \beta - 1)$ term in the Higgs scalar potential minimization condition (Eq.(4.12)) which is itself restricted by the ABDS condition to not be too far removed from m_{weak}^{PU} . From this perspective, it is not surprising that the Higgs sector appears to be highly SM-like at the LHC thus far since there is a decoupling of heavier Higgs particles embedded primarily in the H_d multiplet while H_u multiplet very closely resembles the SM Higgs [4]. Finally, in Figure 5.16 we show the string landscape prediction for first/second generation

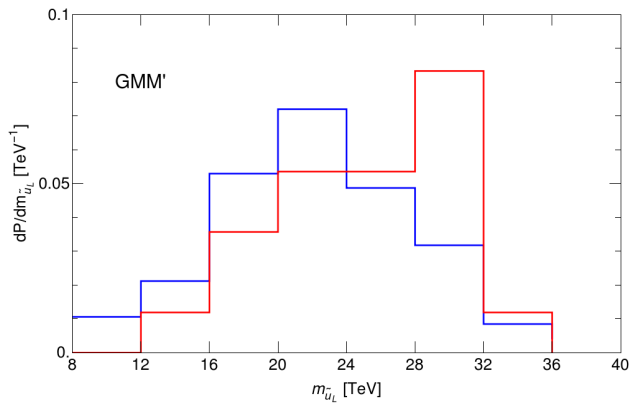


Figure 5.16: Probability distribution $dP/dm_{\tilde{u}_L}$ vs. $m_{\tilde{u}_L}$ for $n_{1/2} = 1$ and $n_0 = 1$ blue, 2 red for general statistical scans over the GMM' model for $m_{3/2} = 20$ TeV, $\mu = 200$ GeV. [4]

scalars as typified by $m_{\tilde{u}_L}$. For the case $n_0 = 1$, then we see that $m_{\tilde{u}_L}$ lie in the range 10 – 35 TeV with a distribution peaking at around $m_{\tilde{u}_L} \sim 22$ TeV. The upper bound on first/second generation scalars arises from 2-loop RGE contributions which can drive top-squark soft terms tachyonic if they get too big, rather than from Yukawa terms (tiny) or D -terms (which largely cancel). As n_0 is increased to 2, then the distribution in $m_{\tilde{u}_L}$ hardens even further with a peak around $m_{\tilde{u}_L} \sim 30$ TeV. Both first and second generation matter scalars are drawn to a common upper bound since the 2-loop RGE terms are flavor independent [4]. This provides a mixed quasi-degeneracy/decoupling solution to the SUSY flavor and CP problems [111], as discussed earlier. All results from general scans of the GMM' parameter space are summarized in the Table 5.1.

mass	$n_0 = 1$	$n_0 = 2$
m_h	125_{-4}^{+1} GeV	125_{-4}^{+1} GeV
$m_{\tilde{g}}$	3.5 ± 2.5 TeV	4 ± 2 TeV
$m_{\tilde{t}_1}$	1.6 ± 0.8 TeV	1.6 ± 0.8 TeV
$m_{\tilde{t}_2}$	3.5 ± 1.5 TeV	3.5 ± 1.5 TeV
m_A	4 ± 2 TeV	4 ± 2 TeV
$m_{\tilde{f}}(1, 2)$	22 ± 10 TeV	30_{-18}^{+6}

Table 5.1: Expected range of Higgs and sparticle masses in the GMM' model from the string landscape with $n_{1/2} = 1$ but with $n_0 = 1$ or $n_0 = 2$.

5.4 Results from Dynamical SUSY breaking in the landscape

From observing nature at a fundamental level we notice different mass scales which seem to obey a hierarchy such that $M_P \gg m_{GUT} \gg m_{weak}$ where M_P is the Planck mass. Looking for an answer as to why this hierarchy is observed is one of the principle goals of particle physics. In QCD, we have an answer: the hadronic mass scale can arise when the gauge coupling evolves to large values such that the fundamental constituents, the quarks, condense to form bound states. From dimensional transmutation, the proton mass can be found even in terms of the Planck mass M_P via $m_{proton} \simeq M_P \exp(-8\pi^2/g^2)$ which yields the correct answer for $g^2 \sim 1.8$ [5]. We have already seen how supersymmetrization of the SM lead to cancellation of quadratic divergences in m_h which otherwise would cause the Higgs mass to blow up to the highest mass scale Λ . Upon implementation of SUSY one is left with only logarithmically divergent contributions to m_h and in fact the MSSM can even be valid up to the GUT or even the Planck scales. Additionally, the weak-scale emerges as a derived consequence of the visible sector SUSY breaking scale m_{soft} which then shifts the concern with the origin of the weak-scale to the origin of the SUSY breaking scale. In gravity-mediated SUSY breaking models, it is common to impose the condition that SUSY is broken spontaneously at the tree level in the hidden sector, possibly via the SUSY breaking Polonyi superpotential: $\hat{W} = m_{hidden}^2(\hat{h} + \beta)$ where \hat{h} is the only hidden sector field. For $\beta = (2 - \sqrt{3})m_P$ (with m_P as the reduced Planck mass $m_P \equiv M_P/\sqrt{8\pi}$) and $m_{hidden} \sim 10^{11}$ GeV, one determines $m_{soft} \sim m_{3/2} \sim m_{weak}$. Thus, the exponentially-suppressed hidden sector mass scale must be put in by hand so that SSB can only accommodate the magnitude of the weak-scale without providing any explanation [5].

A more attractive approach to address the issue of the apparent hierarchy between mass scales follows from the wisdom of QCD, whereby one generates the SUSY breaking scale from dimensional transmutation which then automatically yields an exponential suppression. This is especially desirable in string models where there is only a single mass scale i.e. M_P . Then one could arrange for *dynamical SUSY breaking* (DSB) [156, 157, 158, 159] wherein breaking of SUSY occurs non-perturbatively. One possibility that enables DSB is via hidden sector gaugino condensation [160], where a hidden sector gauge group $SU(N)$ becomes confining at the scale Λ_{GC} and a gaugino condensate occurs with $\langle\lambda\lambda\rangle \sim \Lambda_{GC}^3$ leading to SUSY breaking with the soft terms $m_{soft} \sim \Lambda_{GC}^3/m_P^2$. The associated mass scale [161] is then given by,

$$m_{hidden}^2 \sim m_P^2 \exp\left(-8\pi^2/g_{hidden}^2\right) \quad (5.15)$$

where $m_{hidden}^2 \sim \Lambda_{GC}^3/m_P$. In this case, g_{hidden} is the coupling constant of the confining hidden sector gauge group. It has been shown by Denef and Douglas [84] and by Dine *et al.* [162, 163] that the coupling g_{hidden}^2 is expected to scan uniformly on the landscape, as depicted in Figure 5.17. From Figure 5.17 we can infer that a uniform distribution of soft breaking terms on a log scale are expected i.e. each possible decade of values for m_{soft} is as likely as any other decade [5]. Thus, with $m_{soft} \sim m_{hidden}^2/m_P \sim \Lambda_{GC}^3$, we would expect [164]

$$f_{SUSY}^{DSB} \sim 1/(m_{soft} \log(m_{soft})) \sim 1/m_{soft} \quad (5.16)$$

which provides a uniform distribution of m_{soft} across the decades of possible values. Such a distribution of course favors the lower range of soft term values [5].

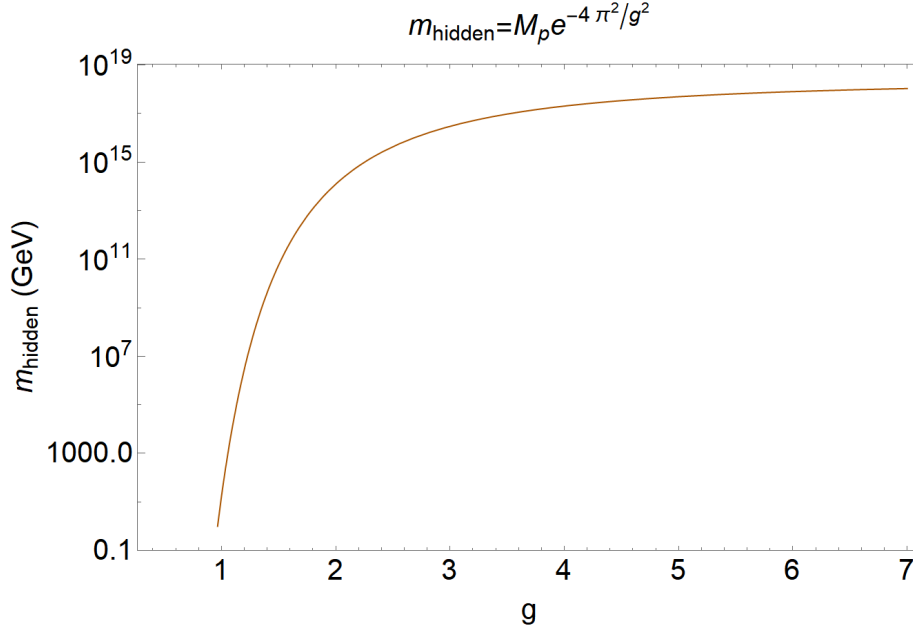


Figure 5.17: Expected SUSY breaking scale m_{hidden} vs. hidden sector coupling g^2 from DSB. [5]

Another possibility is non-perturbative SUSY breaking via instanton effects which similarly leads to an exponential suppression of mass scales [165]. Evidently, at this point the mass scale selection problem has been transferred to the selection of an appropriate value of g_{hidden}^2 [5].

The string landscape picture also proposes its own solution to the origin of mass scales that relies on analyzing the vast array of string vacua of estimated order $\sim 10^{500} - 10^{272,000}$ [84, 166] in II-B flux compactifications [34]. As we have extensively studied in this work thus far, in the landscape with spontaneous SUSY breaking, the F_i and D_α breaking terms are distributed uniformly with the soft terms enjoying a statistical power-law draw $f_{SUSY}^{SSB} \sim m_{soft}^n$ such that $n = 2n_F + n_D - 1$ determine the overall SUSY breaking scale. Such a distribution would tend to favor SUSY breaking at the highest possible mass scales for $n \geq 1$. In fact, it was analyzed in Ref. [167] that the distributions of SUSY breaking scales from vacua for KKLT [41] and LVS [168] flux compactifications resulted in $f_{SUSY} \sim m_{soft}^1$ and $m_{soft} \sim 1/m_{soft}$ respectively

[6]. Furthermore we require an anthropic veto of landscape vacua with no EWSB, those with CCB and those vacua that result in a weak-scale that violates the ABDS anthropic constraint. Thus restricting to such livable vacua tempers the draw to large soft terms such that these terms are not drawn too large such that one ends up in a phenomenologically un-viable vacua with too large a weak-scale or with no EWSB or with CCB.

In this section, we examine the likelihood of habitable vacua exhibiting DSB in the landscape and compare it with the case of SSB in the landscape.

5.4.1 Higgs and sparticle mass distributions in the landscape with DSB

We present the results of calculation of the string landscape probability distributions for the Higgs and sparticle masses under the assumption of $f_{SUSY}^{DSB} \sim 1/m_{soft}$ along with the anthropic condition $f_{EWFT} = \Theta(30 - \Delta_{EW})$ while also vetoing CCB or no EWSB vacua. Our calculations are done within the gravity-mediated three extra parameter Higgs model NUHM3 with the parameter space given by [64, 65, 66, 67, 67, 68, 69]

$$m_0(1,2), m_0(3), m_{1/2}, A_0, \tan\beta, \mu, m_A \text{ (NUHM3)}.$$

We again choose the Isajet [81] SUSY spectrum generator to analyze this parameter space.

We then compare our results with similar calculations performed using the statistical draw

$f_{SUSY}^{SSB} \sim m_{soft}^2$ motivated from [85]. Both these scans are performed over the same space

$$m_0(1, 2) : 0.1 - 60 \text{ TeV}$$

$$m_0(3) : 0.1 - 20 \text{ TeV}$$

$$m_{1/2} : 0.5 - 10 \text{ TeV}$$

$$- A_0 : 0 - 50 \text{ TeV}$$

$$m_A : 0.3 - 10 \text{ TeV}$$

$$\tan \beta : 3 - 60$$

$$\mu = 150 \text{ GeV}.$$

The upper limits to our scan parameter were chosen such that these lie beyond upper bounds imposed by anthropic selection from f_{EFT} . Lower limits are motivated by current LHC search limits, but must also stay clear from the singularity in the f_{SUSY}^{DSB} distribution. Furthermore, fixing μ barely affects our final results since it is chosen to be close to $m_{W,Z,h} \sim 100 \text{ GeV}$ while the soft terms scan as expected in DSB (i.e. $f_{SUSY}^{DSB} \sim 1/m_{soft}$) and SSB (i.e. $f_{SUSY}^{SSB} \sim m_{soft}^n$ with $n = 2$) in independent scans.

The first set of results are presented in four frames shown in Figure 5.18 where we show the distributions for the input Isajet [81] soft parameters. In frame *a*) we show the probability distribution of soft breaking first/second generation scalars $m_0(1, 2)$ from a scan over the NUHM3 parameter space with soft term scanned as f_{SUSY}^{DSB} (in gray) and f_{SUSY}^{SSB} . From this plane we notice that for the case with f_{SUSY}^{DSB} the peak distribution occurs at the lowest allowed $m_0(1, 2)$ values with a tail extending to about $m_0(1, 2) \sim 10 \text{ TeV}$. Thus, one would expect

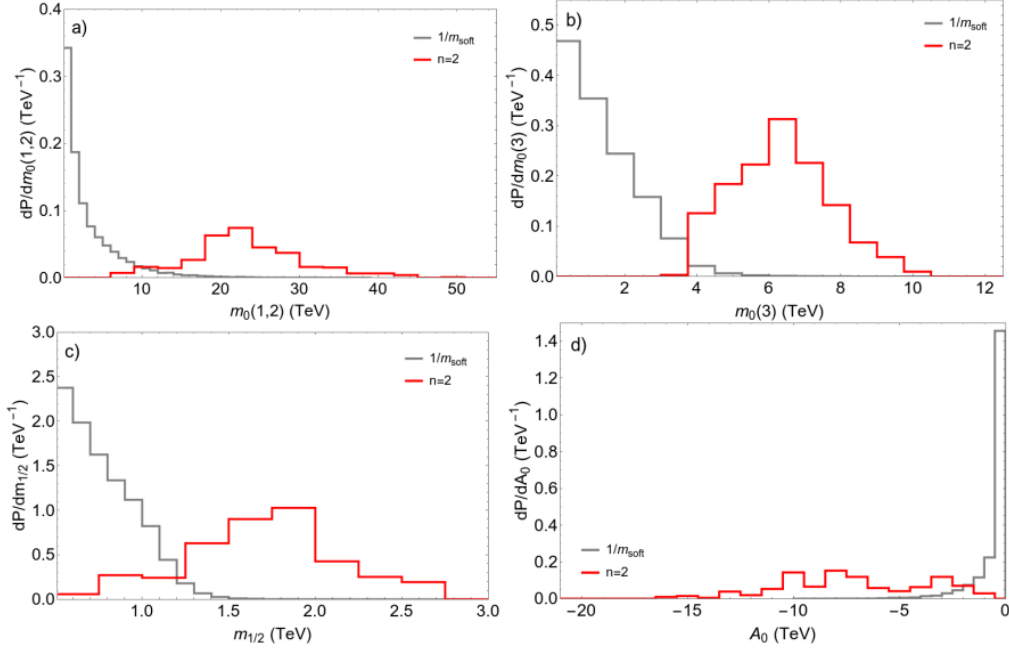


Figure 5.18: Probability distributions of *a)* $m_0(1,2)$, *b)* $m_0(3)$, *c)* $m_{1/2}$, *d)* A_0 for a landscape scan with $f_{SUSY}^{DSB} \sim 1/m_{soft}$ distribution of soft terms (in gray) with $\mu = 150$ GeV. For comparison, we also show the probability distribution for $f_{SUSY}^{SSB} \sim m_{soft}^2$. [5]

relatively light, LHC accessible squarks and sleptons from gravity mediation with DSB in the hidden sector. On the contrary, for f_{SUSY}^{SSB} , the peak occurs at $m_0(1,2) \sim 25$ TeV but they can also be heavier, as signified by the distribution tail extending beyond 40 TeV [5]; such heavy $m_0(1,2)$ states reflects the mixed decoupling/quasi-degeneracy solution to the SUSY flavor and CP problems [111]. In frame *b)* we see the third generation scalar mass probability distributions scanned with f_{SUSY}^{DSB} and with f_{SUSY}^{SSB} . Here again, gravity mediation with DSB in the hidden sector seem to prefer lighter third generation squarks and sleptons signified by the gray distribution peaking around $m_0(3) \sim 1$ TeV with a tail barely extending to ~ 4 TeV (lest $\Sigma_u^u(\tilde{t}_{1,2})$ becomes too large). In contrast, gravity mediation with f_{SUSY}^{SSB} in the hidden sector prefers heavier third generation scalars with distribution peaking at $m_0(3) \sim 7$ TeV

with a tail extending to beyond 12 TeV [5]. Next, in frame *c*) we show the universal gaugino mass $m_{1/2}$ probability distributions for the two cases. Like the previous soft terms, DSB prefers light gauginos as compared to SSB with the gray distribution peaking at much smaller values than is the case with the $n = 2$ (red) distribution peaking just below 2 TeV. Finally, in frame *d*) showing the probability distribution for the trilinear soft terms $-A_0$ shows a similar trend. In the DSB scenario, the most likely expectation from gravity mediation is $A_0 \sim 0$ TeV while in the case with $n = 2$ SSB peak probability arises at $A_0 \sim -4$ TeV and -7 TeV with tails extending higher up to ~ -15 TeV. Larger (negative) values of A_0 as preferred by SSB with $n = 2$ power law draw, allows for large mixing in the stop sector which consequently gives rise to larger m_h [5].

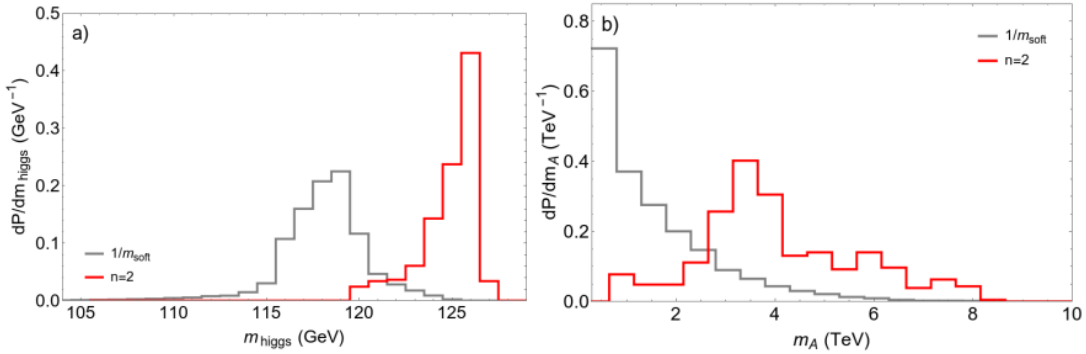


Figure 5.19: Probability distributions of a) m_{higgs} , and b) m_A , for a landscape scan with $f_{SUSY}^{DSB} \sim 1/m_{soft}$ distribution of soft terms (in gray) with $\mu = 150$ GeV. For comparison, we also show the probability distribution for $f_{SUSY}^{SSB} \sim m_{soft}^2$. [5]

The light and heavy Higgs mass probability distributions are presented in Figure 5.19 in frames a) and b) respectively. In frame a), for the case of f_{SUSY}^{DSB} we notice the light Higgs mass peaking at $m_h \sim 118$ GeV with almost no probability extending to ~ 125 GeV, in obvious contradiction with observation. On the other hand, for the case of SSB the distribution

exhibits a sharp peak at $m_h \sim 125 - 126$ GeV which is a result of large trilinear soft terms [5]. The pseudoscalar Higgs mass distributions are depicted in frame *b*) where again DSB seems to predict much lighter $m_A \sim 100 - 200$ GeV leading to large mixing in the Higgs sector and consequently observable deviations in Higgs couplings (see Ref. [144]). Alternatively, the SSB $n = 2$ distribution peaks at $m_A \sim 4$ TeV with a tail extending to ~ 8 TeV. In the latter case, we would expect a decoupled Higgs sector with a very SM-like lightest Higgs scalar h , as suggested by ATLAS/CMS data [5].

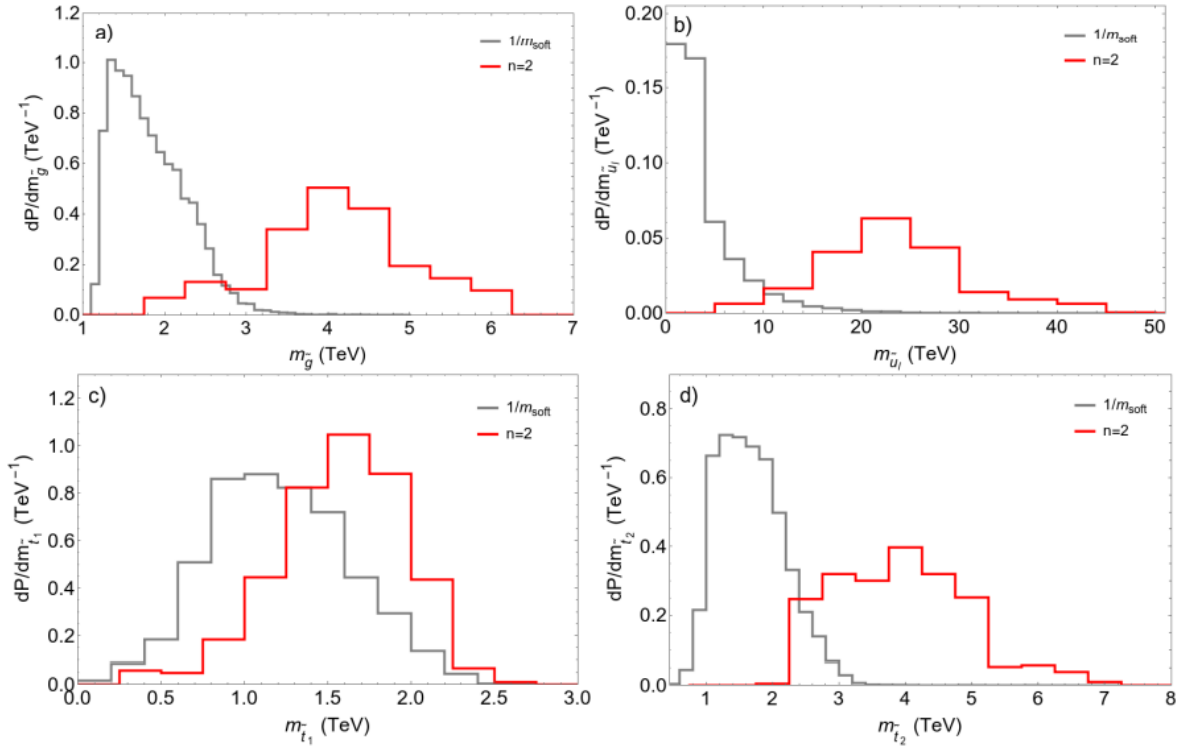


Figure 5.20: Probability distributions of a) $m_{\tilde{g}}$, b) $m_{\tilde{u}_L}$, c) $m_{\tilde{t}_1}$, d) $m_{\tilde{t}_2}$ for a landscape scan with $f_{SUSY}^{DSB} \sim 1/m_{soft}$ distribution of soft terms (in gray) with $\mu = 150$ GeV. For comparison, we also show the probability distribution for $f_{SUSY}^{SSB} \sim m_{soft}^2$. [5]

The final set of results from this analysis is depicted in Figure 5.20. In frame *a*), we show the gluino mass probability distribution; of note here is that the DSB distribution peaks at

~ 1 TeV in sharp contrast with current LHC exclusion limit $m_{\tilde{g}} \lesssim 2.25$ TeV [153, 154]. The SSB distribution however peaks at $\sim 4 - 5$ TeV. The tail of the DSB distribution barely extend beyond ~ 3.5 TeV whereas the SSB distribution tail reaches ~ 6 TeV with almost all of the most likely regions of parameter space lying safely beyond LHC reach. In frame *b*) we show the mass distribution for first generation squark mass m_{u_L} which typifies all first/second generation matter scalars. We see the DSB distribution peaking around $\sim 0 - 3$ TeV range with a tail extending to ~ 10 TeV, which also seemingly excludes them based on LHC limits. The SSB distribution with $n = 2$, on the other hand, peaks $\gtrsim 20$ TeV with a tail reaching beyond ~ 40 TeV, rendering these too heavy for the LHC. Frame *c*) depicts the lighter top squark mass $m_{\tilde{t}_1}$ distribution with DSB yielding peak ~ 1 TeV with reach up to ~ 2.5 TeV. This is stringently bounded by LHC search limit of $m_{\tilde{t}_1} \gtrsim 1.1$ TeV. The SSB distribution for $m_{\tilde{t}_1}$ in contrast exhibits peak at ~ 1.6 TeV with most of the SSB parameter space still open to explore for the LHC. Finally, the heavier top squark $m_{\tilde{t}_2}$ distribution is shown in frame *d*) where the DSB peak occurs at $m_{\tilde{t}_2} \sim 1.5$ TeV whilst the SSB peak occurs at heavier $m_{\tilde{t}_2} \sim 4$ TeV. Thus, substantially heavier \tilde{t}_2 squarks are expected from SSB as opposed to DSB [5].

The common feature that emerges from our exploration of the DSB parameter space (in gravity mediation) suggests much lighter squarks and gauginos, as opposed to SSB parameter space. Furthermore the DSB Higgs mass seems to be much lighter as opposed to observation. Therefore, currently available LHC data seems to rule out almost all of the DSB parameter space while most of the SSB parameter space remains well beyond current search capabilities.

5.5 Examination of soft terms drawn logarithmically on the landscape

As seen in the previous section, for a DSB type scenario in the context of the landscape, the hidden sector gauge coupling g_{hidden}^2 is uniformly distributed within various pocket universes [84] such that the resultant SUSY breaking distribution f_{SUSY} is distributed somewhat uniformly over the decades of values, as shown in Figure 5.17. Then it might also be expected that the soft terms are distributed as a slowly rising (log) distribution. Similar log or log times a power law distribution of soft terms has been advanced by Dine *et al.* previously [163, 164, 169, 170] and has also been an expectation arising out of non-perturbative SUSY breaking due to instanton effects [165]. Motivated by these arguments, it might be interesting to investigate the case in which one employs a milder statistical draw of soft terms on the landscape. As such, in this section we choose a logarithmic draw on soft masses which is indeed much milder than power law draws but still stronger than the $f_{SUSY} \sim 1/m_{soft}$ draw expected from the DSB case investigated in the previous section. Given these, we calculate the statistical distributions of Higgs and sparticle masses in the NUHM3 gravity mediation model assuming a log draw on soft terms i.e. $f_{SUSY} = \log(m_{soft})$. In this study we again use the SUSY spectrum generator Isajet [81] for our calculations.

5.5.1 Higgs and sparticle mass distributions in the landscape with logarithmic draw on soft terms

For the study, we want to compare our results with similar calculations performed by assuming $f_{SUSY} = m_{soft}^n$ in Ref. [85] and to that end we use the same parameter range as in

the last section for our scan,

$$m_0(1, 2) : 0.1 - 60 \text{ TeV}$$

$$m_0(3) : 0.1 - 20 \text{ TeV}$$

$$m_{1/2} : 0.5 - 10 \text{ TeV}$$

$$- A_0 : 0 - 50 \text{ TeV}$$

$$m_A : 0.3 - 10 \text{ TeV}$$

$$\tan \beta : 3 - 60$$

$$\mu = 150 \text{ GeV},$$

wherein all soft parameters are scanned assuming $f_{SUSY} = \log(m_{soft})$ while the superpotential μ term is fixed and $\tan \beta$ is scanned uniformly. The motivations for the selection of upper and lower limits of our scan ranges are the same as for the last section. Furthermore, only the parameter value that successfully create a phenomenologically viable vacua with no CCB, proper EWSB and with $m_{weak}^{PU} \lesssim 4m_{weak}^{OU} \implies \Delta_{EW} \lesssim 30$ are considered relevant for our purposes. The first set of results are shown in Figure 5.21 where we present the probability distributions of input parameters $m_0(1, 2), m_0(3), m_{1/2}$, and A_0 . The $f_{SUSY} = \log(m_{soft})$ distributions are shown as shaded histograms and are compared to scans done for $f_{SUSY} = m_{soft}^n$ with $n = 0$ (typical uniform scan shown in green) and the simplest power law scan with $n = 1$ shown in red. A general trend can be observed from the set of results as expected: the logarithmic draw on soft terms is much milder than the $n = 1$ power law draw but stronger than the uniform selection of soft terms with $n = 0$. In Figure 5.21 frame *a*) we present the probability distributions of first/second generation scalar masses $m_0(1, 2)$ and from the plot one notes that the peak distribution for the log draw occurs at $\sim 10 - 20$ TeV.

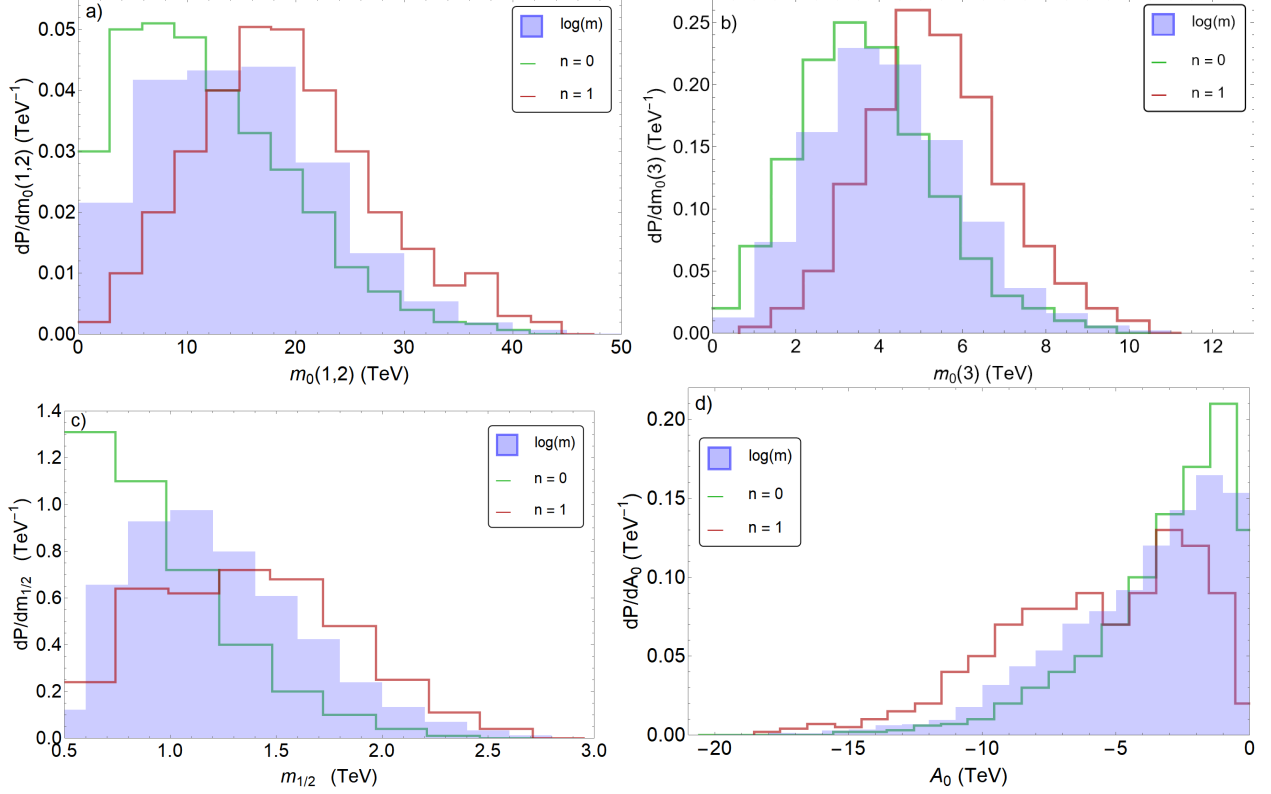


Figure 5.21: Probability distributions of *a*) $m_0(1, 2)$, *b*) $m_0(3)$, *c*) $m_{1/2}$, *d*) A_0 for a scan over the NUHM3 model from a log distribution of soft terms in the string landscape (shaded blue) as compared to distributions with $n = 0$ green, 1 red. For all frames, we fix $\mu = 150$ GeV and [6].

Compared to this, the $n = 1$ draw pulls the distribution more strongly obtaining peaks at $\sim 15 - 20$ TeV whereas the $n = 0$ uniform draw is much milder with peaks < 10 TeV. All three distributions exhibit a long tail extending to $\gtrsim 40$ TeV implying that such large values still potentially provide the mixed decoupling/quasi-degeneracy landscape solution to the SUSY flavor and CP problems, albeit with a small probability. In frame *b*) we depict the third generation scalar $m_0(3)$ probability distributions and again notice that the distribution with $f_{SUSY} = \log(m_{soft})$, with peak probability at ~ 4 TeV, is intermediate between the $n = 0$ and $n = 1$ histograms. Frame *c*) shows a similar trend for the unified gaugino mass $m_{1/2}$ distribution with the log draw yielding peaks at ~ 1.2 TeV with a tail extending to

~ 2.5 TeV; comparatively, the $n = 0$ draw exhibits peaks at only a few TeV range while the $n = 1$ draw shows peaks at much heavier $m_{1/2} \sim 1.5$ TeV, with long tails extending to $m_{1/2} \gtrsim 2.5$ TeV. Finally, in frame *d*) the distribution in $-A_0$ is shown where we see a clear preference for small $|A_0|$ for the $n = 0$ peak occurring at much smaller $|A_0|$ values than for $n = 1$ with peaks at ~ -3.5 TeV and a significant bulge at ~ -7 TeV or for log distribution wherein peak probability occurs at a higher (negative) value of A_0 than was the case for $n = 0$ draw. The smaller A_0 values signal a small mixing in the stop sector which lead to too light of a Higgs mass while large A_0 values seem necessary for maintaining $m_Z^{PU} \lesssim 4m_Z^{OU}$ on account of large cancellations occurring in the Σ_u^u terms. However, anthropic veto of CCB vacua constrains how large A_0 can be and so the distributions in all three cases diminish beyond the peak A_0 values [6].

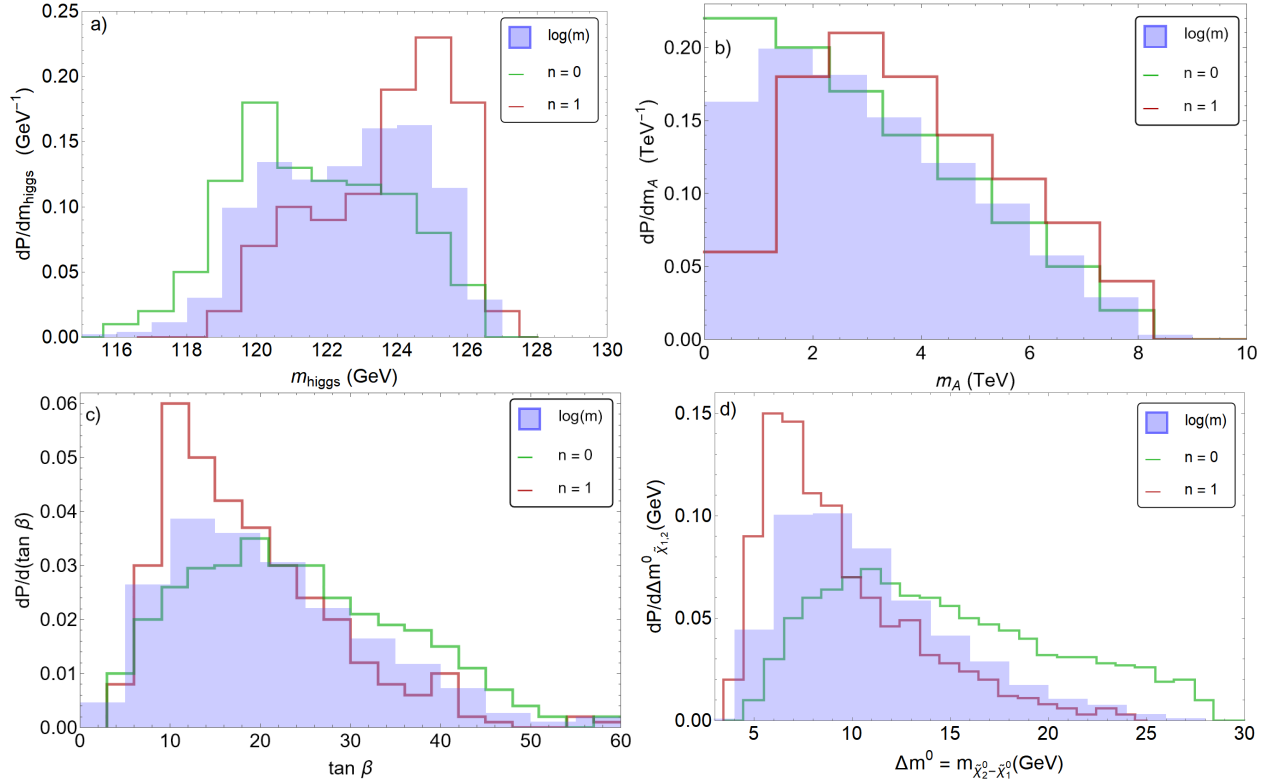


Figure 5.22: Probability distributions of *a*) m_h , *b*) m_A , *c*) $\tan \beta$, *d*) $\Delta m^0 = m_{\tilde{\chi}_2^0} - m_{\tilde{\chi}_1^0}$ for a scan over the NUHM3 model from a log distribution of soft terms in the string landscape (shaded blue) as compared to distributions with $n = 0$ green, 1 red. For all frames, we fix $\mu = 150$ GeV and [6].

Furthermore, in Figure 5.22 we show various probability distributions pertaining to the Higgs/higgsino sector. In Figure 5.22 frame *a*) we present distributions of the resulting light Higgs mass distributions for the three types of statistical draws on soft terms. We notice that with a log distribution of soft terms, the m_h distribution almost has a two-peak structure: a dominant peak around $m_h \sim 125$ GeV and a sub-dominant $m_h \sim 120$ GeV. The dominant large m_h peak coincides with the large $|A_0|$ bulge of Figure 5.21 frame *d*) which leads to large stop mixing lifting the light Higgs mass up to ~ 125 GeV. Thus, for habitable PU with no CCB and proper EWSB with the weak-scale within ABDS bounds, to have a light Higgs with mass similar to what is observed at the LHC, the A_0 term is drawn to as large as possible without violating the aforementioned features of the observable world. This situation is further illustrated in the m_h vs. A_0 plane in Figure 5.23 where we explicitly see a correlation between large $-A_0$ and large $m_h \simeq 125$ GeV. This is a testable prediction of the string landscape picture: a value of $m_h \sim 125$ GeV is reflective of large stop mixing which can be untangled for instance at an e^+e^- collider operating at $\sqrt{s} > 2m_{\tilde{t}_1}$ [171]. Other stringy scenarios - such as G2MSSM [172] or mini-split SUSY [92, 93] obtain $m_h \sim 125$ GeV via very heavy (unnatural) top squarks but with rather small stop mixing. The low $m_h \sim 120$ GeV bump comes from small stop mixing with $-A_0 \lesssim 1$ TeV [6].

In Figure 5.22 frame *b*) we show the pseudoscalar m_A mass distribution where we see peaks around $m_A \sim 1.5 - 2$ TeV with a long tail extending as high as 8 TeV. The upper limit on m_A arises from the $m_{H_d}^2/\tan^2\beta$ contribution to the weak-scale in,

$$\begin{aligned} \frac{m_Z^2}{2} &= \frac{m_{H_d}^2 + \Sigma_d^d - (m_{H_u}^2 + \Sigma_u^u) \tan^2\beta}{\tan^2\beta - 1} - \mu^2 \\ &\simeq -m_{H_u}^2 - \mu^2 - \Sigma_u^u(\tilde{t}_{1,2}). \end{aligned}$$

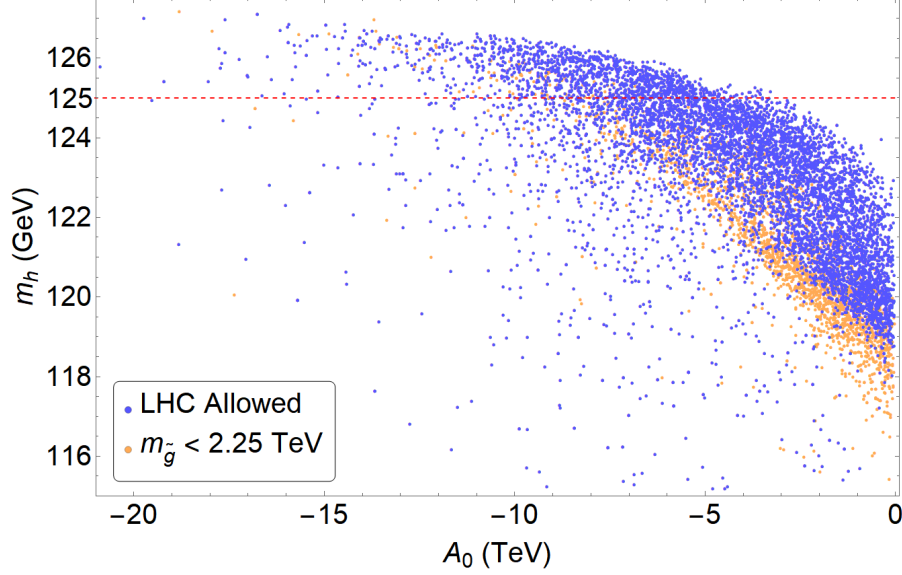


Figure 5.23: Scatter plot of models with appropriate EWSB and $m_Z^{PU} < 4m_Z^{OU}$ in the m_h vs. A_0 plane with $\mu = 150$ GeV. [6]

For $\tan \beta \sim 10$, then $m_A \lesssim 3$ TeV but as $\tan \beta$ gets larger $m_A \sim m_{H_d}$ can become much bigger, as depicted explicitly in Figure 5.24 in the $\tan \beta - m_A$ plane. Such large values of $m_A \gg m_h$ (and consequently m_H and m_{H^\pm}) predict that the Higgs sector looks decoupled, with h behaving largely as a SM-like Higgs boson. Thus, the landscape SUSY prediction is that precision Higgs measurements at HL-LHC or an e^+e^- Higgs factory will see at best only small deviations from SM Higgs properties [6]. Next, in Figure 5.22 frame *c*) we show the probability distribution for $\tan \beta$ which is scanned uniformly in the landscape. The observed trend shows the most probable $\tan \beta$ value lies in the range $\tan \beta \sim 10 - 20$ with a falling tail towards larger values. Large values for $\tan \beta$ yields large bottom squark $\Sigma_u^u(\tilde{b}_1, \tilde{b}_2)$ and tau-lepton contributions to the weak-scale and so is disfavored [6].

In Figure 5.22 frame *d*) we show the light higgsino mass gap $\Delta m^0 \equiv m_{\tilde{\chi}_2^0} - m_{\tilde{\chi}_1^0}$, which is relevant to light higgsino pair production at the LHC via the soft OSDLJMET channel [94, 133, 139, 140, 141, 173, 174, 175]. The prediction with regards to this plane is that a

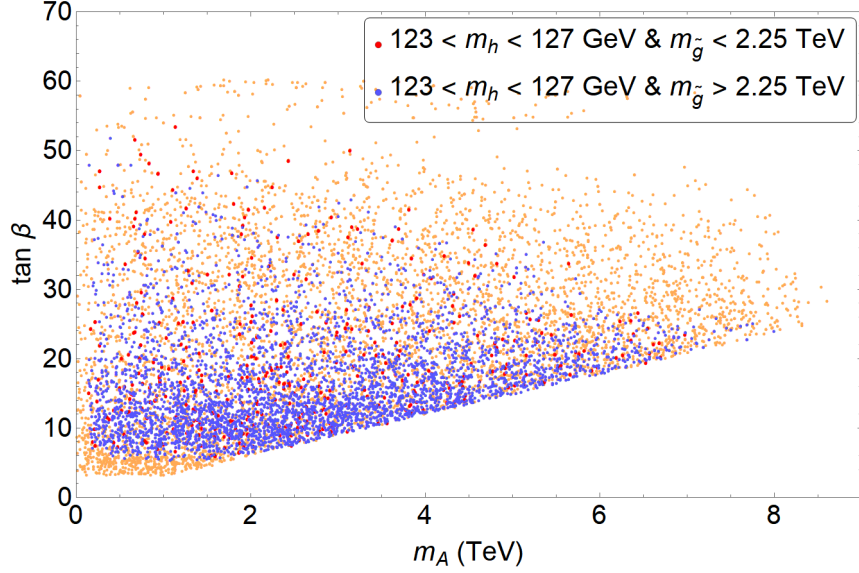


Figure 5.24: Scatter plot of models with appropriate EWSB and $m_Z^{PU} < 4m_Z^{OU}$ in the m_A vs. $\tan\beta$ plane with $\mu = 150$ GeV. The orange dots have $m_h < 123$ GeV. [6]

broad peak probability occurs in the $\Delta m^0 \sim 8 - 10$ GeV range with a tail extending to $15 - 25$ GeV for the case with logarithmic draw on soft terms. However, the large $\Delta m^0 > 14$ GeV tail corresponds to models with too small a light Higgs mass i.e. $m_h < 123$ GeV in addition to yielding $m_{\tilde{g}} \lesssim 2.25$ TeV, as can be seen by the orange dots in the scatter plot for the same scan presented in the m_h vs. Δm^0 plane in Figure 5.25. We see that only the blue points occurring for the smallest $\Delta m^0 \sim 5 - 12$ GeV are LHC safe and as the mass gap gets larger we are pushed into regions ruled out by the LHC. In contrast, the $n = 0$ draw predicts much larger mass gaps while for $n = 1$ power law draw on soft terms predicts $\Delta m^0 \lesssim 10$ GeV [6].

In Figure 5.26 we present probability distributions for various strongly interacting sparticles which are relevant for LHC SUSY searches. Frame *a*) depicts the gluino mass probability distribution $dP/dm_{\tilde{g}}$; we see the log distribution peaking at $\sim m_{\tilde{g}} \gtrsim 2.5 - 3$ TeV, somewhat

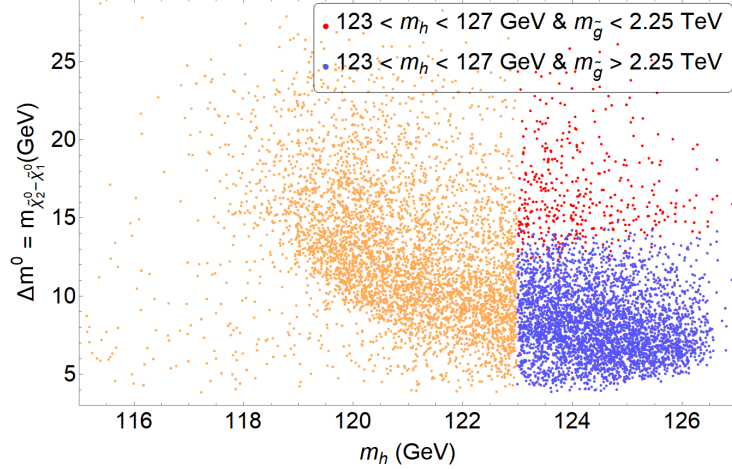


Figure 5.25: Scatter plot of models with appropriate EWSB and $m_Z^{PU} < 4m_Z^{OU}$ in the m_h vs. Δm^0 plane with $\mu = 150$ GeV. The orange dots have $m_h < 123$ GeV. [6]

beyond current LHC limits that require $m_{\tilde{g}} \gtrsim 2.25$ TeV. Thus, a small portion of the log parameter space seems excluded by the present gluino mass limit so that from the perspective of the landscape, it is not surprising that gluino has eluded LHC detection so far. The distribution tails off to $m_{\tilde{g}} \sim 5 - 6$ TeV which implies that an exhaustive search for landscape gluinos would require an energy doubling upgrade to HE-LHC [176, 177]. In the next frame b), an example of the first/second generation squarks typified by $m_{\tilde{u}_i}$ where we notice a broad peak structure at $m_{\tilde{u}_L} \sim 10 - 20$ TeV with a tail extending to ~ 40 TeV. Such high values for the first/second generation squarks are possible since these soft masses are pulled as high as possible in the landscape until their 2-loop RGE contributions to the top squark sector cause these soft terms to run tachyonic resulting in CCB vacua [6]. In frame c) we show implications of a log draw on soft terms for third generation squark mass distributions $dP/dm_{\tilde{t}_1}$, compared with $n = 0$ and $n = 1$ draws. For the log distribution we notice a peak at ~ 1.5 TeV which is again beyond current LHC mass limit of $m_{\tilde{t}_1} \gtrsim 1.1$ TeV. Thus, from the point of view of the landscape it is not surprising that LHC has not observed top-squarks

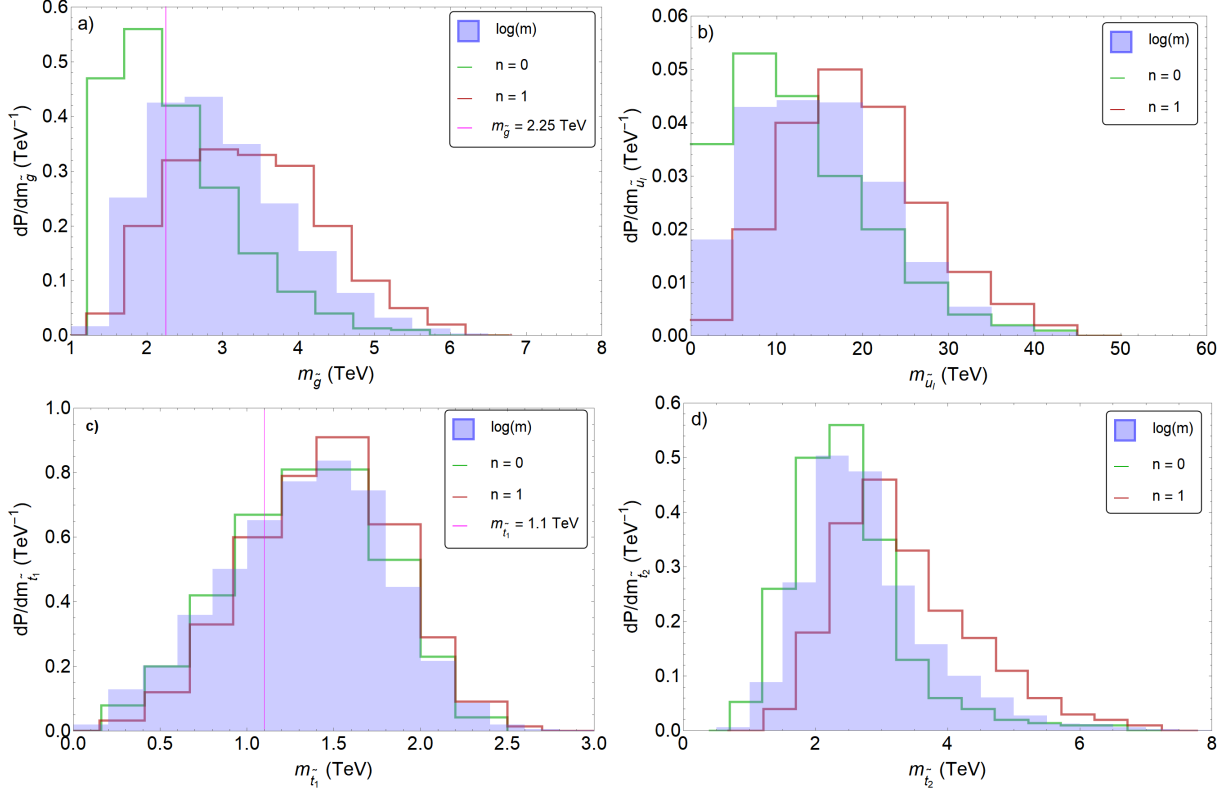


Figure 5.26: Probability distributions of *a)* $m_{\tilde{g}}$, *b)* $m_{\tilde{u}_l}$, *c)* $m_{\tilde{t}_1}$, *d)* $m_{\tilde{t}_2}$ for a scan over the NUHM3 model from a log distribution of soft terms in the string landscape (shaded blue) as compared to distributions with $n = 0$ green , 1 red. For all frames, we fix $\mu = 150$ GeV [6].

since they can be as heavy as $\gtrsim 2.5$ TeV as typified by the distribution tail [6]. Frame *d)* depicts the distribution $dP/dm_{\tilde{t}_2}$ (the heavier top squark eigenstate) which exhibits peaks at $m_{\tilde{t}_2} \sim 3$ TeV with a tail ranging upwards of $\gtrsim 6$ TeV [6].

Thus, we now summarize landscape expectations from various statistical distributions of soft terms arising from employing different moduli stabilization schemes, in Table 5.2. Our calculation show that the landscape prefers power law distribution on soft terms i.e. $f_{SUSY} \sim m_{soft}^n$ with $n = 1$, or 2 rather than a uniform distribution of soft terms for which $n = 0$. Furthermore, we see a general trend in our results in that the case for which $f_{SUSY} \sim \log(m_{soft})$ is intermediate between $n = 0$ and $n = 1$ draw. As such, we see from

model	KKLT [41]	LVS [168]	PS [178]
soft terms	mirage	gravity	gravity
soft dist.	m_{soft}^n	m_{soft}^{-1}	m_{soft}^n
mass dist'ns	[145]	[6]	[85]

Table 5.2: Three models of moduli stabilization along with expected form of soft terms, expected soft term distribution in string II-B landscape and reference for associated statistical distributions of Higgs and sparticle masses. [6]

Figure 5.22 frame *a*), expectations for $m_h \simeq 125$ GeV still holds for a log distribution of soft terms although the Higgs peak at 125 GeV is not as sharp as that observed for power law with $n = 1$ or $n = 2$. Moreover, a log draw of soft terms in the landscape is mostly consistent with power-law draw landscape predictions that sparticles (other than higgsinos) should be out of reach of the current LHC limits, as demonstrated by peak probabilities of sparticle mass distributions occurring beyond current search limits (albeit not as sharply as power-law case) [6]. However, it would seem that LVS type moduli stabilization in the landscape is severely constrained by current LHC data since the expected m_{soft}^{-1} draw in this model produces too light a Higgs along with very light SUSY particles, that seem ruled out by experiment.

Evidently, if experiment confirms SUSY particles within the ranges depicted in our results, one will be able to distinguish mirage mediation from gravity mediation, for instance by extracting running gaugino masses at an e^+e^- collider and checking at what scale they might unify [148]. But as Table 5.2 shows, for the case of gravity mediation based on a single data point of SUSY spectra, there will be no way to differentiate between the different stabilization mechanisms LVS or PS [6].

5.6 Landscape predictions for SUSY Dark Matter

In this section we will present landscape predictions specifically pertaining to supersymmetric DM searches. We have seen that solving the weak-scale naturalness problem requires the introduction of weak-scale SUSY while on the other hand, solving the QCD naturalness problem requires the Peccei-Quinn-Weinberg-Wilczek (PQWW) invisible axion [118, 119, 179, 180, 181, 182]. The SUSY DFSZ axion naturally solves the SUSY μ problem while yielding a little hierarchy i.e. $\mu \ll m_{soft}$. A gravity-safe axionic solution to the strong CP problem can emerge from a strong enough anomaly-free discrete R -symmetry: Z_{24}^R [183]. Consequently, both $U(1)_{PQ}$ and R -parity emerge as accidental, approximate symmetries from the more fundamental discrete R -symmetry which in turn may emerge from compactification of $10 - D$ string theory to $4 - D$ [125]. Thus, in this very attractive scenario the dark matter is expected to consist of two particles: a higgsino-like WIMP which is the LSP and a SUSY DFSZ axion. Typically, the higgsino-like WIMPs are thermally under-produced with relic density $\Omega_{\tilde{\chi}_1^0}^{TP} h^2 \sim (0.1 - 0.2) \times 0.12$ such that the bulk of the DM content is made of SUSY DFSZ axions. However, one needs also include the axion superpartners, the so-called *axino* (\tilde{a}) and the *saxions* (\tilde{s}) into the relic density calculation (along with gravitinos) [184]. A full examination of mixed WIMP-axion DM requires one to calculate the relic density of mixed axion-WIMP DM [185] via solving eight coupled Boltzmann equations starting at re-heating temperature (at the end of inflation) T_R until the era of entropy conservation [186]. The coupled Boltzmann equations track the energy densities of radiation (SM particles), WIMPs, axinos, saxions, gravitinos and axions. Axions and saxions produced as a result of coherent oscillation (CO) and those produced thermally or via heavier particle decays, are treated

separately [184].

5.6.1 Landscape implications for WIMP DM search results from Direct Detection (DD) and Indirect Detection (IDD) Experiments

Firstly, we evaluate the WIMP search limits via ton-scale noble liquid experiments using targets such as Xenon or Argon. To compare WIMP search limits to landscape projections, one must calculate the fractional abundance of WIMPs among the mostly-axionic DM given by $\xi\sigma^{SI}(\tilde{\chi}_1^0, p) \equiv \Omega_{\tilde{\chi}_1^0} h^2 / 0.12$. Our results are displayed in Figure 5.27, where we show the locus of landscape points with a $n = 1$ landscape draw on soft terms in the $\xi\sigma^{SI}(\tilde{\chi}_1^0, p) - m_{\tilde{\chi}_1^0}$ plane using the NUHM3 model. We also include the current search limits from the XENON-100 experiment [187] (black contour) and the XENON1T experiment [56] (red contour), in the plot ². We see that a subset of LHC-allowed points are already excluded (denoted by

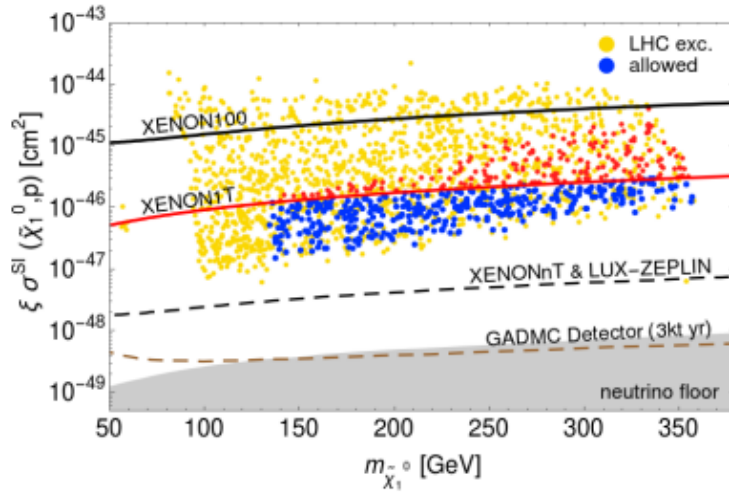


Figure 5.27: Locus of $n = 1$ landscape scan points for the NUHM3 model in the $\xi\sigma^{SI}(\tilde{\chi}_1^0, p)$ vs. $m_{\tilde{\chi}_1^0}$ plane versus recent WIMP search constraints $\mu = 100 - 360$ GeV. Red points are excluded by XENON1T search limits but not by LHC Run 2 constraints. Projected reaches from several future SI DD experiments are also shown. [3]

²After completion of this work, the LZ experiment published even stricter bounds on WIMP DM [188]

red), however the bulk of $n = 1$ landscape points are still allowed, and extend down to an order of magnitude below present limits [3]. These points do not extend all the way to the neutrino floor since in SUSY the WIMPs couple to nucleons primarily via light Higgs exchange and this coupling involves a production of gaugino times higgsino components [189]. For natural SUSY, the WIMP is mostly higgsino albeit with a small but non-negligible gaugino component since gaugino contributions are restricted such that the weak-scale does not exceed the ABDS bound. Thus, from the plot we can infer that projected search limits from XENONnT (multi-ton Xenon detector), with LUX-ZEPLIN (LZ) and other multi-ton-scale detectors should cover the entire $n = 1$ NUHM3 landscape parameter space, even if WIMPs comprise only a portion of the total DM [3].

Next, in the top frame of Figure 5.28 we plot the spin-dependent (SD) direct detection scattering rate in the $\xi\sigma^{SD}(\tilde{\chi}_1^0, p)$ vs. $m_{\tilde{\chi}_1^0}$ plane along with projected $n = 1$ landscape rates. Recent limits from the PICO-60 experiment [190] and IceCube in the W^+W^- annihilation mode [191] are shown. In this plane, we see that the LHC-allowed landscape points tend to lie about an order of magnitude below the current limits. Additionally, the projected future reach of LZ [192], included in the plot, does not quite reach the expected theory region [3]. In the bottom frame of Figure 5.28 we show the indirect WIMP detection rates (IDD) in the $\xi^2\langle\sigma^{SI}v\rangle$ vs. $m_{\tilde{\chi}_1^0}$ plane, where ξ^2 is required since these signals arise from WIMP-WIMP annihilation in the cosmos and is thus suppressed by the fractional WIMP abundance squared [3]. Included on this plot is recent limits from the Fermi-LAT + MAGIC observation of dwarf spheroidal galaxy Segue-1 [193]. The current limit is evidently over an order of magnitude above the expected LHC-allowed non-thermal production of WIMPs which arise from decays of axions/saxions in addition to the thermally-produced neutralinos [3].

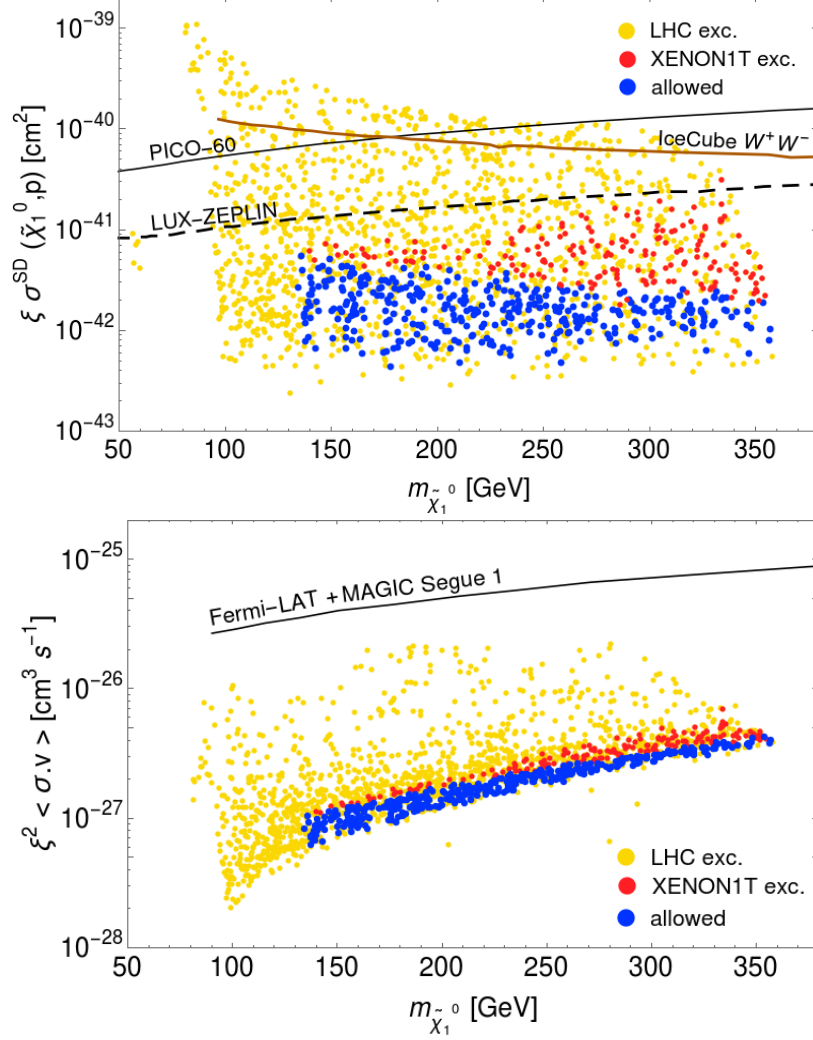


Figure 5.28: Locus of $n = 1$ landscape scan points for the NUHM3 model in the a) $\xi \sigma^{SD}(\tilde{\chi}_1^0, p)$ vs. $m_{\tilde{\chi}_1^0}$ and b) $\xi^2 \langle \sigma^{SI} v \rangle$ vs. $m_{\tilde{\chi}_1^0}$ planes versus recent WIMP search constraints [3].

Therefore, with regards to WIMP searches, it appears that a full complement of data from multi-ton noble liquid SI direct detection experiments should cover the entire $n = 1$, NUHM3 landscape parameter space. This can occur even though in natural SUSY the higgsino-like WIMPs constitute only a portion of parameter space occupied by the $n = 1$ landscape model. On the other hand, even upgraded SD detectors may well fall short of covering the portion of parameter space occupied by the $n = 1$ landscape model. Moreover, it seems highly likely

that IDD WIMP search experiments will also fail to cover the full parameter space since in this case, the expected signal rates are diminished by the square of the fractional WIMP abundance. A similar fate seem probable for SUSY DFSZ axion searches [194] since their coupling $a\gamma\gamma$ is suppressed to much lower values by higgsinos [3].

5.6.2 LHC higgsino discovery plane

Our analysis has shown that a little hierarchy is opening up in that the weak-scale seems to be fairly removed from the scale at which SUSY is softly broken in a hidden sector i.e. $m_{soft} \gg m_{W,Z,h} \sim 100$ GeV. In fact, a landscape pull on soft terms to large values successfully validates the Higgs mass measurement while still rendering the theory natural in the context of the model independent naturalness measure Δ_{EW} extracted from the scalar potential minimization condition,

$$\frac{m_Z^2}{2} = \frac{m_{H_d}^2 + \Sigma_d^d - (m_{H_u}^2 + \Sigma_u^u) \tan^2 \beta}{\tan^2 \beta - 1} - \mu^2 \simeq -m_{H_u}^2 - \mu^2 - \Sigma_u^u(\tilde{t}_{1,2}),$$

such that,

$$\Delta_{EW} = |(\text{max RHS contribution})| / (m_Z^2/2).$$

In this scenario, the natural SUSY parameter space is significantly expanded than was typically expected from older naturalness measures such as Δ_{BG} [58] or Δ_{HS} [74, 75]. Since top squarks enter the minimization condition at one-loop level, they can attain masses into the several TeV regime while remaining natural, with $\Delta_{EW} \lesssim 30$. Gluinos, which enter the minimization condition at two-loop level, can be as heavy as ~ 6 TeV at little cost to naturalness [80, 177]. However, the SUSY conserving Higgs and higgsino mass parameter μ

enters the minimization condition directly which necessitates the Higgs and its superpartner to have comparable masses. Thus, from Δ_{EW} naturalness in the string landscape, we expect the four higgsinos, $\tilde{\chi}_{1,2}^0$ and $\tilde{\chi}_1^\pm$, to be the lightest SUSY particles (LSPs) with mass $\sim 100 - 350$ GeV, while other sparticles that gain masses from soft breaking most likely get pulled beyond present LHC capabilities [94]. In this subsection we analyze the search prospects of these LSPs at the LHC and examine the most likely channels from which higgsino signals are likely to emerge slowly over the next few years amid projected luminosity and energy upgrades to the LHC.

The search for higgsino pair production at the LHC is riddled with difficulties. These difficulties mainly stem from distinguishing very small gaps between the various higgsinos. Specifically mass gaps, $\Delta m^0 \equiv m_{\tilde{\chi}_2^0} - m_{\tilde{\chi}_1^0}$ and $\Delta m^+ \equiv m_{\tilde{\chi}_1^+} - m_{\tilde{\chi}_1^0}$ (following Giudice and Pomarol notation [195]), means that the production of $\tilde{\chi}_1^0\tilde{\chi}_2^0$, $\tilde{\chi}_1^\pm\tilde{\chi}_2^0$ and $\tilde{\chi}_1^+\tilde{\chi}_1^-$ leads to very soft visible decay products, and where most of the energy goes into making the two LSP's rest mass. In addition, $\tilde{\chi}_1^0\tilde{\chi}_1^0j$ production provides a monojet at the level of 1/100 signal/background, where the dominant background comes from Zj production [196]. The reaction $pp \rightarrow \tilde{\chi}_1^0\tilde{\chi}_2^0$ with $\tilde{\chi}_2^0 \rightarrow \mu^+\mu^-\tilde{\chi}_1^0$ was proposed in Ref. [173] which would require a soft dimuon trigger to record the events. It was further proposed [139, 141, 196, 174] to investigate the $\tilde{\chi}_1^0\tilde{\chi}_2^0j$ production where an initial state radiation (ISR) jet at high $p_T \gtrsim 100$ GeV could provide either a jet or MET trigger. Indeed, ATLAS [7] and CMS [175] have followed up on the OSDLJMET signature, which we discussed briefly earlier in section 5.2, and provided limits on such reactions in the $m_{\tilde{\chi}_2^0}$ vs. Δm^0 plane. The prospects of a higgsino discovery looks promising in this plane and henceforth we will label this as the *LHC higgsino discovery plane* [94]. In fact, a recent ATLAS analysis from LHC Run 2 with 139 fb^{-1} finds some

excess of events with low dilepton invariant mass $m(l^+l^-) \sim 5 - 10$ GeV in their SR-E-med analysis shown in Figure 5.29.

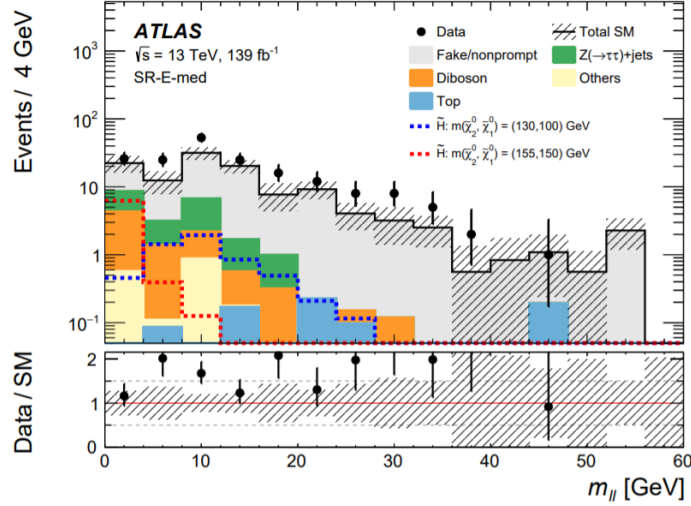


Figure 5.29: ATLAS Collaboration results presented in Fig. 11a of Ref. [7] depicting number of events against the dilepton invariant mass.

The ATLAS and CMS searches in the higgsino discovery plane take place within simplified models which are appropriate for the OSDLJMET search. Here, we want to place the higgsino discovery plane within the context of natural SUSY models and landscape SUSY models so as to provide theoretical context for this plane. To that end we investigate which features of the plane are model-dependent or model-independent, and which portions of the plane are favored by the naturalness and by the string theory landscape. Identifying such regions should help focus OSDLJMET searches onto the most promising portions of the parameter space and also aid in prioritizing searches in the most promising regions over searches with implausible parameter choices [94].

We work with two well-motivated models already examined in the dissertation, namely the NUHM2 and the GMM', to compare the simplified model of the higgsino discovery plane

with expectations from theory. Recall that the parameter space for the NUHM2 model is defined by

$$m_0, m_{1/2}, A_0, \tan \beta, \mu, m_A,$$

while for the GMM' the parameter space is given by

$$\alpha, m_{3/2}, c_m, c_{m3}, a_3, \tan \beta, \mu, m_A.$$

Both the NUHM2 and GMM' models are programmed into the spectrum generator Isajet [81] which we use for our analysis. For simplicity we take $c_m = c_{m3} = (5 \text{ TeV}/\alpha M_s)^2$ so that matter scalar masses are $\sim 5 \text{ TeV}$, equal to the benchmark parameter choice of $m_0 = 5 \text{ TeV}$ in the NUHM2 model. One virtue of the LHC higgsino discovery plane is its relative model independence. Given a certain SUSY model, then for a given set of input parameters one can calculate the (loop-corrected) values [195, 197, 198] of $m_{\tilde{\chi}_2^0}$ and Δm^0 and always locate a point on the discovery plane. Model dependence enters via the assumed value of $m_{\tilde{\chi}_1^\pm}$ and the ATLAS and CMS groups assume $m_{\tilde{\chi}_1^\pm}^* \equiv (m_{\tilde{\chi}_2^0} + m_{\tilde{\chi}_1^0})/2$ which approximately holds at leading order in the deep higgsino region [195]. Upon inclusion of higher order effects into the calculations, deviations to this ansatz begin to set in. However, the details of the relative chargino mass hardly affect the OSDLJMET signature and as a result the higher order effects are not very relevant unless one begins leaving the nearly pure higgsino region where $|\mu| \ll m_{soft}$ [94].

As an illustration, we plot contours of mass difference $\Delta m(\tilde{\chi}_1^\pm) \equiv m_{\tilde{\chi}_1^\pm} - m_{\tilde{\chi}_1^\pm}^*$ between the full one-loop corrected chargino mass from Isajet and the ATLAS/CMS ansatz $m_{\tilde{\chi}_1^\pm}^*$ in Figure 5.30 for the NUHM2 model in the upper frame *a*) and the GMM' model in the lower

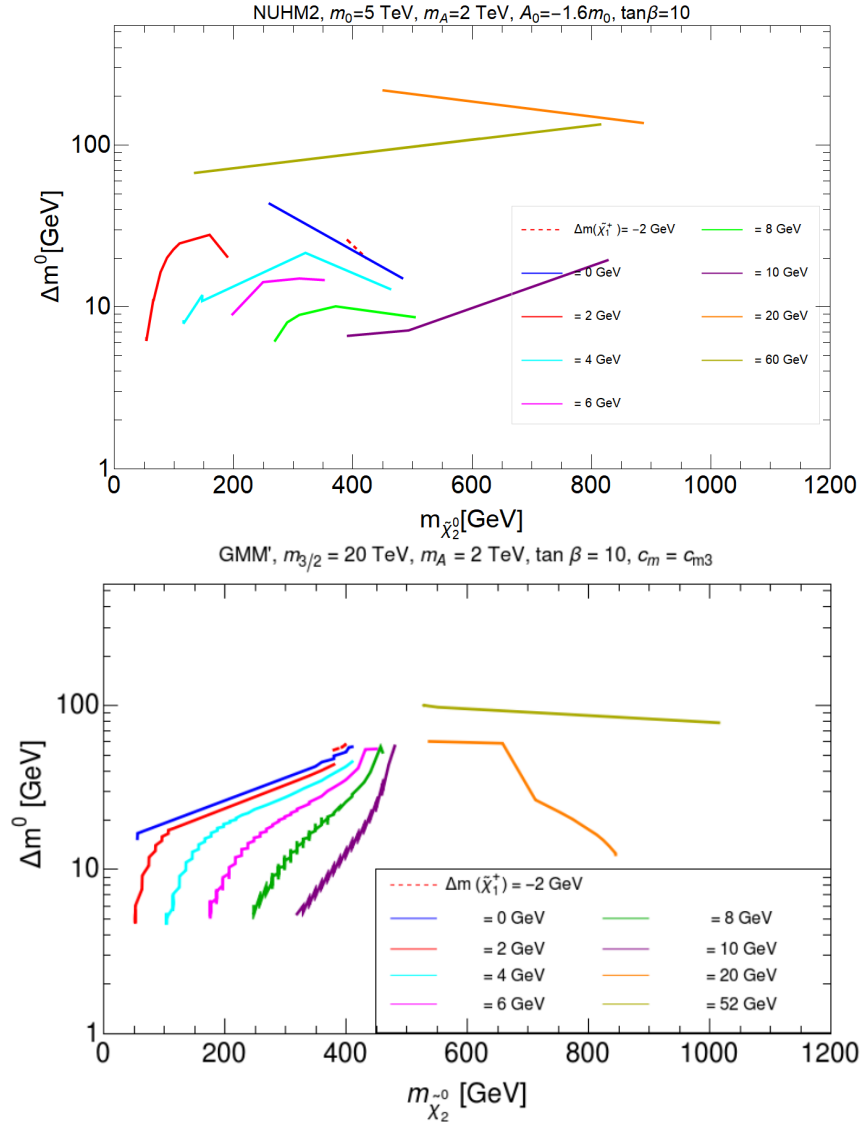


Figure 5.30: Deviations in loop-corrected chargino mass as compared to simplified model value $\Delta m(\tilde{\chi}_1^\pm)$ a) in the NUHM2 model with varying μ and $m_{1/2}$ but with $m_0 = 5$ TeV, $A_0 = -1.6m_0$, $\tan\beta = 10$ and $m_A = 2$ TeV, and in b) in the GMM' model with varying μ and α but with $m_{3/2} = 20$ TeV and $c_m = c_{m3}$. Both models take $m_A = 2$ TeV and $\tan\beta = 10$. [94]

frame b). The blue contour has mass difference zero so is an excellent fit to the ATLAS/CMS ansatz. However, with increasing μ then the mass gaps typically become greater than zero leading to chargino mass becoming larger than the average of the two light neutralinos. In the case of very large μ , then one leaves the light higgsino region and the ansatz no longer holds.

The observed deviation from the simplified model values is not very relevant for the monojet plus soft dilepton searches being considered in this discussion but would be significant for signals like the golden trilepton signal for SUSY that originate from chargino-neutralino production [137].

Next, some aspects of the higgsino discovery plane are shown in Figure 5.31 that are beyond the scope of the ATLAS/CMS simplified models and which depend on the entire SUSY particle mass spectrum. In the top frame *a*), the plot resulted from a scan over the NUHM2 parameters $\mu : 50 - 1000$ GeV (which fixes the higgsino masses) and $m_{1/2} : 100 - 2000$ GeV (which for a given μ value varies the mass gap Δm^0). Since the entire SUSY spectrum is calculated, we can then compute corresponding value of Δ_{EW} for each point in the higgsino discovery plane. The green points have $\Delta_{EW} < 15$ while the magenta points have $\Delta_{EW} < 30$ and hence qualify as natural. Yellow, blue and purple points have $\Delta_{EW} < 100, 200$ and 300 respectively. The grey-shaded region is already excluded by LEP2 searches for the chargino pair production. From the plot, we see that the natural region is bounded by $m_{\tilde{\chi}_2^0} \lesssim 350$ GeV as expected. For small $m_{1/2}$ and $\mu > 350$ GeV, then the $\tilde{\chi}_2^0$ is wino-like and the model can become unnatural even for lower values of $m_{\tilde{\chi}_2^0} \sim 100 - 300$ GeV (which makes up the upper edge of the naturalness envelope in Figure 5.31 frame *a*). For fixed values of $\mu \sim 100 - 300$ GeV but as $m_{1/2}$ increases, then the lightest electroweakinos become increasingly higgsino-like and the mass gap Δm^0 drops below ~ 8 GeV. Precisely where the mass gap value becomes unnatural is partially sensitive to the assumptions of the NUHM2 model. Indeed somewhat lower values of the neutralino gap would have $\Delta_{EW} \lesssim 30$ if one allows generation-dependent matter scalar mass parameters, or if gaugino unification assumption is discarded. The main point, however, is that for small mass gaps, the points become increasingly unnatural in

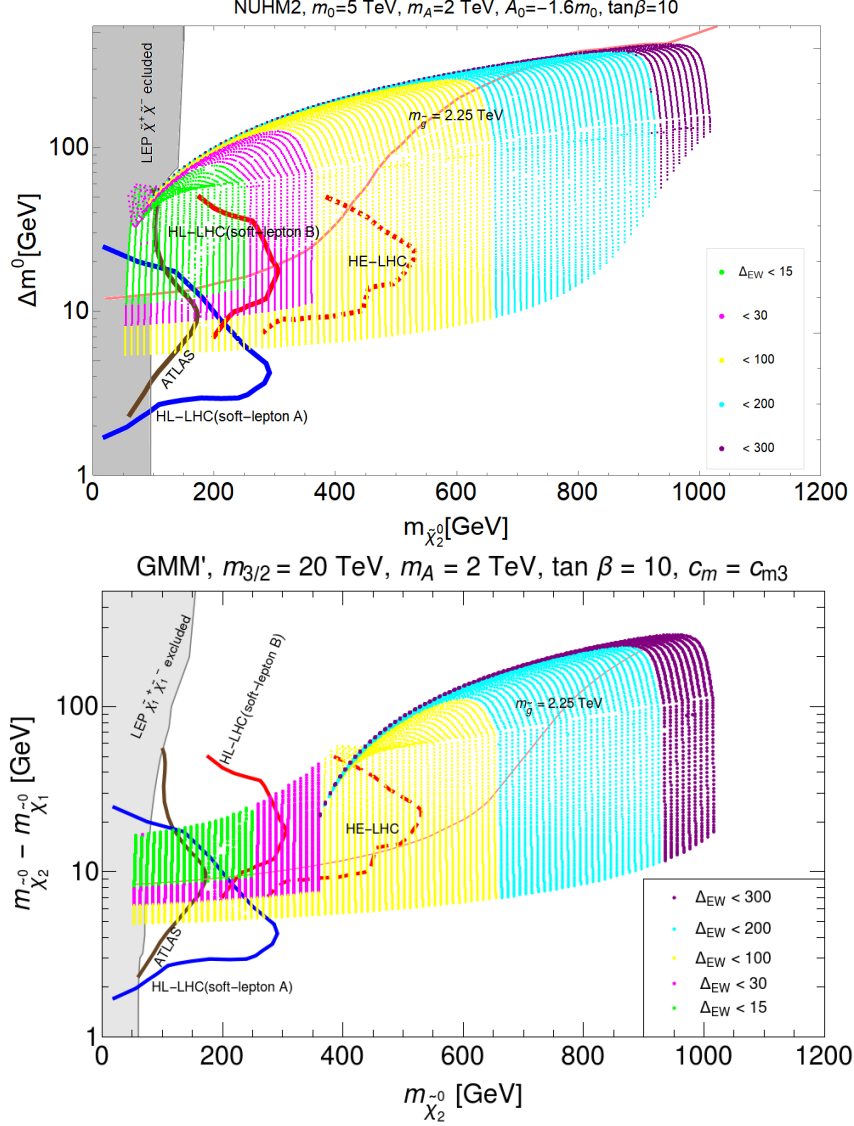


Figure 5.31: Regions of naturalness Δ_{EW} in the light higgsino discovery plane $m_{\tilde{\chi}_2^0}$ vs, $\Delta m^0 \equiv m_{\tilde{\chi}_2^0} - m_{\tilde{\chi}_1^0}$ from a) the NUHM2 model with varying μ and $m_{1/2}$ but with $m_0 = 5$ TeV, $A_0 = -1.6m_0$ and b) the GMM' model with varying μ and α but with $m_{3/2} = 20$ TeV and $c_m = c_{m3}$. For both models, we take $\tan \beta = 10$ and $m_A = 2$ TeV. We also show the present reach of the ATLAS experiment with $139 fb^{-1}$ and the ATLAS (soft lepton A) and the CMS (soft lepton B) projected future reach at the HL-LHC and also CMS at HE-LHC. The region above the $m_{\tilde{g}} = 2.25$ TeV contour is excluded by current LHC Run 2 gluino search analysis. The Higgs mass $m_h \sim 125$ GeV throughout the plane while $m_{\tilde{t}_1} > 1.1$ TeV everywhere. [94]

the NUHM2 case since large $m_{1/2}$ increases $m_{\tilde{g}}$ which feeds into the squark masses which causes $\Sigma_u^u(\tilde{t}_{1,2})$ to become too large. Additionally, the two-loop contributions from $m_{\tilde{g}}$ and

$m_{\tilde{t}_{1,2}}$ can become large as well [199]. This yields an important result: the region of higgsino discovery plane with mass gaps $\Delta m^0 \lesssim 5$ GeV becomes increasingly unnatural and hence less plausible. As previously mentioned, the naturalness lower bound on Δm^0 is somewhat model-dependent and as such can reach $\lesssim 4$ GeV in models like the NUHM3 where the first/second generation scalars take values in the 20 – 40 TeV range. In that case, two-loop RGE effects suppress top squark soft term running, thus allowing for large $m_{1/2}$ values to be natural. Such large $m_{1/2}$ values lead to smaller neutralino mass gaps Δm^0 . While searches in this unnatural region of very low Δm^0 are always warranted, spending an inordinate amount of effort probing such tiny mass gaps should be given lower priority in this rather implausible region. Another feature displayed on the plot in frame *a*) is the LHC gluino exclusion limit shown by the dotted red contour; the region *above* the contour has $m_{\tilde{g}} < 2.25$ TeV and hence is largely excluded by LHC searches in the NUHM2 framework. This exclusion however directly depends on our assumption of gaugino mass unification and in more general models, the allowed natural region might be considerably larger. Also shown is the present ATLAS search contour (brown) for the OSDLJMET signature and the region on the left of this contour is inferred to be excluded. Thus, the *allowed* NUHM2 natural search region has mass gap $\sim 7 - 20$ GeV range, and this is the most plausible region where a SUSY signal may be expected [94]. The lower bound depends on the specific parameter choices adopted and can range down to 4 – 5 GeV for other parameter choices and the current limits do cut well into the natural region of the NUHM2 model. The projected reach of HL-LHC for CMS is denoted by the red contour, while the ATLAS HL-LHC projection is shown by the blue contour. Some of the natural region of the higgsino discovery plane evidently lies beyond the HL-LHC projections. The ATLAS reach extends to lower mass gaps due to the

geometry of the ATLAS detector which allows for the resolution of lower p_T leptons than CMS. Furthermore, the projected HE-LHC reach with $\sqrt{s} = 27$ TeV for CMS is depicted by the red-dashed contour [200]. At face value, it appears as such that the projected HE-LHC reach covers all the natural region of the NUHM2 model for the assumed set of parameters [94].

In the lower frame *b)* of Figure 5.31, we show the same higgsino discovery plane but for the GMM' model where the mirage mediation (MM) value $m_{1/2}^{MM} = \alpha M_s$ varies between 100-2000 GeV. When $m_{1/2}^{MM}$ is at the lower end of the range, one obtains a tachyonic spectra (see Fig. 8 of Ref. [145]) so that no upper edge of unnaturalness ensues as it did for the NUHM2 model case shown in frame *a)* of Figure 5.31, until $m_{\tilde{\chi}_2^0} \gtrsim 400$ GeV. For GMM', depending on α , we expect a compressed spectrum of gaugino masses which means that for a given value of $m_{\tilde{g}}$, the wino and bino masses can be much larger than in the corresponding NUHM2 case with unified gaugino masses. The large wino/bino masses in GMM' results in smaller mass gaps and we find the natural spectra with mass gaps as small as $\Delta m^0 \sim 6$ GeV. We notice that more of the natural region is probed by ATLAS rather than the CMS cuts, in this case. And in fact, more of the natural GMM' parameter space appears to be beyond reach of the HL-LHC. Moreover, a tiny fraction of the magenta region (with $\Delta_{EW} < 30$) lie beyond even the HE-LHC projected reach shown by the dashed red contour. Similar to the NUHM2 case depicted in Figure 5.31 frame *a)*, we see that the region with $\Delta m^0 \lesssim 4 - 5$ GeV becomes increasingly unnatural (the yellow region) [94].

Figure 5.31 suggests therefore, that most of the natural SUSY parameter space is now excluded, including the values with the lowest Δ_{EW} . This is a reflection of the Δ_{EW} measure which is a bottom-up measure of *practical* naturalness wherein smaller Δ_{EW} indicates a more

natural observable \mathcal{O} . In contrast, for an observable \mathcal{O}_1 to be considered more *stringy* natural as compared to observable \mathcal{O}_2 , then \mathcal{O}_1 must lead to more phenomenologically viable vacua, which may be characterized by the weak-scale in a PU. This corresponds to \mathcal{O}_1 leading to more vacua with $m_{weak}^{PU} \lesssim (2 - 5)m_{weak}^{OU}$ which in turn amounts to $\Delta_{EW} < 8 - 50$. For simplicity, we adopt an intermediate value in this range, $\Delta_{EW} < 30$ to yield a phenomenologically viable weak-scale.

To explicitly analyze the stringy natural SUSY parameter space in the higgsino discovery plane, we adopt an $n = 1$ power law draw on gaugino masses since in a wide variety of string models the gaugino masses depend solely on the dilaton field gaining a non-zero VEV, whereas the various moduli contribute subdominantly [4]. Then, for a uniform scan of $\mu > 100$ GeV, with soft terms fixed at $m_0 = 5$ TeV, $A_0 = -1.6m_0$, $m_A = 2$ TeV and for a choice of $\tan\beta = 10$, we generate the corresponding SUSY spectrum in the NUHM2 model. The results are shown in the upper frame *a*) of Figure 5.32 where a higher density of dots correspond to greater stringy naturalness. It is evident from the plot that the region with small mass gap is favored by stringy naturalness over regions with larger mass gap. Thus, much of the stringy natural region still resides well beyond current LHC reach. A similar trend is observed in the case of a landscape scan with the GMM' model shown in Figure 5.32 frame *b*) in that the most densely populated region of parameter space is the low mass gap region making that region more stringy natural. This is consistent with the statistical predictions of stringy naturalness for the sparticle mass spectra in that stringy naturalness pulls the Higgs mass m_h to a peak ~ 125 GeV while gluinos can be pulled as high as $m_{\tilde{g}} \sim 4 \pm 2$ TeV and stops as high as $m_{\tilde{t}_1} \sim 1.5 \pm 0.5$ TeV [85, 103, 145]. For a fixed value of μ , since stringy naturalness pulls gaugino masses as large as possible - subject to maintaining m_{weak}^{PU} to not get too far

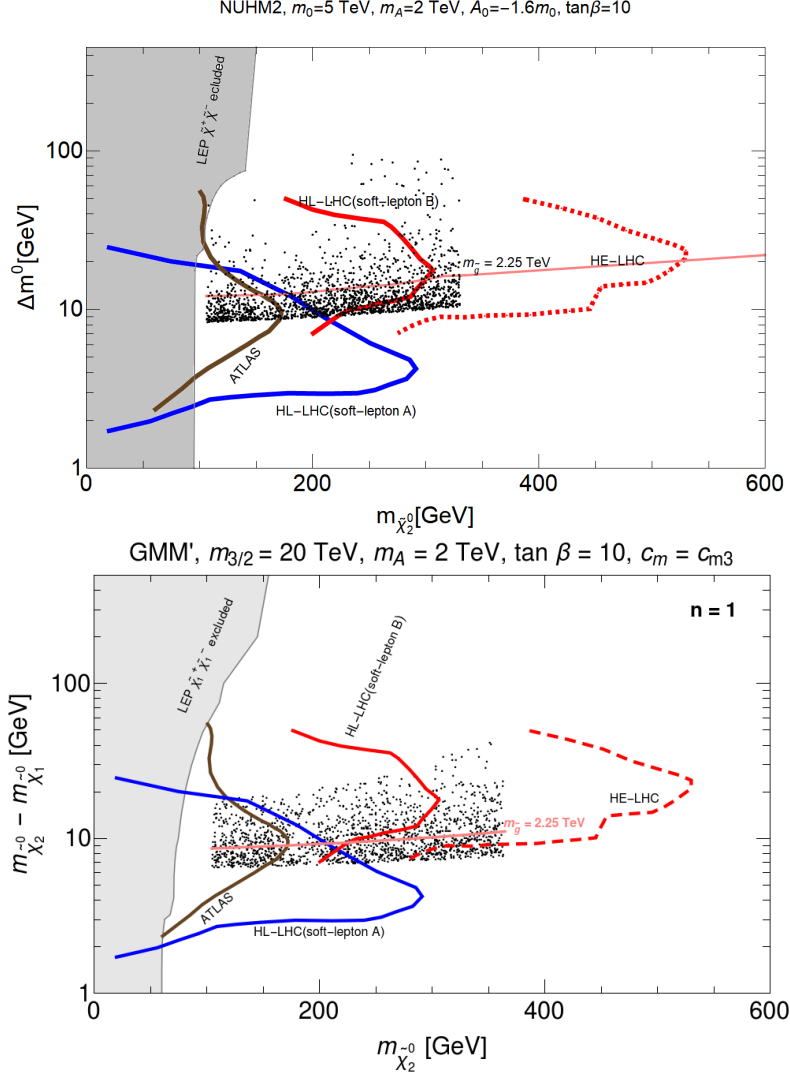


Figure 5.32: Regions of stringy naturalness in the higgsino discovery plane $m_{\tilde{\chi}_2^0}$ vs, $\Delta m^0 \equiv m_{\tilde{\chi}_2^0} - m_{\tilde{\chi}_1^0}$ from a) the NUHM2 model with varying μ and $m_{1/2}$ but with $m_0 = 5$ TeV, $A_0 = -1.6m_0$ and b) the GMM' model with varying μ and α but with $m_{3/2} = 20$ TeV and $c_m = c_{m3}$. For both models, we take $\tan\beta = 10$ and $m_A = 2$ TeV. We also show the present reach of the ATLAS experiment with 139 fb^{-1} and the ATLAS (soft lepton A) and the CMS (soft lepton B) projected future reach at the HL-LHC and also CMS at HE-LHC. The region above the $m_{\tilde{g}} = 2.25$ TeV contour is excluded by current LHC Run 2 gluino search analysis. The Higgs mass $m_h \sim 125$ GeV throughout the plane while $m_{\tilde{t}_1} > 1.1$ TeV everywhere. [94]

beyond m_{weak}^{OU} - then we expect the $m_{\tilde{\chi}_2^0} - m_{\tilde{\chi}_1^0}$ mass gap to be favored on the low allowed side: $\Delta m^0 \sim 5 - 10$ GeV, in both cases.

One can highlight the similarities and differences between the two naturalness considerations made in Figure 5.31 and Figure 5.32. The bottom-up measure Δ_{EW} is universal and applies independently of the details of UV physics. Stringy naturalness however, hinges on the existence of string vacua and their distribution as well as on the atomic principle that led to the cut-off $m_{weak}^{PU} \lesssim (2 - 5)m_{weak}^{OU}$. These additional hypotheses about the nature of UV physics lead to a preference for lower values of Δm^0 . In spite of these differences however, stringy naturalness augmented with the atomic principle, is entirely compatible with electroweak naturalness. This is reflected in the fact that the envelope of points in Figure 5.32 is essentially the same as that in Figure 5.31. Therefore, even if one does not subscribe to the notion of stringy naturalness, they can simply disregard the preference for points with lower Δm^0 apparent in Figure 5.32. However, the takeaway conclusion that naturalness considerations require the neutralino mass gap to be not much below 4 – 5 GeV remains unaltered [94].

Thus, from both notions of naturalness, it may well be that gluinos and squarks are drawn to heavy masses beyond reach of the LHC while the LSP is expected to be mainly higgsino-like with mass around the observed weak-scale. With higgsino pair-production expected to occur at considerable rates at the HL-LHC, the problem lies in identifying the visible energy range. The small mass gaps $m_{\tilde{\chi}_1^\pm} - m_{\tilde{\chi}_1^0}$ and especially $m_{\tilde{\chi}_2^0} - m_{\tilde{\chi}_1^0}$ are expected to be in the 5 – 10 GeV range and most of the reaction energy goes into making the LSP masses $2m_{\tilde{\chi}_1^0}$. As such, it appears that the OSDLJMET signature is the most promising channel for a higgsino DM signal to emerge at the LHC, amid scheduled luminosity and energy upgrades to the ATLAS and CMS detectors.

Chapter 6

Summary and Outlook

The completion of the SM with the discovery of the Higgs at the LHC in 2012 has given rise to a wide variety of perspectives concerning the future of particle physics. According to many physicists, the much anticipated discovery should propel our search for physics beyond the SM, while some, it would seem, have prematurely given up on the prospects of a BSM discovery at the LHC due to its inability to produce results beyond the Higgs thus far. The latter notion mainly arose from some ill-perceived ideas about popular BSM theories such as SUSY and due to older naturalness measures that guided SUSY searches often being guilty of over-simplification that would lead to predictions putting *sparticles* not too far from the weak-scale. In this dissertation, we have addressed such concerns and attempted a sketch of an illustrative map that could lead to potential SUSY discovery in the next decade or so, based on current data, future projections and a more nuanced understanding of previously motivated ideas.

The emergence of the vacuum multiplicity in superstring theory lead to more question marks on the validity of string theory as a probable *theory of everything*: how is one to find a unique vacua among an almost infinitely large number, that could hopefully explain the physical laws of our universe? Here, we have examined how Bousso and Polchinski revised the idea of a habitable landscape consisting of $\sim 10^{500}$ string vacua [50], any of which could support observers like us, provided some pre-existing environmental selection of physical observables such as the value of the cosmological constant. Such *anthropic* reasoning was successfully employed by Weinberg to calculate the value of the cosmological constant to an

incredible precision [45, 46], a decade before observed measurements were published. The principle argument of Weinberg relied on what is known as the *structure principle* which restricts the value of Λ_{cc} to be extremely tiny and positive which then allows for galaxy condensation and structure formation leading to habitable pocket universes in an eternally inflating multiverse. This idea finds a home in the string landscape of vacua with each vacua signifying a pocket universe and we have seen how augmenting it with more anthropic conditions such as,

- ABDS bound on the observed weak-scale (i.e. $m_{weak}^{PU} \lesssim 4m_{weak}^{OU}$) - the condition that allows proper atom formation,
- habitable PU's must exhibit proper breaking of electroweak symmetry,
- vetoing PU's exhibiting charge and colour breaking,

allow us to make robust predictions pertaining to current and future SUSY searches at particle colliders. The next problem to address then becomes how the compact dimensions of the superstring theory are arranged and if it leads to observed phenomena. Of the five superstring constructs available, currently the best understood *compactification* schemes exist for Type IIB. We have made rather general comments on how even the simplest form of compactifications involving *fluxes* and *branes* lead to hundreds of massless scalar fields (i.e. *moduli*) that have so far eluded detection. To address this issue, various *moduli stabilization* methods have been developed such as KKLT [41] and LVS [168]. We have also discussed how SUSY must be a broken symmetry in nature and so, for any potential discovery, one must identify the SUSY breaking scale and each of KKLT and LVS schemes has their own preferences. Soft breaking of SUSY (i.e. without re-introduction of quadratic divergences) in

the hidden sector via KKLT scenario suggests a power-law draw on soft breaking terms (i.e. $f_{SUSY} \sim m_{soft}^1$), as also promoted by Douglas *et.al* [1, 86, 155] in a more general form e.g. $f_{SUSY} \sim m_{soft}^n$, while in the LVS scenario soft term distribution are expected to assume the form, $f_{SUSY} \sim m_{soft}^{-1}$. If soft terms are indeed distributed as a power law in the landscape, then we have seen how it pushes most of the particles in the SUSY spectrum well beyond the observed weak-scale. On the other hand, the $1/m_{soft}$ distribution still expects the SUSY spectrum not too far removed from the weak-scale and a Higgs mass $m_h < 123$ GeV, which stands in sharp contrast to experimental observations thus far.

As its name suggests, superstring theory includes supersymmetry in its formulation and thus even though it seems highly unlikely to directly detect fundamental strings with current energy capabilities of colliders, a robust litmus test for existence of an underlying string theory is manifestation of SUSY in nature. However, exactly how SUSY is broken in the hidden sector is still a mystery and SUSY models promoted in the literature assumes various mechanisms via which SUSY breaking is communicated to the visible sector. We have primarily analysed models based around two of the most motivated mechanisms namely, gravity mediated SUSY breaking and mirage mediated SUSY breaking while also briefly touching on aspects of dynamical SUSY breaking (DSB) wherein SUSY breaking occurs non-perturbatively either via gaugino condensation or via instanton effects. However, not all models are made equal and we have seen how some models are more *natural* than others and the more natural model is in turn a more likely occurrence in the string landscape than an unnatural one. To this end, we have thoroughly discussed how the principle of naturalness has traditionally been implemented with considerable success in terms of discovering new particles such as the charm quark [47]. Moreover, we have compared and contrasted different

naturalness measures and seen how the Δ_{EW} measure is a more accurate measure rather than older measures like Δ_{BG} and Δ_{HS} due to some crucial details glossed over in the calculation of the latter measures. Consequently, a low value of Δ_{EW} , signifying a more natural model, successfully allows for the experimentally observed values of the Higgs mass while limits for other measures are not expected to be meaningful. Alternatively, in the context of the landscape, we have required m_{weak}^{PU} to be within the ABDS window which, in the absence of fine-tuning, corresponds to $\Delta_{EW} \lesssim 30$.

Additionally, in this dissertation, we have examined the concept of *stringy naturalness* which is a more nuanced notion of naturalness that prefers sparticle masses to be as heavy as possible provided one yields viable phenomenological results such as proper EWSB and no CCB on top of the anthropic requirement of $m_{weak}^{PU} \lesssim 4m_{weak}^{OU}$. Using this construct, we have concluded that spontaneous SUSY breaking via gravity or mirage mediation (i.e. models like NUHM2, NUHM3 and GMM') in Type IIB superstring theory with KKLT type flux compactification is more stringy natural and hence is the more likely outcome in the string landscape rather than DSB or LVS type scenarios. This conclusion can be drawn based off of all current data available. Furthermore, we have built on future projected data to make specific predictions for collider SUSY and DM searches. The following list is a summary of the most important predictions that has been made in the dissertation,

- The lightest SUSY particle known as the higgsino, which is a DM candidate along with the axions, is the only particle in the SUSY spectrum of natural models that should be expected to have mass around the weak-scale (i.e. $m_{\tilde{\chi}_1^0} \sim 100 - 350$ GeV). This expectation stems from the fact that the higgsino (and Higgs) superpotential mass

parameter μ is related to the weak-scale magnitude as,

$$m_Z^2/2 \simeq -m_{H_u}^2 - \Sigma_u^u(\tilde{t}_{1,2}) - \mu^2$$

which is used in Δ_{EW} calculation such that,

$$\Delta_{EW} = |(\text{max RHS contribution})|/(m_Z^2/2)$$

is low meaning that μ must not be too far removed from the magnitude of the observed weak-scale since it enters directly into the equation.

- Even though higgsinos are expected to be around the weak-scale, searches face difficulties due to the four eigenstates of the higgsinos - two neutralinos and two charginos - being almost mass degenerate. Therefore, higgsino searches rely on identifying very small mass gaps (e.g. $m_{\chi_2^0} - m_{\chi_1^0} \sim 4 - 10$ GeV) to make a discovery. The most promising search channel for this purpose is the $pp \rightarrow \chi_2^0 - \chi_1^0 \rightarrow l^+l^- \chi_1^0 \chi_1^0$ which leads to the OSDLJMET signature which produces opposite-sign dileptons along with two higgsinos (identified as \cancel{E}_T) in the final state. The dilepton invariant mass is bounded by the difference in neutralino masses which is expected to be tiny and stringy naturalness expects the most probable discovery in this channel being in the range $\Delta m \sim 5 - 10$ GeV, but not much below 5 GeV, which is currently being explored by the LHC.
- The third generation squarks $\tilde{t}_{1,2}$ are expected to be in the 1 – 3 TeV range, with current limits of exclusion at the LHC set at $m_{\tilde{t}_1} \gtrsim 1.1$ TeV but with projected reach of the HL-LHC to be up to ~ 1.7 TeV, a significant portion of the landscape allowed

top squark parameter space will be probed.

- First and second generation squarks can be heavier still, with masses ranging upwards of tens of TeV's. Such heavy masses for the first/second generation squarks are brought about due to their small Yukawa couplings (leading to small contributions to the weak-scale). This then enables a mixed decoupling quasi-degeneracy solution to the SUSY flavor and CP problems.
- Current gluino search exclusion limits are set around ~ 2.25 TeV but the landscape can allow these to be as heavy as 6 TeV.
- Crucially, what all these observations indicate is that all present LHC observations are in accord with landscape predictions: i.e. a SM-like Higgs with mass ~ 125 GeV but no sign of sparticles as of yet since most of these should be beyond current limits, apart from the light but notoriously elusive higgsinos.

References

- [1] L. SUSSKIND, SUPERSYMMETRY BREAKING IN THE ANTHROPIC LANDSCAPE, in: From Fields to Strings: Circumnavigating Theoretical Physics, WORLD SCIENTIFIC, 2005, pp. 1745–1749. doi:10.1142/9789812775344_0040. URL https://doi.org/10.1142/9789812775344_0040
- [2] H. Baer, V. Barger, S. Salam, Naturalness versus stringy naturalness (with implications for collider and dark matter searches, Phys. Rev. Research. 1 (2019) 023001. arXiv:1906.07741, doi:10.1103/PhysRevResearch.1.023001.
- [3] H. Baer, V. Barger, S. Salam, H. Serce, K. Sinha, LHC SUSY and WIMP dark matter searches confront the string theory landscape, JHEP 04 (2019) 043. arXiv:1901.11060, doi:10.1007/JHEP04(2019)043.
- [4] H. Baer, V. Barger, S. Salam, D. Sengupta, String landscape guide to soft susy breaking terms, Physical Review D 102 (7) (10 2020). doi:10.1103/physrevd.102.075012. URL <https://www.osti.gov/biblio/1851225>
- [5] H. Baer, V. Barger, S. Salam, H. Serce, Supersymmetric particle and higgs boson masses from the landscape: Dynamical versus spontaneous supersymmetry breaking, Physical Review D 104 (11) (dec 2021). doi:10.1103/physrevd.104.115025. URL <https://doi.org/10.1103/physrevd.104.115025>
- [6] H. Baer, V. Barger, S. Salam, D. Sengupta, Landscape Higgs boson and sparticle mass predictions from a logarithmic soft term distribution, Phys. Rev. D 103 (3) (2021) 035031. arXiv:2011.04035, doi:10.1103/PhysRevD.103.035031.
- [7] G. Aad, et al., Search for new phenomena with top quark pairs in final states with one lepton, jets, and missing transverse momentum in pp collisions at $\sqrt{s} = 13$ TeV with the ATLAS detector, JHEP 04 (2021) 174. arXiv:2012.03799, doi:10.1007/JHEP04(2021)174.
- [8] S. L. Glashow, Partial-symmetries of weak interactions, Nuclear Physics 22 (4) (1961) 579–588. doi:[https://doi.org/10.1016/0029-5582\(61\)90469-2](https://doi.org/10.1016/0029-5582(61)90469-2). URL <https://www.sciencedirect.com/science/article/pii/0029558261904692>
- [9] S. Weinberg, A model of leptons, Phys. Rev. Lett. 19 (1967) 1264–1266. doi:10.1103/PhysRevLett.19.1264. URL <https://link.aps.org/doi/10.1103/PhysRevLett.19.1264>
- [10] A. Salam, J. C. Ward, Electromagnetic and weak interactions, Phys. Lett. 13 (1964) 168–171. doi:10.1016/0031-9163(64)90711-5.
- [11] P. W. Higgs, Broken symmetries and the masses of gauge bosons, Phys. Rev. Lett. 13 (1964) 508–509. doi:10.1103/PhysRevLett.13.508. URL <https://link.aps.org/doi/10.1103/PhysRevLett.13.508>

- [12] F. Englert, R. Brout, Broken symmetry and the mass of gauge vector mesons, *Phys. Rev. Lett.* 13 (1964) 321–323. doi:10.1103/PhysRevLett.13.321.
URL <https://link.aps.org/doi/10.1103/PhysRevLett.13.321>
- [13] G. Hinshaw, D. Larson, E. Komatsu, D. N. Spergel, C. L. Bennett, J. Dunkley, M. R. Nolte, M. Halpern, R. S. Hill, N. Odegard, et al., Nine-year wilkinson microwave anisotropy probe (wmap) observations: Cosmological parameter results, *The Astrophysical Journal Supplement Series* 208 (2) (2013) 19. doi:10.1088/0067-0049/208/2/19.
URL <http://dx.doi.org/10.1088/0067-0049/208/2/19>
- [14] P. A. R. Ade, N. Aghanim, M. Arnaud, M. Ashdown, J. Aumont, C. Baccigalupi, A. J. Banday, R. B. Barreiro, J. G. Bartlett, et al., Planck2015 results, *Astronomy & Astrophysics* 594 (2016) A13. doi:10.1051/0004-6361/201525830.
URL <http://dx.doi.org/10.1051/0004-6361/201525830>
- [15] S. Perlmutter, G. Aldering, G. Goldhaber, R. A. Knop, P. Nugent, P. G. Castro, S. Deustua, S. Fabbro, A. Goobar, D. E. Groom, et al., Measurements of and from 42 highredshift supernovae, *The Astrophysical Journal* 517 (2) (1999) 565586. doi:10.1086/307221.
URL <http://dx.doi.org/10.1086/307221>
- [16] P. Zyla, et al., Review of Particle Physics, *PTEP* 2020 (8) (2020) 083C01. doi:10.1093/ptep/ptaa104.
- [17] H. Baer, X. Tata, *Weak Scale Supersymmetry: From Superfields to Scattering Events*, Cambridge University Press, 2006. doi:10.1017/CB09780511617270.
- [18] C. CSÁKI, The minimal supersymmetric standard model, *Modern Physics Letters A* 11 (08) (1996) 599613. doi:10.1142/s021773239600062x.
URL <http://dx.doi.org/10.1142/S021773239600062X>
- [19] Y. Nambu, Quasi-particles and gauge invariance in the theory of superconductivity, *Phys. Rev.* 117 (1960) 648–663. doi:10.1103/PhysRev.117.648.
URL <https://link.aps.org/doi/10.1103/PhysRev.117.648>
- [20] J. Goldstone, Field Theories with Superconductor Solutions, *Nuovo Cim.* 19 (1961) 154–164. doi:10.1007/BF02812722.
- [21] A. Shomer, A pedagogical explanation for the non-renormalizability of gravity (2007). arXiv:0709.3555.
- [22] J. Polchinski, a. O. M. C. Safari, *String Theory*, no. v. 1, Cambridge University Press, 1998.
URL <https://books.google.com/books?id=EyaqtQEACAAJ>
- [23] J. Polchinski, *String Theory: Volume 2, Superstring Theory and Beyond*, Cambridge Monographs on Mathematical Physics, Cambridge University Press, 2005.
URL <https://books.google.com/books?id=IkFSngEACAAJ>

- [24] K. Becker, M. Becker, J. H. Schwarz, *String Theory and M-Theory: A Modern Introduction*, Cambridge University Press, 2006. doi:10.1017/CB09780511816086.
- [25] K. Wray, *An introduction to string theory*, Berkeley University (2011) 58–59.
- [26] F. Gliozzi, J. Scherk, D. I. Olive, Supersymmetry, Supergravity Theories and the Dual Spinor Model, *Nucl. Phys. B* 122 (1977) 253–290. doi:10.1016/0550-3213(77)90206-1.
- [27] R. J. Szabo, *An introduction to string theory and D-brane dynamics : with problems and solutions / Richard J. Szabo.*, 2nd Edition, Imperial College Press ; Distributed by World Scientific, London : Hackensack, N.J., 2011.
- [28] E. Witten, String theory dynamics in various dimensions, *Nuclear Physics B* 443 (12) (1995) 85126. doi:10.1016/0550-3213(95)00158-o.
URL [http://dx.doi.org/10.1016/0550-3213\(95\)00158-0](http://dx.doi.org/10.1016/0550-3213(95)00158-0)
- [29] T. Kaluza, Zum Unitätsproblem der Physik, *Sitzungsberichte der Königlich Preußischen Akademie der Wissenschaften* (Berlin (1921) 966–972.
- [30] O. Klein, Quantentheorie und fünfdimensionale Relativitätstheorie, *Zeitschrift für Physik* 37 (12) (1926) 895–906. doi:10.1007/BF01397481.
- [31] M. R. Douglas, R. Kallosh, Compactification on negatively curved manifolds, *Journal of High Energy Physics* 2010 (6) (jun 2010). doi:10.1007/jhep06(2010)004.
URL <https://doi.org/10.1007%2Fjhep06%282010%29004>
- [32] M. R. Douglas, The String Theory Landscape, *Universe* 5 (7) (2019) 176. doi:10.3390/universe5070176.
- [33] E. Silverstein, TASI lectures on cosmological observables and string theory, in: *New Frontiers in Fields and Strings*, WORLD SCIENTIFIC, 2016. doi:10.1142/9789813149441_0009.
URL https://doi.org/10.1142%2F9789813149441_0009
- [34] M. R. Douglas, S. Kachru, Flux compactification, *Reviews of Modern Physics* 79 (2) (2007) 733–796. doi:10.1103/revmodphys.79.733.
URL <https://doi.org/10.1103%2Frevmodphys.79.733>
- [35] G. D. Coughlan, W. Fischler, E. W. Kolb, S. Raby, G. G. Ross, Cosmological Problems for the Polonyi Potential, *Phys. Lett. B* 131 (1983) 59–64. doi:10.1016/0370-2693(83)91091-2.
- [36] T. Banks, D. B. Kaplan, A. E. Nelson, Cosmological implications of dynamical supersymmetry breaking, *Physical Review D* 49 (2) (1994) 779–787. doi:10.1103/physrevd.49.779.
URL <https://doi.org/10.1103%2Fphysrevd.49.779>

- [37] B. de Carlos, J. Casas, F. Quevedo, E. Roulet, Model-independent properties and cosmological implications of the dilaton and moduli sectors of 4d strings, *Physics Letters B* 318 (3) (1993) 447–456. doi:10.1016/0370-2693(93)91538-x.
URL <https://doi.org/10.1016%2F0370-2693%2893%2991538-x>
- [38] J. MALDACENA, C. NUÑEZ, SUPERGRAVITY DESCRIPTION OF FIELD THEORIES ON CURVED MANIFOLDS AND a NO GO THEOREM, *International Journal of Modern Physics A* 16 (05) (2001) 822–855. doi:10.1142/s0217751x01003937.
URL <https://doi.org/10.1142%2Fs0217751x01003937>
- [39] G. Ren, *Aspects of string compactification*, 2011.
- [40] J. Polchinski, Dirichlet branes and ramond-ramond charges, *Physical Review Letters* 75 (26) (1995) 4724–4727. doi:10.1103/physrevlett.75.4724.
URL <https://doi.org/10.1103%2Fphysrevlett.75.4724>
- [41] S. Kachru, R. Kallosh, A. Linde, S. P. Trivedi, de sitter vacua in string theory, *Physical Review D* 68 (4) (aug 2003). doi:10.1103/physrevd.68.046005.
URL <https://doi.org/10.1103%2Fphysrevd.68.046005>
- [42] R. Bousso, J. Polchinski, Quantization of four-form fluxes and dynamical neutralization of the cosmological constant, *Journal of High Energy Physics* 2000 (06) (2000) 006–006. doi:10.1088/1126-6708/2000/06/006.
URL <https://doi.org/10.1088%2F1126-6708%2F2000%2F06%2F006>
- [43] M. R. Douglas, The statistics of string/m theory vacua, *Journal of High Energy Physics* 2003 (05) (2003) 046–046. doi:10.1088/1126-6708/2003/05/046.
URL <https://doi.org/10.1088%2F1126-6708%2F2003%2F05%2F046>
- [44] L. Susskind, The anthropic landscape of string theory (2003). doi:10.48550/ARXIV.HEP-TH/0302219.
URL <https://arxiv.org/abs/hep-th/0302219>
- [45] S. Weinberg, Anthropic bound on the cosmological constant, *Phys. Rev. Lett.* 59 (1987) 2607–2610. doi:10.1103/PhysRevLett.59.2607.
URL <https://link.aps.org/doi/10.1103/PhysRevLett.59.2607>
- [46] S. Weinberg, The cosmological constant problem, *Rev. Mod. Phys.* 61 (1989) 1–23. doi:10.1103/RevModPhys.61.1.
URL <https://link.aps.org/doi/10.1103/RevModPhys.61.1>
- [47] M. K. Gaillard, B. W. Lee, J. L. Rosner, Search for charm, *Rev. Mod. Phys.* 47 (1975) 277–310. doi:10.1103/RevModPhys.47.277.
URL <https://link.aps.org/doi/10.1103/RevModPhys.47.277>
- [48] M. Dine, Naturalness under stress (2015). doi:10.48550/ARXIV.1501.01035.
URL <https://arxiv.org/abs/1501.01035>

- [49] G. 't Hooft, Naturalness, chiral symmetry, and spontaneous chiral symmetry breaking, *NATO Sci. Ser. B* 59 (1980) 135–157. doi:10.1007/978-1-4684-7571-5_9.
- [50] R. Bousso, J. Polchinski, The string theory landscape, *Scientific American* 291 (2004) 78–87. doi:10.1038/scientificamerican0904-78.
- [51] A. Linde, A brief history of the multiverse (2015). doi:10.48550/ARXIV.1512.01203. URL <https://arxiv.org/abs/1512.01203>
- [52] V. Agrawal, S. M. Barr, J. F. Donoghue, D. Seckel, Anthropic considerations in multiple-domain theories and the scale of electroweak symmetry breaking, *Phys. Rev. Lett.* 80 (1998) 1822–1825. doi:10.1103/PhysRevLett.80.1822. URL <https://link.aps.org/doi/10.1103/PhysRevLett.80.1822>
- [53] V. Agrawal, S. M. Barr, J. F. Donoghue, D. Seckel, Viable range of the mass scale of the standard model, *Phys. Rev. D* 57 (1998) 5480–5492. doi:10.1103/PhysRevD.57.5480. URL <https://link.aps.org/doi/10.1103/PhysRevD.57.5480>
- [54] H. Baer, V. Barger, D. Martinez, S. Salam, Radiative natural supersymmetry emergent from the string landscape (2022). doi:10.48550/ARXIV.2202.07046. URL <https://arxiv.org/abs/2202.07046>
- [55] B. S. Acharya, Supersymmetry, ricci flat manifolds and the string landscape (2019). doi:10.48550/ARXIV.1906.06886. URL <https://arxiv.org/abs/1906.06886>
- [56] E. Aprile, J. Aalbers, F. Agostini, M. Alfonsi, L. Althueser, F. Amaro, M. Anthony, F. Arneodo, L. Baudis, B. Bauermeister, M. Benabderrahmane, T. Berger, P. Breur, A. Brown, A. Brown, E. Brown, S. Bruenner, G. Bruno, R. Budnik, C. Capelli, J. Cardoso, D. Cichon, D. Coderre, A. Colijn, J. Conrad, J. Cussonneau, M. Decowski, P. de Perio, P. D. Gangi, A. D. Giovanni, S. Diglio, A. Elykov, G. Eurin, J. Fei, A. Ferella, A. Fieguth, W. Fulgione, A. G. Rosso, M. Galloway, F. Gao, M. Garbini, C. Geis, L. Grandi, Z. Greene, H. Qiu, C. Hasterok, E. Hogenbirk, J. Howlett, R. Itay, F. Joerg, B. Kaminsky, S. Kazama, A. Kish, G. Koltman, H. Landsman, R. Lang, L. Levinson, Q. Lin, S. Lindemann, M. Lindner, F. Lombardi, J. Lopes, J. Mahlstedt, A. Manfredini, T. M. Undagoitia, J. Masbou, D. Masson, M. Messina, K. Micheneau, K. Miller, A. Molinaro, K. Morå, M. Murra, J. Naganoma, K. Ni, U. Oberlack, B. Pelssers, F. Piastra, J. Pienaar, V. Pizzella, G. Plante, R. Podvianiuk, N. Priel, D. R. García, L. Rauch, S. Reichard, C. Reuter, B. Riedel, A. Rizzo, A. Rocchetti, N. Rupp, J. dos Santos, G. Sartorelli, M. Scheibelhut, S. Schindler, J. Schreiner, D. Schulte, M. Schumann, L. S. Lavina, M. Selvi, P. Shagin, E. Shockley, M. Silva, H. Simgen, D. Thers, F. Toschi, G. Trincherro, C. Tunnell, N. Upole, M. Vargas, O. Wack, H. Wang, Z. Wang, Y. Wei, C. Weinheimer, C. Wittweg, J. Wulf, J. Ye, Y. Zhang, T. Z. and, Dark matter search results from a one ton-year exposure of XENON1t, *Physical Review Letters* 121 (11) (sep 2018). doi:10.1103/physrevlett.121.111302. URL <https://doi.org/10.1103%2Fphysrevlett.121.111302>

- [57] J. R. Ellis, K. Enqvist, D. V. Nanopoulos, F. Zwirner, Observables in Low-Energy Superstring Models, *Mod. Phys. Lett. A* 1 (1986) 57. doi:10.1142/S0217732386000105.
- [58] R. Barbieri, G. Giudice, Upper bounds on supersymmetric particle masses, *Nuclear Physics B* 306 (1) (1988) 63–76. doi:https://doi.org/10.1016/0550-3213(88)90171-X.
URL <https://www.sciencedirect.com/science/article/pii/055032138890171X>
- [59] S. Dimopoulos, G. Giudice, Naturalness constraints in supersymmetric theories with non-universal soft terms, *Physics Letters B* 357 (4) (1995) 573–578. doi:10.1016/0370-2693(95)00961-j.
URL <https://doi.org/10.1016%2F0370-2693%2895%2900961-j>
- [60] G. W. Anderson, D. J. Castaño, Challenging weak-scale supersymmetry at colliders, *Physical Review D* 53 (5) (1996) 2403–2410. doi:10.1103/physrevd.53.2403.
URL <https://doi.org/10.1103%2Fphysrevd.53.2403>
- [61] R. Barbieri, A. Strumia, About the fine-tuning price of LEP, *Physics Letters B* 433 (1-2) (1998) 63–66. doi:10.1016/s0370-2693(98)00577-2.
URL <https://doi.org/10.1016%2Fs0370-2693%2898%2900577-2>
- [62] S. Dimopoulos, H. Georgi, Softly broken supersymmetry and $su(5)$, *Nuclear Physics B* 193 (1) (1981) 150–162. doi:https://doi.org/10.1016/0550-3213(81)90522-8.
URL <https://www.sciencedirect.com/science/article/pii/0550321381905228>
- [63] H. Baer, A. Mustafayev, S. Profumo, A. Belyaev, X. Tata, Neutralino cold dark matter in a one-parameter extension of the minimal supergravity model, *Physical Review D* 71 (9) (may 2005). doi:10.1103/physrevd.71.095008.
URL <https://doi.org/10.1103%2Fphysrevd.71.095008>
- [64] D. Matalliotakis, H. P. Nilles, Implications of nonuniversality of soft terms in supersymmetric grand unified theories, *Nucl. Phys. B* 435 (1995) 115–128. arXiv:hep-ph/9407251, doi:10.1016/0550-3213(94)00487-Y.
- [65] M. Olechowski, S. Pokorski, Electroweak symmetry breaking with nonuniversal scalar soft terms and large $\tan\beta$ solutions, *Phys. Lett. B* 344 (1995) 201–210. arXiv:hep-ph/9407404, doi:10.1016/0370-2693(94)01571-S.
- [66] P. Nath, R. L. Arnowitt, Nonuniversal soft SUSY breaking and dark matter, in: 1st International Conference on Particle Physics and the Early Universe, 1997, pp. 203–210. arXiv:hep-ph/9801259, doi:10.1142/9789814447263_0020.
- [67] J. R. Ellis, K. A. Olive, Y. Santoso, The MSSM parameter space with nonuniversal Higgs masses, *Phys. Lett. B* 539 (2002) 107–118. arXiv:hep-ph/0204192, doi:10.1016/S0370-2693(02)02071-3.
- [68] J. R. Ellis, T. Falk, K. A. Olive, Y. Santoso, Exploration of the MSSM with nonuniversal Higgs masses, *Nucl. Phys. B* 652 (2003) 259–347. arXiv:hep-ph/0210205, doi:10.1016/S0550-3213(02)01144-6.

- [69] H. Baer, A. Mustafayev, S. Profumo, A. Belyaev, X. Tata, Direct, indirect and collider detection of neutralino dark matter in SUSY models with non-universal Higgs masses, *JHEP* 07 (2005) 065. arXiv:hep-ph/0504001, doi:10.1088/1126-6708/2005/07/065.
- [70] H. Baer, V. Barger, D. Mickelson, How conventional measures overestimate electroweak fine-tuning in supersymmetric theory, *Phys. Rev. D* 88 (2013) 095013. doi:10.1103/PhysRevD.88.095013.
URL <https://link.aps.org/doi/10.1103/PhysRevD.88.095013>
- [71] A. Mustafayev, X. Tata, Supersymmetry, naturalness and light higgsinos, *Indian Journal of Physics* 88 (9) (2014) 991–1004. doi:10.1007/s12648-014-0504-8.
URL <https://doi.org/10.1007/s12648-014-0504-8>
- [72] H. Baer, V. Barger, D. Mickelson, M. Padeffke-Kirkland, SUSY models under siege: LHC constraints and electroweak fine-tuning, *Physical Review D* 89 (11) (jun 2014). doi:10.1103/physrevd.89.115019.
URL <https://doi.org/10.1103/physrevd.89.115019>
- [73] H. Baer, V. Barger, M. Savoy, Supergravity gauge theories strike back: there is no crisis for SUSY but a new collider may be required for discovery, *Physica Scripta* 90 (6) (2015) 068003. doi:10.1088/0031-8949/90/6/068003.
URL <https://doi.org/10.1088/0031-8949/90/6/068003>
- [74] M. Papucci, J. T. Ruderman, A. Weiler, Natural SUSY endures, *Journal of High Energy Physics* 2012 (9) (sep 2012). doi:10.1007/jhep09(2012)035.
URL [https://doi.org/10.1007/jhep09\(2012\)035](https://doi.org/10.1007/jhep09(2012)035)
- [75] C. Brust, A. Katz, S. Lawrence, R. Sundrum, SUSY, the third generation and the LHC, *Journal of High Energy Physics* 2012 (3) (mar 2012). doi:10.1007/jhep03(2012)103.
URL [https://doi.org/10.1007/jhep03\(2012\)103](https://doi.org/10.1007/jhep03(2012)103)
- [76] M. Carena, H. Haber, Higgs boson theory and phenomenology, *Progress in Particle and Nuclear Physics* 50 (1) (2003) 63–152. doi:10.1016/s0146-6410(02)00177-1.
URL [https://doi.org/10.1016/s0146-6410\(02\)00177-1](https://doi.org/10.1016/s0146-6410(02)00177-1)
- [77] H. Baer, V. Barger, A. Mustafayev, Implications of a 125 gev higgs scalar for the lhc supersymmetry and neutralino dark matter searches, *Phys. Rev. D* 85 (2012) 075010. doi:10.1103/PhysRevD.85.075010.
URL <https://link.aps.org/doi/10.1103/PhysRevD.85.075010>
- [78] H. Baer, V. Barger, P. Huang, A. Mustafayev, X. Tata, Radiative natural supersymmetry with a 125 GeV higgs boson, *Physical Review Letters* 109 (16) (oct 2012). doi:10.1103/physrevlett.109.161802.
URL <https://doi.org/10.1103/physrevlett.109.161802>
- [79] H. Baer, V. Barger, P. Huang, D. Mickelson, A. Mustafayev, X. Tata, Radiative natural supersymmetry: Reconciling electroweak fine-tuning and the higgs boson mass, *Physical*

- Review D 87 (11) (jun 2013). doi:10.1103/physrevd.87.115028.
 URL <https://doi.org/10.1103%2Fphysrevd.87.115028>
- [80] H. Baer, V. Barger, M. Savoy, Upper bounds on sparticle masses from naturalness or how to disprove weak scale supersymmetry, *Physical Review D* 93 (3) (feb 2016). doi:10.1103/physrevd.93.035016.
 URL <https://doi.org/10.1103%2Fphysrevd.93.035016>
- [81] H. Baer, F. E. Paige, S. D. Protopescu, X. Tata, Isajet 7.40: A monte carlo event generator for pp , $\bar{p}p$, and e^+e^- reactions (1998). doi:10.48550/ARXIV.HEP-PH/9810440.
 URL <https://arxiv.org/abs/hep-ph/9810440>
- [82] G. L. Kane, C. F. Kolda, L. Roszkowski, J. D. Wells, Study of constrained minimal supersymmetry, *Phys. Rev. D* 49 (1994) 6173–6210. arXiv:hep-ph/9312272, doi:10.1103/PhysRevD.49.6173.
- [83] M. R. Douglas, Basic results in vacuum statistics, *Comptes Rendus Physique* 5 (9-10) (2004) 965–977. doi:10.1016/j.crhy.2004.09.008.
 URL <https://doi.org/10.1016%2Fj.crhy.2004.09.008>
- [84] F. Denef, M. R. Douglas, Distributions of flux vacua, *Journal of High Energy Physics* 2004 (05) (2004) 072–072. doi:10.1088/1126-6708/2004/05/072.
 URL <https://doi.org/10.1088%2F1126-6708%2F2004%2F05%2F072>
- [85] H. Baer, V. Barger, H. Serce, K. Sinha, Higgs and superparticle mass predictions from the landscape, *JHEP* 03 (2018) 002. arXiv:1712.01399, doi:10.1007/JHEP03(2018)002.
- [86] N. Arkani-Hamed, S. Dimopoulos, S. Kachru, Predictive landscapes and new physics at a tev (2005). doi:10.48550/ARXIV.HEP-TH/0501082.
 URL <https://arxiv.org/abs/hep-th/0501082>
- [87] G. F. Giudice, R. Rattazzi, Living dangerously with low-energy supersymmetry, *Nuclear Physics B* 757 (1-2) (2006) 19–46. doi:10.1016/j.nuclphysb.2006.07.031.
 URL <https://doi.org/10.1016%2Fj.nuclphysb.2006.07.031>
- [88] G. F. Giudice, A. Strumia, Probing high-scale and split supersymmetry with higgs mass measurements, *Nuclear Physics B* 858 (1) (2012) 63–83. doi:10.1016/j.nuclphysb.2012.01.001.
 URL <https://doi.org/10.1016%2Fj.nuclphysb.2012.01.001>
- [89] G. Elor, H.-S. Goh, L. J. Hall, P. Kumar, Y. Nomura, Environmentally selected WIMP dark matter with high-scale supersymmetry breaking, *prd* 81 (9) (2010) 095003. arXiv:0912.3942, doi:10.1103/PhysRevD.81.095003.
- [90] N. Arkani-Hamed, S. Dimopoulos, Supersymmetric unification without low energy supersymmetry and signatures for fine-tuning at the LHC, *Journal of High Energy Physics* 2005 (06) (2005) 073–073. doi:10.1088/1126-6708/2005/06/073.
 URL <https://doi.org/10.1088%2F1126-6708%2F2005%2F06%2F073>

- [91] N. Arkani-Hamed, S. Dimopoulos, G. Giudice, A. Romanino, Aspects of split supersymmetry, *Nuclear Physics B* 709 (1-2) (2005) 3–46. doi:10.1016/j.nuclphysb.2004.12.026.
URL <https://doi.org/10.1016%2Fj.nuclphysb.2004.12.026>
- [92] A. Arvanitaki, N. Craig, S. Dimopoulos, G. Villadoro, Mini-split, *Journal of High Energy Physics* 2013 (2) (feb 2013). doi:10.1007/jhep02(2013)126.
URL <https://doi.org/10.1007%2Fjhep02%282013%29126>
- [93] N. Arkani-Hamed, A. Gupta, D. E. Kaplan, N. Weiner, T. Zorawski, Simply unnatural supersymmetry (2012). doi:10.48550/ARXIV.1212.6971.
URL <https://arxiv.org/abs/1212.6971>
- [94] H. Baer, V. Barger, S. Salam, D. Sengupta, X. Tata, The LHC higgsino discovery plane for present and future SUSY searches, *Phys. Lett. B* 810 (2020) 135777. arXiv:2007.09252, doi:10.1016/j.physletb.2020.135777.
- [95] V. S. Kaplunovsky, J. Louis, Model-independent analysis of soft terms in effective supergravity and in string theory, *Physics Letters B* 306 (3-4) (1993) 269–275. doi:10.1016/0370-2693(93)90078-v.
URL <https://doi.org/10.1016%2F0370-2693%2893%2990078-v>
- [96] A. Brignole, Towards a theory of soft terms for the supersymmetric standard model, *Nuclear Physics B* 422 (1-2) (1994) 125–171. doi:10.1016/0550-3213(94)00068-9.
URL <https://doi.org/10.1016%2F0550-3213%2894%2900068-9>
- [97] E. Cremmer, S. Ferrara, L. Girardello, A. Van Proeyen, Yang-Mills Theories with Local Supersymmetry: Lagrangian, Transformation Laws and SuperHiggs Effect, *Nucl. Phys. B* 212 (1983) 413. doi:10.1016/0550-3213(83)90679-X.
- [98] A. BRIGNOLE, L. E. IBÁÑEZ, C. MUÑOZ, SOFT SUPERSYMMETRY-BREAKING TERMS FROM SUPERGRAVITY AND SUPERSTRING MODELS, in: *Perspectives on Supersymmetry*, WORLD SCIENTIFIC, 1998, pp. 125–148. doi:10.1142/9789812839657_0003.
URL https://doi.org/10.1142%2F9789812839657_0003
- [99] S. P. MARTIN, A SUPERSYMMETRY PRIMER, in: *Perspectives on Supersymmetry*, WORLD SCIENTIFIC, 1998, pp. 1–98. doi:10.1142/9789812839657_0001.
URL https://doi.org/10.1142%2F9789812839657_0001
- [100] H. Baer, V. Barger, H. Serce, X. Tata, Natural generalized mirage mediation, *Phys. Rev. D* 94 (2016) 115017. doi:10.1103/PhysRevD.94.115017.
URL <https://link.aps.org/doi/10.1103/PhysRevD.94.115017>
- [101] K. Choi, A. Falkowski, H. Nilles, M. Olechowski, Soft supersymmetry breaking in klt flux compactification, *Nuclear Physics B* 718 (1) (2005) 113–133. doi:<https://doi.org/10.1016/j.nuclphysb.2005.04.032>.
URL <https://www.sciencedirect.com/science/article/pii/S0550321305003482>

- [102] K. R. Dienes, C. Kolda, Twenty open questions in supersymmetric particle physics (1997). doi:10.48550/ARXIV.HEP-PH/9712322.
URL <https://arxiv.org/abs/hep-ph/9712322>
- [103] H. Baer, V. Barger, M. Savoy, H. Serce, The higgs mass and natural supersymmetric spectrum from the landscape, *Physics Letters B* 758 (2016) 113–117. doi:10.1016/j.physletb.2016.05.010.
URL <https://doi.org/10.1016%2Fj.physletb.2016.05.010>
- [104] M. Dine, A. E. Nelson, Y. Nir, Y. Shirman, New tools for low energy dynamical supersymmetry breaking, *Physical Review D* 53 (5) (1996) 2658–2669. doi:10.1103/physrevd.53.2658.
URL <https://doi.org/10.1103%2Fphysrevd.53.2658>
- [105] G. Giudice, R. Rattazzi, Theories with gauge-mediated supersymmetry breaking, *Physics Reports* 322 (6) (1999) 419–499. doi:10.1016/s0370-1573(99)00042-3.
URL <https://doi.org/10.1016%2Fs0370-1573%2899%2900042-3>
- [106] L. Randall, R. Sundrum, Out of this world supersymmetry breaking, *Nuclear Physics B* 557 (1-2) (1999) 79–118. doi:10.1016/s0550-3213(99)00359-4.
URL <https://doi.org/10.1016%2Fs0550-3213%2899%2900359-4>
- [107] G. F. Giudice, R. Rattazzi, M. A. Luty, H. Murayama, Gaugino mass without singlets, *Journal of High Energy Physics* 1998 (12) (1998) 027–027. doi:10.1088/1126-6708/1998/12/027.
URL <https://doi.org/10.1088%2F1126-6708%2F1998%2F12%2F027>
- [108] J. A. Bagger, T. Moroi, E. Poppitz, Anomaly mediation in supergravity theories, *Journal of High Energy Physics* 2000 (04) (2000) 009–009. doi:10.1088/1126-6708/2000/04/009.
URL <https://doi.org/10.1088%2F1126-6708%2F2000%2F04%2F009>
- [109] P. Binétruy, M. K. Gaillard, B. D. Nelson, One loop soft supersymmetry breaking terms in superstring effective theories, *Nuclear Physics B* 604 (1-2) (2001) 32–74. doi:10.1016/s0550-3213(00)00759-8.
URL <https://doi.org/10.1016%2Fs0550-3213%2800%2900759-8>
- [110] S. L. Glashow, J. Iliopoulos, L. Maiani, Weak interactions with lepton-hadron symmetry, *Phys. Rev. D* 2 (1970) 1285–1292. doi:10.1103/PhysRevD.2.1285.
URL <https://link.aps.org/doi/10.1103/PhysRevD.2.1285>
- [111] H. Baer, V. Barger, D. Sengupta, Landscape solution to the susy flavor and cp problems, *Phys. Rev. Research* 1 (2019) 033179. doi:10.1103/PhysRevResearch.1.033179.
URL <https://link.aps.org/doi/10.1103/PhysRevResearch.1.033179>
- [112] N. Arkani-Hamed, S. Dimopoulos, S. Kachru, Predictive landscapes and new physics at a tev (2005). doi:10.48550/ARXIV.HEP-TH/0501082.
URL <https://arxiv.org/abs/hep-th/0501082>

- [113] G. F. Giudice, A. Masiero, A Natural Solution to the μ Problem in Supergravity Theories, *Phys. Lett. B* 206 (1988) 480–484. doi:[10.1016/0370-2693\(88\)91613-9](https://doi.org/10.1016/0370-2693(88)91613-9).
- [114] J. E. Kim, H. Nilles, The μ -problem and the strong cp-problem, *Physics Letters B* 138 (1) (1984) 150–154. doi:[https://doi.org/10.1016/0370-2693\(84\)91890-2](https://doi.org/10.1016/0370-2693(84)91890-2).
URL <https://www.sciencedirect.com/science/article/pii/0370269384918902>
- [115] U. Ellwanger, C. Hugonie, A. M. Teixeira, The next-to-minimal supersymmetric standard model, *Physics Reports* 496 (1-2) (2010) 1–77. doi:[10.1016/j.physrep.2010.07.001](https://doi.org/10.1016/j.physrep.2010.07.001).
URL <https://doi.org/10.1016%2Fj.physrep.2010.07.001>
- [116] K. J. Bae, E. J. Chun, S. H. Im, Cosmology of the DFSZ axino, *Journal of Cosmology and Astroparticle Physics* 2012 (03) (2012) 013–013. doi:[10.1088/1475-7516/2012/03/013](https://doi.org/10.1088/1475-7516/2012/03/013).
URL <https://doi.org/10.1088%2F1475-7516%2F2012%2F03%2F013>
- [117] K. J. Bae, H. Baer, E. J. Chun, Mixed axion/neutralino dark matter in the SUSY DFSZ axion model, *Journal of Cosmology and Astroparticle Physics* 2013 (12) (2013) 028–028. doi:[10.1088/1475-7516/2013/12/028](https://doi.org/10.1088/1475-7516/2013/12/028).
URL <https://doi.org/10.1088%2F1475-7516%2F2013%2F12%2F028>
- [118] M. Dine, W. Fischler, M. Srednicki, A simple solution to the strong cp problem with a harmless axion, *Physics Letters B* 104 (3) (1981) 199–202. doi:[https://doi.org/10.1016/0370-2693\(81\)90590-6](https://doi.org/10.1016/0370-2693(81)90590-6).
URL <https://www.sciencedirect.com/science/article/pii/0370269381905906>
- [119] A. R. Zhitnitsky, On Possible Suppression of the Axion Hadron Interactions. (In Russian), *Sov. J. Nucl. Phys.* 31 (1980) 260.
- [120] S. M. Barr, D. Seckel, Planck-scale corrections to axion models, *Phys. Rev. D* 46 (1992) 539–549. doi:[10.1103/PhysRevD.46.539](https://doi.org/10.1103/PhysRevD.46.539).
URL <https://link.aps.org/doi/10.1103/PhysRevD.46.539>
- [121] R. Holman, S. D. Hsu, T. W. Kephart, E. W. Kolb, R. Watkins, L. M. Widrow, Solutions to the strong-CP problem in a world with gravity, *Physics Letters B* 282 (1-2) (1992) 132–136. doi:[10.1016/0370-2693\(92\)90491-1](https://doi.org/10.1016/0370-2693(92)90491-1).
URL <https://doi.org/10.1016%2F0370-2693%2892%2990491-1>
- [122] M. Kamionkowski, J. March-Russell, Planck-scale physics and the peccei-quinn mechanism, *Physics Letters B* 282 (1-2) (1992) 137–141. doi:[10.1016/0370-2693\(92\)90492-m](https://doi.org/10.1016/0370-2693(92)90492-m).
URL <https://doi.org/10.1016%2F0370-2693%2892%2990492-m>
- [123] R. Kallosh, A. Linde, D. Linde, L. Susskind, Gravity and global symmetries, *Physical Review D* 52 (2) (1995) 912–935. doi:[10.1103/physrevd.52.912](https://doi.org/10.1103/physrevd.52.912).
URL <https://doi.org/10.1103%2Fphysrevd.52.912>

- [124] K. Babu, I. Gogoladze, K. Wang, Stabilizing the axion by discrete gauge symmetries, *Physics Letters B* 560 (3-4) (2003) 214–222. doi:10.1016/s0370-2693(03)00411-8. URL <https://doi.org/10.1016%2Fs0370-2693%2803%2900411-8>
- [125] H. P. Nilles, Stringy origin of discrete r-symmetries (2017). doi:10.48550/ARXIV.1705.01798. URL <https://arxiv.org/abs/1705.01798>
- [126] H. M. Lee, S. Raby, M. Ratz, G. G. Ross, R. Schieren, K. Schmidt-Hoberg, P. K. Vaudrevange, Discrete r symmetries for the MSSM and its singlet extensions, *Nuclear Physics B* 850 (1) (2011) 1–30. doi:10.1016/j.nuclphysb.2011.04.009. URL <https://doi.org/10.1016%2Fj.nuclphysb.2011.04.009>
- [127] H. Baer, V. Barger, D. Sengupta, Gravity safe, electroweak natural axionic solution to strong CP and SUSY μ problems, *Physics Letters B* 790 (2019) 58–63. doi:10.1016/j.physletb.2019.01.007. URL <https://doi.org/10.1016%2Fj.physletb.2019.01.007>
- [128] H. P. Nilles, P. K. S. Vaudrevange, Geography of fields in extra dimensions: String theory lessons for particle physics, *Modern Physics Letters A* 30 (10) (2015) 1530008. doi:10.1142/s0217732315300086. URL <https://doi.org/10.1142%2Fs0217732315300086>
- [129] W. Buchmuller, K. Hamaguchi, O. Lebedev, M. Ratz, Local grand unification (2005). doi:10.48550/ARXIV.HEP-PH/0512326. URL <https://arxiv.org/abs/hep-ph/0512326>
- [130] Search for supersymmetry in final states with missing transverse momentum and multiple b -jets in proton-proton collisions at $\sqrt{s} = 13$ TeV with the ATLAS detector (7 2018).
- [131] A. M. Sirunyan, et al., Search for top squark pair production in pp collisions at $\sqrt{s} = 13$ TeV using single lepton events, *JHEP* 10 (2017) 019. arXiv:1706.04402, doi:10.1007/JHEP10(2017)019.
- [132] A. M. Sirunyan, et al., Search for additional neutral MSSM Higgs bosons in the $\tau\tau$ final state in proton-proton collisions at $\sqrt{s} = 13$ TeV, *JHEP* 09 (2018) 007. arXiv:1803.06553, doi:10.1007/JHEP09(2018)007.
- [133] M. Aaboud, et al., Search for electroweak production of supersymmetric states in scenarios with compressed mass spectra at $\sqrt{s} = 13$ TeV with the ATLAS detector, *Phys. Rev. D* 97 (5) (2018) 052010. arXiv:1712.08119, doi:10.1103/PhysRevD.97.052010.
- [134] H. Baer, V. Barger, J. S. Gainer, P. Huang, M. Savoy, D. Sengupta, X. Tata, Gluino reach and mass extraction at the LHC in radiatively-driven natural SUSY, *Eur. Phys. J. C* 77 (7) (2017) 499. arXiv:1612.00795, doi:10.1140/epjc/s10052-017-5067-3.

- [135] H. Baer, V. Barger, M. Padeffke-Kirkland, X. Tata, Naturalness implies intra-generational degeneracy for decoupled squarks and sleptons, *Phys. Rev. D* 89 (2014) 037701. doi:10.1103/PhysRevD.89.037701.
URL <https://link.aps.org/doi/10.1103/PhysRevD.89.037701>
- [136] H. Baer, V. Barger, P. Huang, D. Mickelson, A. Mustafayev, W. Sreethawong, X. Tata, Same-sign diboson signature from supersymmetry models with light higgsinos at the LHC, *Physical Review Letters* 110 (15) (apr 2013). doi:10.1103/physrevlett.110.151801.
URL <https://doi.org/10.1103%2Fphysrevlett.110.151801>
- [137] H. Baer, V. Barger, P. Huang, D. Mickelson, A. Mustafayev, W. Sreethawong, X. Tata, Radiatively-driven natural supersymmetry at the LHC, *Journal of High Energy Physics* 2013 (12) (dec 2013). doi:10.1007/jhep12(2013)013.
URL <https://doi.org/10.1007%2Fjhep12%282013%29013>
- [138] H. Baer, V. Barger, J. S. Gainer, M. Savoy, D. Sengupta, X. Tata, Aspects of the same-sign diboson signature from wino pair production with light higgsinos at the high luminosity LHC, *Physical Review D* 97 (3) (feb 2018). doi:10.1103/physrevd.97.035012.
URL <https://doi.org/10.1103%2Fphysrevd.97.035012>
- [139] Z. Han, G. D. Kribs, A. Martin, A. Menon, Hunting quasidegenerate higgsinos, *Phys. Rev. D* 89 (2014) 075007. doi:10.1103/PhysRevD.89.075007.
URL <https://link.aps.org/doi/10.1103/PhysRevD.89.075007>
- [140] H. Baer, A. Mustafayev, X. Tata, Monojet plus soft dilepton signal from light higgsino pair production at lhc14, *Phys. Rev. D* 90 (2014) 115007. doi:10.1103/PhysRevD.90.115007.
URL <https://link.aps.org/doi/10.1103/PhysRevD.90.115007>
- [141] C. Han, D. Kim, S. Munir, M. Park, Accessing the core of naturalness, nearly degenerate higgsinos, at the LHC, *Journal of High Energy Physics* 2015 (4) (apr 2015). doi:10.1007/jhep04(2015)132.
URL <https://doi.org/10.1007%2Fjhep04%282015%29132>
- [142] X. Cid Vidal, et al., Report from Working Group 3: Beyond the Standard Model physics at the HL-LHC and HE-LHC, CERN Yellow Rep. Monogr. 7 (2019) 585–865. arXiv:1812.07831, doi:10.23731/CYRM-2019-007.585.
- [143] H. Baer, M. Bisset, C. Kao, X. Tata, Detecting higgs boson decays to neutralinos at hadron supercolliders, *Phys. Rev. D* 50 (1994) 316–324. doi:10.1103/PhysRevD.50.316.
URL <https://link.aps.org/doi/10.1103/PhysRevD.50.316>
- [144] K. J. Bae, H. Baer, N. Nagata, H. Serce, Prospects for higgs coupling measurements in susy with radiatively-driven naturalness, *Phys. Rev. D* 92 (2015) 035006. doi:10.1103/PhysRevD.92.035006.
URL <https://link.aps.org/doi/10.1103/PhysRevD.92.035006>

- [145] H. Baer, V. Barger, D. Sengupta, Mirage mediation from the landscape, *Physical Review Research* 2 (1) (mar 2020). doi:10.1103/physrevresearch.2.013346.
URL <https://doi.org/10.1103/physrevresearch.2.013346>
- [146] K. Choi, A. Falkowski, H. P. Nilles, M. Olechowski, S. Pokorski, Stability of flux compactifications and the pattern of supersymmetry breaking, *Journal of High Energy Physics* 2004 (11) (2004) 076–076. doi:10.1088/1126-6708/2004/11/076.
URL <https://doi.org/10.1088/1126-6708/2004/11/076>
- [147] H. Baer, V. Barger, D. Mickelson, A. Mustafayev, X. Tata, Physics at a higgsino factory, *Journal of High Energy Physics* 2014 (6) (jun 2014). doi:10.1007/jhep06(2014)172.
URL [https://doi.org/10.1007/jhep06\(2014\)172](https://doi.org/10.1007/jhep06(2014)172)
- [148] H. Baer, M. Berggren, K. Fujii, J. List, S.-L. Lehtinen, T. Tanabe, J. Yan, ILC as a natural SUSY discovery machine and precision microscope: From light higgsinos to tests of unification, *Physical Review D* 101 (9) (may 2020). doi:10.1103/physrevd.101.095026.
URL <https://doi.org/10.1103/physrevd.101.095026>
- [149] K. Choi, K.-S. Jeong, K. ichi Okumura, Phenomenology of mixed modulus-anomaly mediation in fluxed string compactifications and brane models, *Journal of High Energy Physics* 2005 (09) (2005) 039–039. doi:10.1088/1126-6708/2005/09/039.
URL <https://doi.org/10.1088/1126-6708/2005/09/039>
- [150] A. Falkowski, O. Lebedev, Y. Mambrini, SUSY phenomenology of KKLT flux compactifications, *Journal of High Energy Physics* 2005 (11) (2005) 034–034. doi:10.1088/1126-6708/2005/11/034.
URL <https://doi.org/10.1088/1126-6708/2005/11/034>
- [151] K. Choi, K. S. Jeong, T. Kobayashi, K. ichi Okumura, TeV scale mirage mediation and natural little supersymmetric hierarchy, *Physical Review D* 75 (9) (may 2007). doi:10.1103/physrevd.75.095012.
URL <https://doi.org/10.1103/physrevd.75.095012>
- [152] M. Endo, M. Yamaguchi, K. Yoshioka, Bottom-up approach to moduli dynamics in heavy gravitino scenario: Superpotential, soft terms, and sparticle mass spectrum, *Physical Review D* 72 (1) (jul 2005). doi:10.1103/physrevd.72.015004.
URL <https://doi.org/10.1103/physrevd.72.015004>
- [153] K. Uno, Search for squarks and gluinos in final states with jets and missing transverse momentum at $\sqrt{s} = 13$ TeV using 139 fb^{-1} data with the ATLAS detector, *PoS LeptonPhoton2019* (2019) 186. doi:10.22323/1.367.0186.
- [154] Search for supersymmetry in proton-proton collisions at 13 TeV in final states with jets and missing transverse momentum (2019).
- [155] M. R. Douglas, Statistical analysis of the supersymmetry breaking scale (2004). doi:10.48550/ARXIV.HEP-TH/0405279.
URL <https://arxiv.org/abs/hep-th/0405279>

- [156] E. Witten, Dynamical Breaking of Supersymmetry, Nucl. Phys. B 188 (1981) 513. doi:10.1016/0550-3213(81)90006-7.
- [157] E. Poppitz, S. P. Trivedi, Dynamical supersymmetry breaking, Ann. Rev. Nucl. Part. Sci. 48 (1998) 307–350. arXiv:hep-th/9803107, doi:10.1146/annurev.nucl.48.1.307.
- [158] Y. Shadmi, Y. Shirman, Dynamical supersymmetry breaking, Rev. Mod. Phys. 72 (2000) 25–64. arXiv:hep-th/9907225, doi:10.1103/RevModPhys.72.25.
- [159] M. Dine, J. D. Mason, Supersymmetry and Its Dynamical Breaking, Rept. Prog. Phys. 74 (2011) 056201. arXiv:1012.2836, doi:10.1088/0034-4885/74/5/056201.
- [160] S. Ferrara, L. Girardello, H. P. Nilles, Breakdown of Local Supersymmetry Through Gauge Fermion Condensates, Phys. Lett. B 125 (1983) 457. doi:10.1016/0370-2693(83)91325-4.
- [161] I. Affleck, M. Dine, N. Seiberg, Exponential Hierarchy From Dynamical Supersymmetry Breaking, Phys. Lett. B 140 (1984) 59–62. doi:10.1016/0370-2693(84)91047-5.
- [162] T. Banks, M. Dine, E. Gorbatov, Is there a string theory landscape?, JHEP 08 (2004) 058. arXiv:hep-th/0309170, doi:10.1088/1126-6708/2004/08/058.
- [163] M. Dine, E. Gorbatov, S. D. Thomas, Low energy supersymmetry from the landscape, JHEP 08 (2008) 098. arXiv:hep-th/0407043, doi:10.1088/1126-6708/2008/08/098.
- [164] M. Dine, The Intermediate scale branch of the landscape, JHEP 01 (2006) 162. arXiv:hep-th/0505202, doi:10.1088/1126-6708/2006/01/162.
- [165] I. Affleck, M. Dine, N. Seiberg, Supersymmetry Breaking by Instantons, Phys. Rev. Lett. 51 (1983) 1026. doi:10.1103/PhysRevLett.51.1026.
- [166] W. Taylor, Y.-N. Wang, The F-theory geometry with most flux vacua, JHEP 12 (2015) 164. arXiv:1511.03209, doi:10.1007/JHEP12(2015)164.
- [167] I. Broeckel, M. Cicoli, A. Maharana, K. Singh, K. Sinha, Moduli Stabilisation and the Statistics of SUSY Breaking in the Landscape, JHEP 10 (2020) 015. arXiv:2007.04327, doi:10.1007/JHEP09(2021)019.
- [168] V. Balasubramanian, P. Berglund, J. P. Conlon, F. Quevedo, Systematics of moduli stabilisation in Calabi-Yau flux compactifications, JHEP 03 (2005) 007. arXiv:hep-th/0502058, doi:10.1088/1126-6708/2005/03/007.
- [169] M. DINE, SUPERSYMMETRY, NATURALNESS AND THE LANDSCAPE, in: PAS-COS 2004, World Scientific Publishing Company, 2005. doi:10.1142/9789812701756_0093.
URL https://doi.org/10.1142/9789812701756_0093

- [170] M. Dine, D. O'Neil, Z. Sun, Branches of the landscape, *Journal of High Energy Physics* 2005 (07) (2005) 014–014. doi:10.1088/1126-6708/2005/07/014.
URL <https://doi.org/10.1088/1126-6708/2005/07/014>
- [171] A. Arbey, et al., Physics at the e+ e- Linear Collider, *Eur. Phys. J. C* 75 (8) (2015) 371. arXiv:1504.01726, doi:10.1140/epjc/s10052-015-3511-9.
- [172] G. Kane, P. Kumar, R. Lu, B. Zheng, Higgs Mass Prediction for Realistic String/M Theory Vacua, *Phys. Rev. D* 85 (2012) 075026. arXiv:1112.1059, doi:10.1103/PhysRevD.85.075026.
- [173] H. Baer, V. Barger, P. Huang, Hidden SUSY at the LHC: the light higgsino-world scenario and the role of a lepton collider, *Journal of High Energy Physics* 2011 (11) (nov 2011). doi:10.1007/jhep11(2011)031.
URL <https://doi.org/10.1007/jhep11%282011%29031>
- [174] H. Baer, V. Barger, M. Savoy, X. Tata, Multichannel assault on natural supersymmetry at the high luminosity LHC, *Phys. Rev. D* 94 (3) (2016) 035025. arXiv:1604.07438, doi:10.1103/PhysRevD.94.035025.
- [175] Search for new physics in the compressed mass spectra scenario using events with two soft opposite-sign leptons and missing momentum energy at 13 TeV (2016).
- [176] H. Baer, V. Barger, J. S. Gainer, H. Serce, X. Tata, Reach of the high-energy LHC for gluinos and top squarks in SUSY models with light Higgsinos, *Phys. Rev. D* 96 (11) (2017) 115008. arXiv:1708.09054, doi:10.1103/PhysRevD.96.115008.
- [177] H. Baer, V. Barger, J. S. Gainer, D. Sengupta, H. Serce, X. Tata, LHC luminosity and energy upgrades confront natural supersymmetry models, *Phys. Rev. D* 98 (7) (2018) 075010. arXiv:1808.04844, doi:10.1103/PhysRevD.98.075010.
- [178] M. Berg, M. Haack, B. Körs, Stabilization of the compactification volume by quantum corrections, *Physical Review Letters* 96 (2) (jan 2006). doi:10.1103/physrevlett.96.021601.
URL <https://doi.org/10.1103/physrevlett.96.021601>
- [179] R. D. Peccei, H. R. Quinn, CP Conservation in the Presence of Instantons, *Phys. Rev. Lett.* 38 (1977) 1440–1443. doi:10.1103/PhysRevLett.38.1440.
- [180] S. Weinberg, A New Light Boson?, *Phys. Rev. Lett.* 40 (1978) 223–226. doi:10.1103/PhysRevLett.40.223.
- [181] F. Wilczek, Problem of Strong P and T Invariance in the Presence of Instantons, *Phys. Rev. Lett.* 40 (1978) 279–282. doi:10.1103/PhysRevLett.40.279.
- [182] J. E. Kim, Weak Interaction Singlet and Strong CP Invariance, *Phys. Rev. Lett.* 43 (1979) 103. doi:10.1103/PhysRevLett.43.103.

- [183] H. Baer, V. Barger, D. Sengupta, Gravity safe, electroweak natural axionic solution to strong CP and SUSY μ problems, *Physics Letters B* 790 (2019) 58–63. doi:10.1016/j.physletb.2019.01.007.
URL <https://doi.org/10.1016%2Fj.physletb.2019.01.007>
- [184] H. Baer, V. Barger, D. Sengupta, S. Salam, K. Sinha, Status of weak scale supersymmetry after LHC run 2 and ton-scale noble liquid WIMP searches, *The European Physical Journal Special Topics* 229 (21) (2020) 3085–3141. doi:10.1140/epjst/e2020-000020-x.
URL <https://doi.org/10.1140%2Fepjst%2Fe2020-000020-x>
- [185] H. Baer, A. Lessa, S. Rajagopalan, W. Sreethawong, Mixed axion/neutralino cold dark matter in supersymmetric models, *Journal of Cosmology and Astroparticle Physics* 2011 (06) (2011) 031–031. doi:10.1088/1475-7516/2011/06/031.
URL <https://doi.org/10.1088%2F1475-7516%2F2011%2F06%2F031>
- [186] H. Baer, A. Lessa, W. Sreethawong, Coupled boltzmann calculation of mixed axion/neutralino cold dark matter production in the early universe, *Journal of Cosmology and Astroparticle Physics* 2012 (01) (2012) 036–036. doi:10.1088/1475-7516/2012/01/036.
URL <https://doi.org/10.1088%2F1475-7516%2F2012%2F01%2F036>
- [187] E. Aprile, J. Aalbers, F. Agostini, M. Alfonsi, F. D. Amaro, M. Anthony, F. Arneodo, P. Barrow, L. Baudis, B. Bauermeister, M. L. Benabderrahmane, T. Berger, P. A. Breur, A. Brown, E. Brown, S. Bruenner, G. Bruno, R. Budnik, L. Bütikofer, J. Calvén, J. M. R. Cardoso, M. Cervantes, D. Cichon, D. Coderre, A. P. Colijn, J. Conrad, J. P. Cussonneau, M. P. Decowski, P. de Perio, P. Di Gangi, A. Di Giovanni, S. Diglio, E. Duchovni, J. Fei, A. D. Ferella, A. Fieguth, D. Franco, W. Fulgione, A. Gallo Rosso, M. Galloway, F. Gao, M. Garbini, C. Geis, L. W. Goetzke, Z. Greene, C. Grignon, C. Hasterok, E. Hogenbirk, R. Itay, B. Kaminsky, G. Kessler, A. Kish, H. Landsman, R. F. Lang, D. Lellouch, L. Levinson, M. Le Calloch, C. Levy, Q. Lin, S. Lindemann, M. Lindner, J. A. M. Lopes, A. Manfredini, T. Marrodán Undagoitia, J. Masbou, F. V. Massoli, D. Masson, D. Mayani, Y. Meng, M. Messina, K. Micheneau, B. Miguez, A. Molinario, M. Murra, J. Naganoma, K. Ni, U. Oberlack, S. E. A. Orrigo, P. Pakarha, B. Pelssers, R. Persiani, F. Piastra, J. Pienaar, M.-C. Piro, G. Plante, N. Priel, L. Rauch, S. Reichard, C. Reuter, A. Rizzo, S. Rosendahl, N. Rupp, J. M. F. dos Santos, G. Sartorelli, M. Scheibelhut, S. Schindler, J. Schreiner, M. Schumann, L. Scotto Lavina, M. Selvi, P. Shagin, M. Silva, H. Simgen, M. v. Sivers, A. Stein, D. Thers, A. Tiseni, G. Trincherro, C. D. Tunnell, R. Wall, H. Wang, M. Weber, Y. Wei, C. Weinheimer, J. Wulf, Y. Zhang, Xenon100 dark matter results from a combination of 477 live days, *Phys. Rev. D* 94 (2016) 122001. doi:10.1103/PhysRevD.94.122001.
URL <https://link.aps.org/doi/10.1103/PhysRevD.94.122001>
- [188] J. Aalbers, et al., First Dark Matter Search Results from the LUX-ZEPLIN (LZ) Experiment (7 2022). arXiv:2207.03764.
- [189] H. Baer, V. Barger, D. Mickelson, Direct and indirect detection of higgsino-like WIMPs: Concluding the story of electroweak naturalness, *Physics Letters B* 726 (1-3) (2013)

330–336. doi:10.1016/j.physletb.2013.08.060.
URL <https://doi.org/10.1016%2Fj.physletb.2013.08.060>

- [190] C. Amole, et al., Dark Matter Search Results from the PICO-60 C₃F₈ Bubble Chamber, *Phys. Rev. Lett.* 118 (25) (2017) 251301. arXiv:1702.07666, doi:10.1103/PhysRevLett.118.251301.
- [191] M. G. Aartsen, et al., Search for annihilating dark matter in the Sun with 3 years of IceCube data, *Eur. Phys. J. C* 77 (3) (2017) 146, [Erratum: *Eur.Phys.J.C* 79, 214 (2019)]. arXiv:1612.05949, doi:10.1140/epjc/s10052-017-4689-9.
- [192] D. Akerib, C. Akerlof, S. Alsum, H. Araújo, M. Arthurs, X. Bai, A. Bailey, J. Balajthy, S. Balashov, D. Bauer, J. Belle, P. Beltrame, T. Benson, E. Bernard, T. Biesiadzinski, K. Boast, B. Boxer, P. Brás, J. Buckley, V. Bugaev, S. Burdin, J. Busenitz, C. Carels, D. Carlsmith, B. Carlson, M. Carmona-Benitez, C. Chan, J. Cherwinka, A. Cole, A. Cottle, W. Craddock, A. Currie, J. Cutter, C. Dahl, L. de Viveiros, A. Dobi, J. Dobson, E. Druszkiewicz, T. Edberg, W. Edwards, A. Fan, S. Fayer, S. Fiorucci, T. Fruth, R. Gaitskell, J. Genovesi, C. Ghag, M. Gilchriese, M. van der Grinten, C. Hall, S. Hans, K. Hanzel, S. Haselschwardt, S. Hertel, S. Hillbrand, C. Hjemsfelt, M. Hoff, J.-K. Hor, D. Huang, C. Ignarra, W. Ji, A. Kaboth, K. Kamdin, J. Keefner, D. Khaitan, A. Khazov, Y. Kim, C. Kocher, E. Korolkova, H. Kraus, H. Krebs, L. Kreczko, B. Krikler, V. Kudryavtsev, S. Kyre, J. Lee, B. Lenardo, D. Leonard, K. Lesko, C. Levy, J. Li, J. Liao, F.-T. Liao, J. Lin, A. Lindote, R. Linehan, W. Lippincott, X. Liu, M. Lopes, B. L. Paredes, W. Lorenzon, S. Luitz, J. Lyle, P. Majewski, A. Manalaysay, R. Mannino, C. Maupin, D. McKinsey, Y. Meng, E. Miller, J. Mock, M. Monzani, J. Morad, E. Morrison, B. Mount, A. Murphy, H. Nelson, F. Neves, J. Nikoleyczik, K. O’Sullivan, I. Olcina, M. Olevitch, K. Oliver-Mallory, K. Palladino, S. Patton, E. Pease, B. Penning, A. Piepke, S. Powell, R. Preece, K. Pushkin, B. Ratcliff, J. Reichenbacher, C. Rhyne, A. Richards, J. Rodrigues, R. Rosero, P. Rossiter, J. Saba, M. Sarychev, R. Schnee, M. Schubnell, P. Scovell, S. Shaw, T. Shutt, J. Silk, C. Silva, K. Skarpaas, W. Skulski, M. Solmaz, V. Solovov, P. Sorensen, I. Stancu, M. Stark, T. Stiegler, K. Stifter, M. Szydagis, W. Taylor, R. Taylor, D. Taylor, D. Temples, P. Terman, K. Thomas, M. Timalisina, W. To, A. Tomás, T. Tope, M. Tripathi, C. Tull, L. Tvrznikova, U. Utku, J. Va’vra, A. Vacheret, J. Verbus, E. Voirin, W. Waldron, J. Watson, R. Webb, D. White, T. Whitis, W. Wisniewski, M. Witherell, F. Wolfs, D. Woodward, S. Worm, M. Yeh, J. Yin, I. Y. and, Projected WIMP sensitivity of the LUX-ZEPLIN dark matter experiment, *Physical Review D* 101 (5) (mar 2020). doi:10.1103/physrevd.101.052002.
URL <https://doi.org/10.1103%2Fphysrevd.101.052002>
- [193] Limits to dark matter annihilation cross-section from a combined analysis of MAGIC and fermi-LAT observations of dwarf satellite galaxies, *Journal of Cosmology and Astroparticle Physics* 2016 (02) (2016) 039–039. doi:10.1088/1475-7516/2016/02/039.
URL <https://doi.org/10.1088%2F1475-7516%2F2016%2F02%2F039>

- [194] K. J. Bae, H. Baer, H. Serce, Prospects for axion detection in natural SUSY with mixed axion-higgsino dark matter: back to invisible?, *JCAP* 06 (2017) 024. [arXiv:1705.01134](https://arxiv.org/abs/1705.01134), [doi:10.1088/1475-7516/2017/06/024](https://doi.org/10.1088/1475-7516/2017/06/024).
- [195] G. F. Giudice, A. Pomarol, Mass degeneracy of the higgsinos, *Physics Letters B* 372 (3) (1996) 253–258. [doi:https://doi.org/10.1016/0370-2693\(96\)00060-3](https://doi.org/10.1016/0370-2693(96)00060-3).
URL <https://www.sciencedirect.com/science/article/pii/0370269396000603>
- [196] H. Baer, A. Mustafayev, X. Tata, Monojets and monophotons from light higgsino pair production at lhc14 , *Phys. Rev. D* 89 (2014) 055007. [doi:10.1103/PhysRevD.89.055007](https://doi.org/10.1103/PhysRevD.89.055007).
URL <https://link.aps.org/doi/10.1103/PhysRevD.89.055007>
- [197] D. Pierce, A. Papadopoulos, The complete radiative corrections to the gaugino and higgsino masses in the minimal supersymmetric model, *Nuclear Physics B* 430 (2) (1994) 278–292. [doi:10.1016/0550-3213\(94\)00303-3](https://doi.org/10.1016/0550-3213(94)00303-3).
URL <https://doi.org/10.1016%2F0550-3213%2894%2900303-3>
- [198] D. M. Pierce, J. A. Bagger, K. T. Matchev, R.-J. Zhang, Precision corrections in the minimal supersymmetric standard model, *Nuclear Physics B* 491 (1-2) (1997) 3–67. [doi:10.1016/s0550-3213\(96\)00683-9](https://doi.org/10.1016/s0550-3213(96)00683-9).
URL <https://doi.org/10.1016%2Fs0550-3213%2896%2900683-9>
- [199] A. Dedes, P. Slavich, Two-loop corrections to radiative electroweak symmetry breaking in the MSSM, *Nuclear Physics B* 657 (2003) 333–354. [doi:10.1016/s0550-3213\(03\)00173-1](https://doi.org/10.1016/s0550-3213(03)00173-1).
URL <https://doi.org/10.1016%2Fs0550-3213%2803%2900173-1>
- [200] A. Canepa, T. Han, X. Wang, The Search for Electroweakinos, *Ann. Rev. Nucl. Part. Sci.* 70 (2020) 425–454. [arXiv:2003.05450](https://arxiv.org/abs/2003.05450), [doi:10.1146/annurev-nucl-031020-121031](https://doi.org/10.1146/annurev-nucl-031020-121031).